# INFLUENCE OF SEISMIC SOURCE AND GROUND MOTION MODELING ON THE PROBABILISTIC SEISMIC HAZARD ASSESSMENT OF THE CITY OF VAN AFTER THE 23 OCTOBER 2011 $M_W$7.2 EARTHQUAKE

A THESIS SUBMITTED TO
THE GRADUATE SCHOOL OF NATURAL AND APPLIED SCIENCES
OF
MIDDLE EAST TECHNICAL UNIVERSITY

BY

MEHTAP ŞENYURT

IN PARTIAL FULFILLMENT OF THE REQUIREMENTS
FOR
THE DEGREE OF MASTER OF SCIENCE
IN
CIVIL ENGINEERING

SEPTEMBER 2013

Approval of the thesis:

**INFLUENCE OF SEISMIC SOURCE AND GROUND MOTION MODELING ON THE PROBABILISTIC SEISMIC HAZARD ASSESSMENT OF THE CITY OF VAN AFTER THE 23 OCTOBER 2011 $M_W$7.2 EARTHQUAKE**

submitted by **MEHTAP ŞENYURT** in partial fulfillment of the requirements for the degree of **Master of Science in Civil Engineering Department, Middle East Technical University** by**,**

Prof. Dr., Canan Özgen _____
Dean, Graduate School of **Natural and Applied Sciences**

Prof. Dr., Ahmet Cevdet Yalçıner _____
Head of Department, **Civil Engineering Dept., METU**

Prof. Dr., Sinan Akkar _____
Supervisor, **Civil Engineering Dept., METU**

Assist. Prof. Dr., M. Tolga Yılmaz _____
Co-Supervisor, **Engineering Sciences Dept., METU**

**Examining Committee Members:**

Assoc. Prof. Dr., Ayşegül Askan Gündoğan _____
Department of Civil Engineering, METU

Prof. Dr., Sinan Akkar _____
Department of Civil Engineering, METU

Assoc. Prof. Dr., Zafer Evis _____
Department of Engineering Sciences, METU

Assoc. Prof. Dr., Altuğ Erberik _____
Department of Civil Engineering, METU

Ulubey Çeken, M.Sc _____
Prime Ministry Disaster & Emergency Management Presidency

**Date:** 04.09.2013

**I hereby declare that all information in this document has been obtained and presented in accordance with academic rules and ethical conduct. I also declare that, as required by these rules and conduct, I have fully cited and referenced all material and results that are not original to this work.**

Name, Last Name: Mehtap ŞENYURT

Signature :

# ABSTRACT

## INFLUENCE OF SEISMIC SOURCE AND GROUND MOTION MODELING ON THE PROBABILISTIC SEISMIC HAZARD ASSESSMENT OF THE CITY OF VAN AFTER THE 23 OCTOBER 2011 $M_W$7.2 EARTHQUAKE

Şenyurt, Mehtap
MSc. Department of Civil Engineering
Supervisor: Prof. Dr. Sinan Akkar
Co-Supervisor: Assist. Prof. Dr. M. Tolga Yılmaz

September 2013, 81 pages

Reliable assessment of seismic hazard is the most important step for seismic design and performance assessment of structural systems. However, the inherent uncertainty in earthquakes as well as modeling of ground motion may affect the hazard computed for a particular region. This study investigates the influence of seismic source and ground motion modeling on probabilistic seismic hazard assessment (PSHA). The study considers the seismicity around the city of Van to achieve its objective as this city was hit by a major earthquake on 23 October 2011 ($M_w$ 7.2) that was followed by another significant event on 9 November 2011 ($M_w$ 5.6). These two earthquakes caused loss of a substantial number of lives and left many locals homeless with a huge socio-economic impact. They re-emphasized the importance of seismic induced hazard in the region and uncertainties involved both in source and ground-motion variability to quantify hazard in the region. The importance of each input parameter in PSHA is depicted by studying the uncertainties that are ranked through sensitivity analysis. A multi-parameter approach that is proposed by Rabinowitz and Steinberg (1991) is utilized in sensitivity analysis. The method not only indicates the individual effects of each input parameter but also portrays the interaction between the input PSHA parameters. The study accounts for the uncertainty in PSHA by considering the variations in the estimation of ground motion intensity measure, the level

of standard deviation, earthquake catalog information, selection of recurrence models, selection of maximum magnitude and slip rate of the faults in the region of interest. The individual effects of these parameters and their mutual interactions are examined by using the aforementioned multi-parameter sensitivity approach. The calculations are done for peak ground acceleration (PGA) as well as pseudo-spectral acceleration (PSA) ordinates at T = 0.2s and T = 1.0s (i.e., PSA(T=0.2s) and PSA(T=1.0s)). The return periods chosen for the sensitivity analyses are 72, 475 and 2475 years that are used by the Turkish Earthquake Code (TEC, 2007) for seismic design and performance assessment of building structures. The discussions presented in this thesis can be used for deriving the design spectra for the above return periods for future engineering studies in the city of Van and surrounding regions.

Keywords: Probabilistic seismic hazard assessment; sensitivity analysis; seismic hazard of the city of Van; seismotectonics of Eastern Anatolia; 23 October and 9 November 2011 Van earthquakes

# ÖZ

## SİSMİK KAYNAK VE YER HAREKETİ TAHMİN DENKLEMLERİNE BAĞLI MODELLEME BELİRSİZLİĞİNİN OLASILIKSAL SİSMİK TEHLİKE HESAPLARINA ETKİSİ

Şenyurt, Mehtap
Yüksek Lisans, İnşaat Mühendisliği Bölümü
Tez Yöneticisi: Prof. Dr. Sinan Akkar
Ortak Tez Yöneticisi: Yrd. Doç. Dr. M. Tolga Yılmaz

Eylül 2013, 81 sayfa

Mühendislik yapılarının tasarımılari icin sismik tehlikenin guvenilir bir sekilde hesaplanmasi gerekir. Bununla beraber sismik kaynak ve yer hareketi tahmin denklemlerine bağlı belirsizlikler bir bolge veya spesifik bir nokta icin yapilan sismik tehlike hesaplarının sonuclarini ciddi sekilde etkileyebilir. Bu çalışma, sismik kaynak ve yer hareketi modellerine bağlı belirsizliklerin olasiliksal sismik tehlike hesaplarına olan etkilerini irdelemistir. Bu amac dogrultusunda Van sehri ve cevresindeki sismik aktivite dikkate alinarak bu bolgenin olasiliksal sismik tehlike hesaplari uzerinde calisilmistir. Van sehri, 23 Ekim 2011 (Mw 7.2) ve 9 Kasım 2011 (Mw 5.6) depremlerinde buyuk buyuk hasar gormus, bu depremler sonuc meydana gelen can ve mal kayiplari sonucu sosyo-ekonomik acidan ciddi yaralar almistir. Van ve civarinda yasanan bu yikici depremler bölgenin sismotektonik ve yer hareketi modelleri açısından belirsizliklerinin irdelenmesinin gerekliliğini, Van sehri ve cevresi icin yapilacak sismik tehlike hesaplarindaki onemleri acisindan bir kez daha göstermiştir. Olasiliksal sismik tehlike hesaplarında rol alan parametrelerin hesap sonuclarina olan etkileri duyarlılık analizleri ile belirlenir. Bu çalışma Rabinowitz ve Steinberg (1991) tarafından önerilen coklu parametre yontemi olasiliksal sismik tehlike hesaplarinda kullanilan parametrelerin etkilerini belirlemeye yonelik duyarlılık analizlerinde kullanmistir. Rabinowitz ve Steinberg (1991) yöntemi her parametrenin ayrı ayrı sismik tehlike hesaplarına olan etkilerini incelerken

parametrelerin birbirleriyle olan etkileşimlerini de dikkate alabilmektedir. Bu tez kapsamında, yer hareketi tahmin denklemleri seçiminden kaynaklanan belirsizlikler, tahmin denklemlerinin standart sapmalarının belirlenmesinden kaynaklanan belirsizlikler, çalışılan bölge için derlenen deprem katalog bilgilerinden kaynaklanabilecek belirsizlikler, deprem tekerrür modellerinin seçiminden dogabilecek belirsizlikler, sismik kaynaklardaki en büyük deprem magnitudu ve fayların atım miktarındaki belirsizlikler irdelenmiştir. Duyarlılık analizleriye, yukarıda bahsi geçen parametrelerdeki belirsizliklerin tehlike hesaplarina olan etkisi ve onemi PGA (en buyuk yatay yer ivmesi), 0.2s ve 1.0s periyotlarındaki spektral ivme değerleri icin calisilmistir. Duyarlilik hesaplari icin secilen spektral ivme tekrar periyotlari sirasiyla 2475 yıl, 475 yıl ve 72 yıl olup bu degerler Turk Deprem Yonetmeligi tarafindan bina tasarimi ve deprem etkileri altinda bina performans tahkiki icin kullanilmaktadir. Bu tezin sonucunda elde edilen gözlemler, yukarıdaki tekrar periyotları ve Van bölgesi için gelecekte yapılabilecek mühendislik çalışmaları için tasarım spektrumlarının türetilmesi amacıyla kullanılabilir.

Anahtar kelimeler: Olasiliksal sismik tehlike hesaplari; duyarlilik analizleri; Van sehrinin sismik tehlike analizi; Dogu Anadolu'nun sismotektonigi; 23 Ekim ve 9 Kasim 2011 Van depremleri

*To My Family*

# ACKNOWLEDGMENTS

I would like to express my deepest gratitude to my supervisor Prof. Dr. Sinan Akkar for his guidance, advice, criticism, encouragements and insight throughout the research.

I would also like to thank to Assist. Prof. Dr. M. Tolga Yılmaz for his support and advice during this research.

I would like to express my sincere thanks to my friends for their friendship, support and motivation.

Finally, I would like to express my deepest appreciation to my parents Songül Şenyurt, Recep Şenyurt, my sister Gözde and my brother Cengiz Burak, for the support, understanding and motivation that they provided me throughout my life. I would also thank my nephew Lina for being in my life and making me smile whenever I need.

# TABLE OF CONTENTS

# LIST OF TABLES

TABLES

# LIST OF FIGURES

FIGURES

# CHAPTER 1

# INTRODUCTION

## 1.1 General

The objective of using probabilistic seismic hazard analysis (PSHA) is to determine the seismic design loads for a certain exceedance level that matches with the needs of a given engineering project. To this end, the primary output obtained from PSHA is the uniform hazard spectrum of different exceedance probabilities that is computed from hazard curves at different spectral periods. The hazard curves show the variation of spectral ordinates (or peak ground motion values) against annual exceedance rates. As PSHA accounts for the uncertainties in different components (e.g., seismic sources, their activity, distribution of ground motion) that contribute to the entire computational process, a priori knowledge about the significance of uncertainty in each component is important for the justification of PSHA outputs. Such prior information can be achieved via sensitivity analysis.

Sensitivity analysis is the study of how the variation or the uncertainty in the output of a mathematical model can be apportioned. In general, sensitivity analysis investigates the robustness of a study when it includes some form of mathematical modeling (Saltelli et al., 2008). In essence the sensitivity analysis tries to identify the significance of uncertainties in the mathematical model. This thesis studies the significance of uncertainty in PSHA input parameters by considering the seismic hazard of Van and surrounding regions as a particular case. The study aims at emphasizing the efficiency and usefulness of the multi-parameter sensitivity analysis method that is capable of considering the direct effects and interactions of each PSHA input on hazard estimations. The versatility of this analysis is tested by using the city of Van as it was recently hit by the 23 October ($M_w$ 7.2) and 9 November ($M_w$ 5.6) 2011 earthquakes. Besides, the seismic studies for the city of Van and surroundings are, unfortunately, insufficient that increase the unknowns while assessing the hazard in the region. Thus, the chosen location (i.e., Van and surroundings) to understand the efficiency of the multi-parameter sensitivity method in ranking the PSHA

input parameters for their influence on hazard results is believed to be reasonable. The thesis essentially can be of use for establishing the logic-tree applications for seismic sources and ground-motion prediction equations while estimating the ground-motion amplitudes of future earthquakes that would occur in the vicinity of the Van city.

The following section summarizes the literature studies that use different sensitivity analysis approaches to under significance of various components of PSHA in hazard estimations. The chapter ends with defining the major objectives of this study.

## 1.2 Literature Survey

As it is emphasized in the introductory section of this chapter, PSHA decomposes the influence of seismic sources and ground-motion variability for estimating the effects of future earthquakes on structures. The seismic sources are modeled by means of temporal and spatial distributions. The ground motion variability is modeled as log-normal distribution. Each one of these models require certain assumptions and the level of uncertainty in these assumptions or the consistency of tools used while developing the source and ground-motion models make an impact on the results of PSHA. To understand the significance of uncertainty in each component of PSHA various researchers have conducted sensitivity analysis.

McGuire and Shedlock (1981) studied the effects of mean rupture lengths, standard deviation of ground-motion prediction equations (GMPEs), variations in b-value, maximum magnitude and activity rate for the probabilistic seismic hazard assessment of San Francisco (Bay Area). Their basic assumption while conducting the sensitivity analyses is the independency of uncertainties associated with each one of these parameters. In other words, McGuire and Shedlock (1981) assume that the uncertainty in any one of these parameters do not trigger (increase or decrease) the uncertainty in the other relevant input parameter. In a latter study, Toro and McGuire (1987) indicated that the uncertainty in seismic input parameters can be investigated systematically by the application of logic-tree method. In the current PSHA practice, logic trees are widely used to capture epistemic uncertainty in the model parameters used for seismic sources and ground-motion variability (Bommer, 2012).

In a separate study, Atkinson and Charlwood (1983) looked into the variability in seismogenic zones, upper magnitude limits, magnitude recurrence parameters, median and standard deviation of GMPEs as well as deep and shallow seismicity for PSHA of Vancouver, British Columbia. The methodology used by Atkinson and Charlwood (1983) is similar to that of McGuire and Shedlock (1981); the authors vary each input parameter one at a time and overlook the likely interaction between the parameters. They observe that

uncertainties in upper magnitude limits, magnitude recurrence parameters dominate the hazard results for Vancouver.

In 1991, Rabinowitz and Steinberg study almost all seismic input parameters that contribute to the probabilistic seismic hazard assessment results of Jerusalem. Different than the aforementioned studies, Rabinowitz and Steinberg (1991) use multi-parameter sensitivity analysis approach that accounts for the individual effects of seismic input parameters as well as their interaction within each other to assess their importance in seismic hazard results. In essence, these authors indicate that the interaction between the upper magnitude bound and GMPE estimations can be significant in the PSHA of Jerusalem.

The sensitivity study by Annaka and Ohki (1992) varies each seismic input parameter individually (a methodology similar to McGuire and Shedlock (1981) or Atkinson and Charlwood (1983)) to emphasize the significance of earthquake occurrence and GMPEs in the PSHA results of Japan. Following a similar approach, Rabez and Slejko (2000) as well as Hassaballa et al. (2011) indicate the importance of uncertainty in seismic source and ground-motion estimation parameters while investigating the PSHA results of Italy and Sudan, respectively.

Studies by Grünthal and Wahlström (2008) investigate the sensitivity of each model parameter used in the PSHA of Germany by considering different weights in the logic-tree approach. Their logic-tree includes different seismic source parameters, magnitudes and GMPEs. The sensitivity analysis of Grünthal and Wahlström (2008) assesses the significance of variability in each parameter by using the hazard curves of peak ground acceleration (PGA). Sokolov et al. (2009) focus on varying every single seismic input parameter (e.g., maximum magnitude, different ground-motion predictive models, focal depths and their distribution, standard deviation associated with GMPEs, etc) to investigate their role on the seismic hazard assessment Romania. Wang and Gao (1996) introduce different spatial distribution functions to evaluate their importance in the hazard studies of China. In her study, Yilmaz (2008) focused on the probabilistic seismic hazard assessment of Bursa and Jordan by following an approach similar to Grünthal and Wahlström (2008). Yilmaz (2008) varies the logic-tree weights to understand the significance of GMPEs, rupture length, seismic sources and earthquake recurrence models in PSHA.

The common point in the sensitivity analyses used by the above studies, except for the one employed in Rabinowitz and Steinberg (1991), is that the effects of model parameters are elucidated without considering their likely interaction with each other. Moreover, they do not systematically investigate the combined variability effects of the model parameters.

## 1.3 Major Objectives of the Study and Organization

The main focus of this study is to assess the efficiency of multi-parameter sensitivity analysis approach (Rabinowitz and Steinberg, 1991) for the determination of the significance of uncertainty in model parameters used in PSHA. The PSHA input parameters considered in the study consist of variables used in the source and ground-motion modeling that may play a role in the final hazard results. The thesis uses the seismic hazard assessment of the city of Van and the surroundings as the case study because two recent earthquakes (23 October and 9 November 2011) shook this city increasing the importance of seismic hazard assessment of the region. The seismicity of Van and surroundings has not been studied in detail as in the case of other seismic prone regions or cities (e.g., the Marmara or Aegean regions) in Turkey, which makes the results of this study important to describe the significance of uncertainty in each input parameter while assessing the seismic hazard of the region in a probabilistic manner. Moreover, the increased levels of uncertainty in each seismic input parameter for the city of Van and surroundings make this study as a good case to verify the efficiency of multi-parameter sensitivity analysis that combines the effects and interactions of seismic input parameters in a systematic way. Finally, the review documented on the seismicity of Van and surroundings can be used in the relevant studies of earthquake induced risk mitigation for the Eastern Anatolia.

The thesis is composed of 5 chapters to achieve the above stated objectives. The first chapter introduces the major focus points of this study and presents a literature review on previous PSHA-based sensitivity analyses. The second chapter describes the main components of probabilistic seismic hazard assessment and factors influencing the uncertainty of each component in PSHA. These are discussed one by one to assess their role in the final results of PSHA. The third chapter discusses the sensitivity methods used in PSHA by emphasizing their differences among each other. A significant part of this chapter focuses on the multi-parameter sensitivity analysis and presents its details in order to understand the case study discussed in Chapter 4. The seismicity and seismotectonic review of Van and surroundings are the introductory topics of Chapter 4 and they are followed by the description of seismic input parameters considered in the sensitivity analyses for the probabilistic seismic hazard assessment of the city of Van. The descriptions of the considered seismic input parameters for the sensitivity analysis also consist of the ranges used to address the uncertainty in each seismic input parameter. The results of multi-parameter sensitivity analysis, the role of each considered seismic input parameter on the hazard results of the Van city are also presented in Chapter 4. The last chapter summarizes the results and major conclusions observed from this study.

# CHAPTER 2

# PROBABILISTIC SEISMIC HAZARD ANALYSIS: EMPHASIS ON UNCERTAINTIES

## 2.1 General

Probabilistic seismic hazard analysis (PSHA) estimates the ground-motion level with a certain probability of annual exceedance. The main output of PSHA is the hazard curve. This curve shows the annual exceedance rate (frequency) of a particular ground-motion parameter higher than a pre-determined threshold level. The ground-motion parameter of interest is usually chosen as peak ground acceleration (PGA) or pseudo-spectral acceleration (PSA) due to their common engineering significance (Figure 2.1). In essence, modern design codes use these parameters computed for a particular annual exceedance rate to establish the design spectrum envelope for their use in the seismic design of buildings located on specific geographical coordinates.

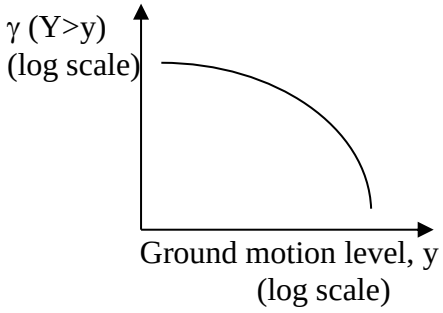


Figure 2.1 A representative hazard curve

Probabilistic seismic hazard analysis involves four basic steps: specification of the seismic source(s), characterization of the rate of earthquake magnitude occurrences on each source (i.e., magnitude-recurrence relationships), selection of ground-motion prediction

equation(s) (i.e., attenuation relationships) and finally integral computations to build hazard curve. Figure 2.2 illustrates these elements schematically that lead to determination of ground-motion design parameters to be considered in structural design. The process can be summarized as establishing a probabilistic model of strong-motion amplitudes that can be exceeded during a period of exposure time in the future. Considering the limitations (difficulties) in the characterization of seismic sources, wave travel paths and site responses, all sources of uncertainty that have a significant effect on the hazard results should be reflected in the calculations. The subsequent sections of this chapter present the basic steps of PSHA and the methods for dealing with the unavoidable problem of uncertainty in a seismic hazard analysis.

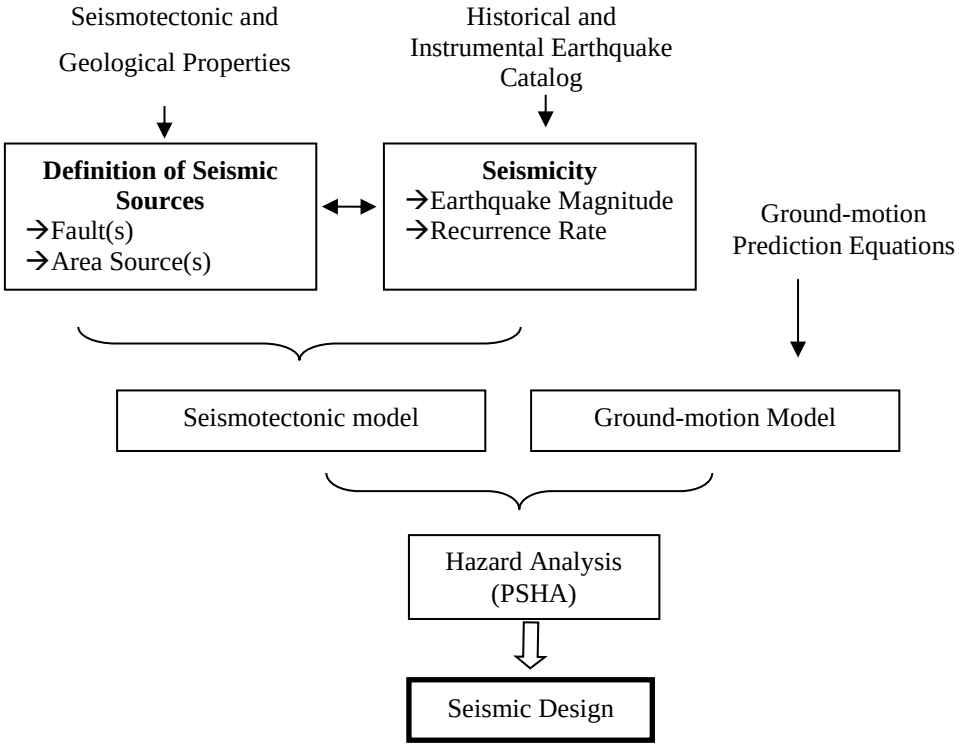


Figure 2.2 Flowchart showing the fundamental elements of PSHA

## 2.2. Definition of Seismic Sources

The first step in probabilistic seismic hazard assessment is the characterization of seismic sources that significantly contribute to the seismic hazard in the area of interest. The available seismic and geological (i.e., seismotectonic) information must be carefully compiled for developing adequate models of seismic sources. As for the first step, the spatial coordinates of seismic sources are described. Basically two source types (line and

area sources) are considered in source characterization. The line-source is used for modeling the occurrences of earthquakes on a mapped active fault. The area sources are useful for modeling the seismicity on tectonic regions where the spatial locations of future earthquakes involve significant uncertainty. Figure 2.3 illustrates a map of line sources, area sources and spatial distribution of seismic events in the area of interest considered in this study. As for the second step, the likely occurrence of future earthquakes on each source should be modeled.

The locations and kinematic properties of line (fault) sources are studied by earth scientists. The line sources are commonly modeled as multi-planar systems where the earthquake ruptures are distributed over finite fault planes. These models also depend on the estimation of rupture geometry and seismic activity rate. The activity rate depends on the rate of seismic moment accumulation on a fault, and consequently on the average slip rate on a fault (Abrahamson, 2006). Slip rates are obtained from geological measurements and relative plate motions, or by the remote sensing techniques (Westaway, 2003; Reilinger et al., 2006). The geological measurements are generally imperfect since geomorphic processes continuously alter the offsets of landforms and the geological materials (Zechar and Frankel, 2009). If displacement and age measurements involve significant uncertainty, slip rate estimates cannot be precise. Moreover, the maximum magnitude ($M_{max}$) that can occur on a fault can be properly estimated, if detailed geological and paleoseismological data are available. The value of $M_{max}$ can also be estimated by using empirical relationships (e.g., Wells and Coppersmith, 1994; Leonard, 2010) that use the fault geometry. This thesis considers the major faults with verified tectonic activity in Holocene, so that any further discussion on seismic sources are avoided. The activities of considered faults are verified by recorded destructive earthquakes during the instrumental period, and by published maps of fault rupture. Figure 2.3 identifies two main faults as the sources significantly contributing to the hazard in the area of interest (the city of Van and surroundings). The characteristics of these faults will be examined in Chapter 4.

The presences of unmapped active faults as well as the spatial distribution of earthquakes that cannot be associated with known faults are handled by area source models that are based on regional seismicity. Thus, area sources account for the occurrence of future earthquakes where the spatial uncertainty in earthquake distribution is considerably large. Hence, the events that cannot be attributed to any line source are assumed to be generated by unknown tectonic structures on the background of known faults. The occurrences of those events are modeled by area, or background-seismicity sources. The background sources are assumed to produce earthquakes of a certain magnitude interval, to have a uniform spatial distribution of seismicity. This thesis includes the non-overlapping area sources, depicted as cells of $0.5^{o}$ by the gray squares in Figure 2.3 for modeling the background seismicity. The seismological properties of the background sources will also be explained in Chapter 4.

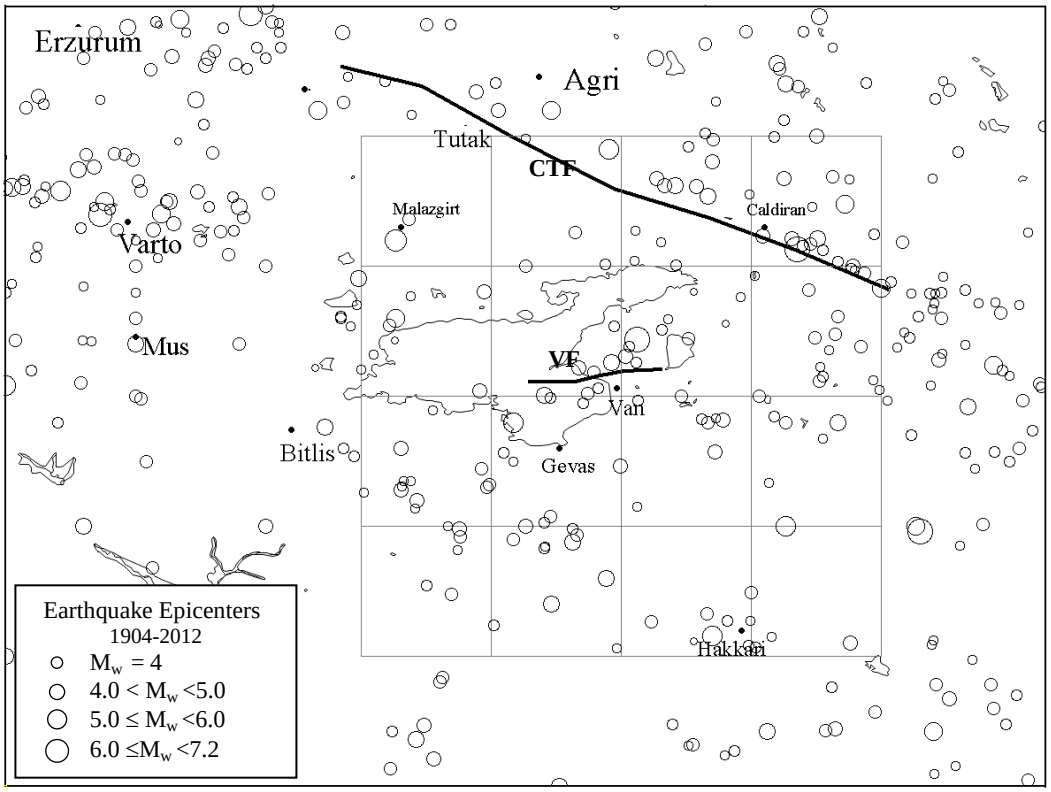


Figure 2.3 A representative figure showing the fault sources (black lines), area sources (gray squares), and spatial distribution of seismic events included in the earthquake catalog compiled for the Van area; region of interest in this thesis (CTF: Caldiran-Tutak Fault, VF: Van Fault)

The geographical dimensions of background area sources should be optimum because the inaccuracy in uniformity assumption for an area source would yield lower erroneous hazard results particularly when moderate-to-low seismicity dominates the area of interest. Moreover the sample size of earthquakes in an area will decrease as its dimensions become smaller. This, in turn, may increase the uncertainty in seismic activity rates. The characteristics of an area source are based mainly on the records of seismic activity and the available information on tectonic structures. For regions of uncertain tectonic structures and for relatively low levels of seismicity, the bias in the delineation of source boundaries and inaccurate $M_{max}$ (maximum magnitude that can occur in the background) increase the subjectivity in source characterization of area sources. This subjectivity can be surmounted to a certain extent by using the gridded spatial smoothing method (Frankel, 1995). This method assumes that the destructive future earthquakes will take place near the estimated epicenters of historical earthquakes. The method divides the study area into grid cells and computes the rate of earthquake magnitudes larger than a threshold in each grid cell. The

last step of the method involves spatial smoothing of seismicity rates in each grid cell by some empirical functions (Frankel, 1995).

## 2.3. Probabilistic characterization of seismicity

The second step in PSHA is the characterization of seismicity that leads to a probabilistic description of occurrence of future earthquakes within a certain magnitude interval. To this end, earthquake catalogs should be compiled for the seismic sources of interest. The catalog compilation consists of magnitude unification, declustering analysis, and completeness analysis. The frequency of exceeding a specific magnitude by future earthquakes is then estimated for each source. These topics are described in the following sections.

### 2.3.1. Earthquake Magnitude Scales and Magnitude Unification in Earthquake Catalog Compilation

There are several magnitude scales and most of them are based on the amplitude measurements of specific seismic wave types. These seismic waves represent particular frequency ranges due to the differences in the frequency response characteristics of seismometers. Thus, magnitude scales differ while describing the size of the same earthquake (McCalpin, 1996). In earthquake catalogs the size of earthquakes are usually given in different magnitude scales. The most commonly used magnitude scales are local (or Richter) magnitude ($M_L$), surface-wave magnitude ($M_s$), body-wave magnitude ($m_b$) and moment magnitude ($M_w$).

Local magnitude scale, $M_L$ is the first commonly applied magnitude scale in USA (Richter, 1935). It is based on the peak amplitude of the Wood-Anderson seismometer at a period of about 0.8s. The peak amplitudes of the Wood-Anderson seismometer are normalized to a standard epicentral distance of 100 km. The local magnitude scale can accurately show the energy released by an earthquake up to $M_L$6.5. However, it saturates at about $M_L$6.5 and consequently underestimates the actual energy release in larger ranges of the magnitude.

Surface-wave magnitude scale, $M_s$ is proposed to surmount the saturation problem of local magnitude scale for larger earthquakes. The measurement technique is similar to local magnitude scale except that the amplitudes of long-period surface-waves from shallow earthquakes are used. The seismometers that are capable of measuring surface-waves have a natural period of 20s and they can record distant events. Thus, $M_s$ is measured on long-period seismographs that are not necessarily deployed at stations close to the earthquake source. These features overcome the problem of magnitude saturation observed in $M_L$ up to a certain extent. The large-size earthquakes produce long-period waveforms that are captured better by long-period seismometers. Since such seismometers can capture seismic

waveforms at distant stations, the clipping of waveforms is not frequent as in the case of Wood-Anderson seismometers. These advantages lead to unbiased measurement of earthquake size by $M_s$ for magnitudes less than 8 (Kramer, 1996). Nevertheless, the dependency of $M_s$ on wave amplitude and seismometer frequency band eventually causes magnitude saturation.

The body wave magnitude, $m_b$, is often used for measuring the sizes of deep earthquakes in which the surface wave amplitudes are too small to measure. It is based on the amplitude of P-wave at a period of 1 s (Gutenberg, 1945). This magnitude scaling also suffers from magnitude saturation due to the limitations in the frequency band of the seismometer.

Currently, the most widely used magnitude is the moment magnitude scale, $M_w$. The moment magnitude, which is defined by Hanks and Kanamori (1979), is based on the seismic moment, $M_o$, of an earthquake rather than the peak amplitudes of the seismograms at different periods (or frequency intervals). The seismic moment is defined as

$$M_0 = D * A * \mu \tag{2.1}$$

where D is the average slip displacement, A is the area of the ruptured fault surface and μ is the average shear rigidity of the rock, which is typically $3*10^{11}$ dyne/cm$^2$ for crustal events (Aki, 1965). Average slip displacement is estimated from the observed surface displacements on the fault plane and ruptured area is obtained from the product of length and estimated depth of the ruptured fault plane. Moment magnitude is directly related to seismic moment which represents the total amount of energy released at the source as shown in Eq. (2.2).

$$M_w = \frac{2}{3} * \log_{10}(M_0) - 10.7 \tag{2.2}$$

The moment magnitude scale, being independent of the seismic wave amplitudes and seismometer limitations, is developed to overcome the saturation problem of other aforementioned magnitude scales. In this study, the other magnitude scales are converted to the moment magnitude scale by empirical magnitude conversion relationships for homogenizing the magnitude scale in the earthquake catalog compiled for the city of Van and surrounding regions. There are various empirical magnitude conversion relationships in the literature (e.g., Grünthal et al., 2009; Ulusay et al., 2004; Akkar et al., 2010; Zare and Bard, 2002). They calculate the expected moment magnitude, $M_w$, from $M_s$, $M_L$ and $m_b$. The moment magnitude estimations of these relationships can be considerably different from each other for a variety of reasons. Insufficient sample size of the earthquake data with different magnitude scales, different regression techniques resulting in differences in the regression coefficients of empirical magnitude conversion relationships can be counted as some of the reasons behind these differences. Moreover, while establishing a

relationship for $M_L$ vs. $M_w$ conversion, regional $M_L$ should be used as this magnitude scale can vary from one region to the other due to the differences in its computation process. Therefore, the choice for the empirical relationship on magnitude-scale conversion can affect the characterization of seismicity in a region. Figure 2.4 depicts the variation of moment magnitude when different empirical relationships are considered. The effects of using different empirical magnitude conversion relationships on the hazard results is discussed in Chapter 4 by using the particular hazard study (seismic hazard of the city of Van) of this thesis.

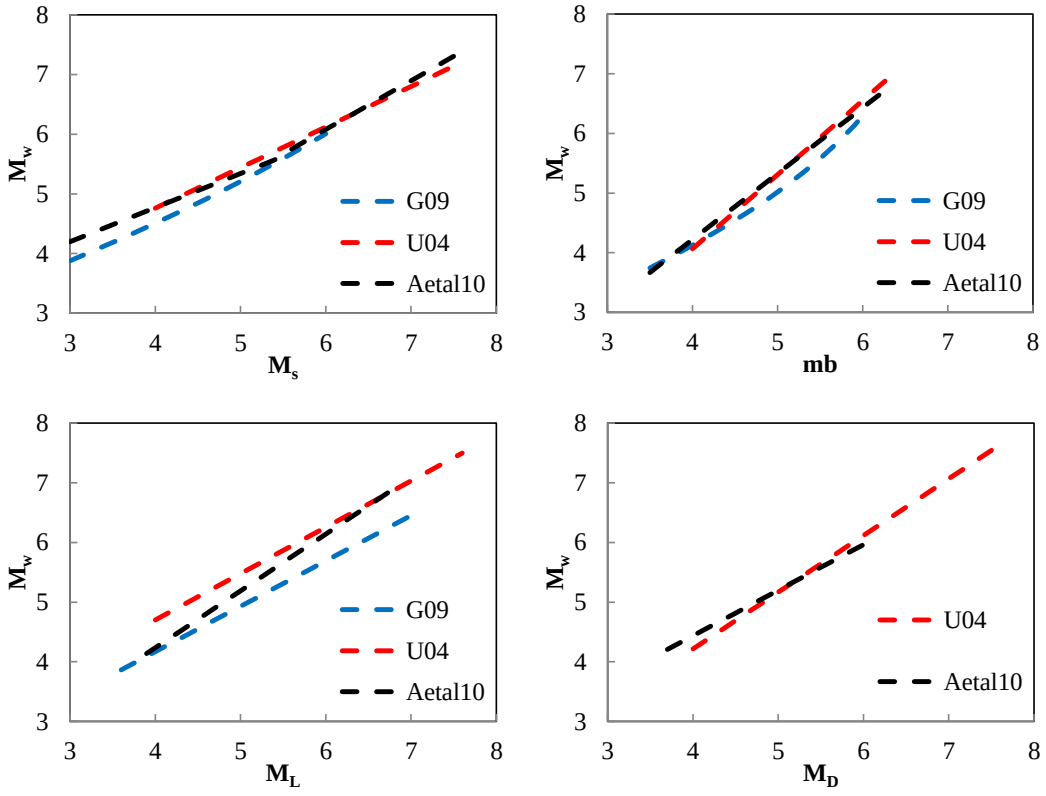


Figure 2.4 Comparison of empirical magnitude conversion relationships used for this study: G04: Grünthal et al. (2009); U04: Ulusay et al. (2004); Aetal10: Akkar et al. (2010); ZB02: Zare and Bard (2002)

### 2.3.2. Declustering and Completeness Analysis

Seismic activity of a region is investigated from historical and contemporary seismic event catalogs that are compiled from published reports, books or scientific articles and several seismological agencies. Figure 2.3 shows the distribution of events reported by the unified catalog compiled in this study from the earthquake catalogs of Kandilli Observatory and Earthquake Research Institute, KOERI, (*http://www.koeri.boun.edu.tr/*) and International Seismological Center, ISC, (*http://www.isc.ac.uk/*). The most reliable information on

earthquake magnitude, earthquake occurrence time and epicentral location should be selected for each event while compiling the catalog. The compiled catalog is used for interpreting and building earthquake occurrence models on the seismicity of sources (Section 2.3.3). For a more robust hazard analysis, it is assumed that occurrences of earthquakes are independent from each other. However, foreshocks and aftershocks definitely violate this assumption. Thus, before the computation of earthquake recurrence rates, the compiled catalog has to be examined and improved as the catalogs provided by seismic agencies (e.g., KOERI and ISC) contain a non-uniform composition of mainshock, foreshock and aftershock earthquakes along with duplicated earthquake entries. In the first step, duplicated and dependent events (i.e., aftershock and foreshock events) are removed and the seismic moments of the dependent events are added to the seismic moment of the main event to implicitly calculate the maximum moment release on a particular seismic source under a certain time interval. This process is called as declustering of the catalog and is computed by running the computer program ZMAP (Wyss et al., 2001a) in this study. The algorithm of Reasenberg (1985) is chosen during the declustering analysis. The Reasenberg algorithm links up aftershocks within an earthquake cluster: if event A triggers event B, and if event B triggers event C, then all of these events are considered to belong to one common cluster. Earthquakes occurring within a certain time and distance windows of the mainshock are considered as dependent events and are removed from the catalog. The intervals of time and distance windows are defined by the mainshock magnitude. The earthquakes occurring within the specified time and distance windows are associated to form clusters and each cluster is replaced by an equivalent earthquake that has a moment magnitude consistent with the sum of seismic moments in the cluster. To relate an aftershock to a mainshock requires defining the intervals of distance and time lag between the two. Thus, the look-ahead time for un-clustered events, the maximum look-ahead time for clustered events, the maximum error in epicenter coordinates and the maximum error in hypocenter depth must to be estimated. The determination of time and space closeness between the mainshock and its aftershock contains uncertainty that should be taken into account during the improvement of earthquake catalogs.

Once the consistency in magnitude scale is provided and dependent events are removed from the catalog, the catalog is assessed for its completeness. An earthquake catalogue is complete for magnitude $m_i$ within a specific time interval, if all events within magnitude $m_i$ that occurred during that period are available in the earthquake catalog. Estimation of the time interval in which the catalog is complete is often difficult and subjective. The most common method for estimating the completeness period is proposed by Stepp (1973). The completeness process consists of making plots of the cumulative number of events against time. The determination of the completeness interval is dependent on the particular time distribution of earthquakes for the considered seismic zone. Figure 2.5 represents the probable complete time intervals for smaller and larger magnitude ranges. The red and blue dashed arrows on the figure show the beginning of time periods for the completeness of considered magnitude ranges. The intervals in between the blue and red dashed arrows

depict the possible trends for the complete time interval for small magnitude events. The figure implies that, in particular, for small magnitude events, the determination of the complete time interval is rather uncertain. The uncertainty in determination of the completeness interval affects the statistical interpretations on regional seismicity.

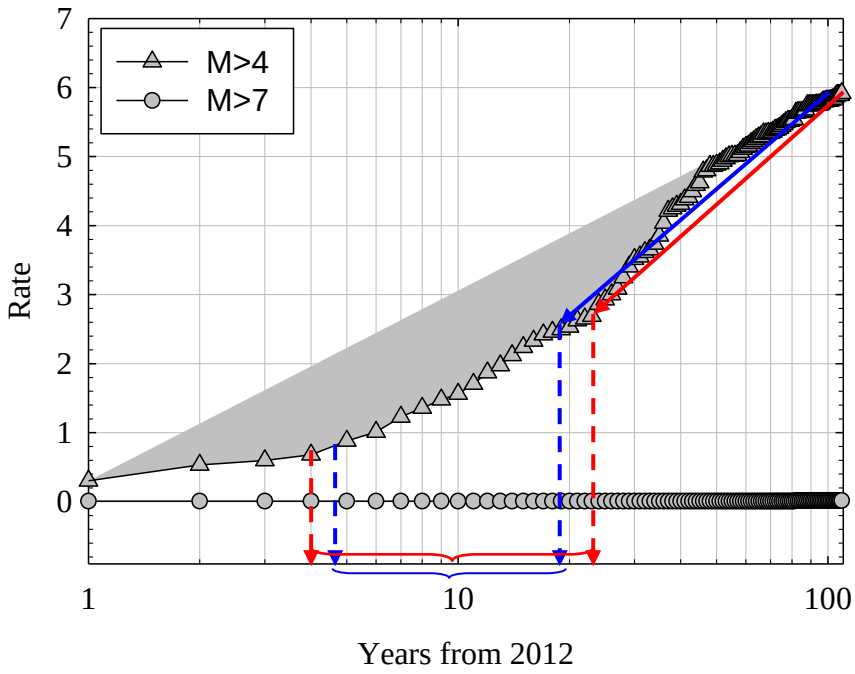


Figure 2.5 A representative figure that shows the complete time intervals for different magnitude ranges that are assessed from the declustered earthquake catalog compiled for this study (the city of Van and surroundings)

### 2.3.3. Establishing Probability Models for Earthquake Recurrence

The final step in representing earthquake occurrences is to express the frequency of each earthquake magnitude, namely the magnitude-recurrence relationship for a seismic source. The following section describes the frequently used relationships for this process.

#### 2.3.3.1. Frequency Distribution of Magnitudes

After defining source characteristics and the seismicity of the considered region, the frequency of earthquake occurrences on the source is expressed by the magnitude-recurrence models. The magnitude-recurrence models express the rate of events with magnitudes exceeding a threshold. The magnitude-recurrence relationship is basically defined by a magnitude distribution function given in Eq. (2.3)

$$n = \nu_{Mmin} \int_{m=M}^{Mmax} f_m(m)dm \tag{2.3}$$

The term $\nu_{Mmin}$ in Eq. (2.3) represents the rate of events exceeding $M_{min}$, and $f_m(m)$ denotes the magnitude density function.

Due to the randomness observed in the numbers of large, moderate and small magnitude earthquakes, probability density functions of magnitude are defined. Exponential (Gutenberg-Richer), truncated exponential and characteristic magnitude models are frequently used for the characterization of seismicity on a source. The exponential model is useful for simulating the magnitude recurrence on faulting zones and seismic belts. The characteristic model is more appropriate for characterizing individual faults which tend to produce earthquakes within a specific magnitude range (Youngs and Coppersmith, 1985). This study considers characteristic magnitude model in order to define seismic activity of fault sources. The characteristic earthquakes with magnitudes consistent with fault dimensions can occur only on mapped active faults. Since it is very difficult to separate low-magnitude events from the events originating from background sources (particularly due to the error in epicenter locations), all events with magnitudes less than the characteristic magnitude are considered as background events surrounding the faults. The background source seismicity is modeled by an exponential relationship.

Exponential model that is proposed by Gutenberg and Richter (1956) expresses the frequency of earthquakes by a logarithmic relation

$$log_{10}(n) = a + bM \tag{2.4}$$

where $a$ is the seismic activity rate and $b$ represents the likelihood of larger magnitudes in total activity. The logarithmic relationship can be reduced to a power relationship by the substitution of $\nu_{Mmin} = 10^a$ (activity term) and $\beta = b\ ln(10)$ in Eq. (2.4).

$$n = \nu_{Mmin} e^{-\beta(M - M_{min})} \tag{2.5}$$

The term, $n$ refers to the annual exceedance rate of magnitudes ($M$) above $M_{min}$. The minimum magnitude margin is generally defined by considering the limitations of earthquake catalogs and significance in hazard calculations.

The estimation of recurrence parameters $\nu_{Mmin}$ and β can be based on a maximum likelihood method, which is extended to the case of events grouped over unequal observational periods. β can be obtained by an iterative scheme (Weichert, 1980) using the following relationship

$$\frac{\sum_i t_i\ m_i\ exp(-\beta m_i)}{\sum_j t_j\ m_j\ exp(-\beta m_j)} = \frac{\sum_i \nu_i\ m_i}{n} = \overline{m} \tag{2.6}$$

The parameter $t_i$ in Eq. (2.6) refers to time intervals in which the catalog is complete for magnitude class $m_i$, parameter $\nu_i$ is the number of events in magnitude class $m_i$ and $n$ is the sum of $\nu_i$ .

Since each seismic source has the ability of generating a certain range of earthquakes in size, the data tend to truncate towards larger magnitudes. The data tend to truncate at maximum magnitude but the fitted line deviates from the observed magnitude value as seen in Figure 2.6. Thus, truncated exponential (or truncated Gutenberg-Richter) distribution model is proposed (Eq. (2.7)) that caps the annual frequency of earthquakes for a given maximum magnitude (McGuire, 2004). This way the magnitude frequencies can be determined by accounting for the physical limitations of the source. Figure 2.6 illustrates the observations of earthquake magnitudes along with exponential and truncated exponential magnitude recurrence models applied on the seismic activity around the city of Van. Black circles represent the actual variation of annual exceedance frequencies (rates), straight and dashed lines depict the exponential (Gutenberg-Richter) and truncated exponential magnitude-recurrence relationships, respectively.

$$f_m^{TE} = \frac{\beta \exp[-\beta(M-M_{min})]}{1-exp[-\beta(M_{max}-M_{min})]} \tag{2.7}$$

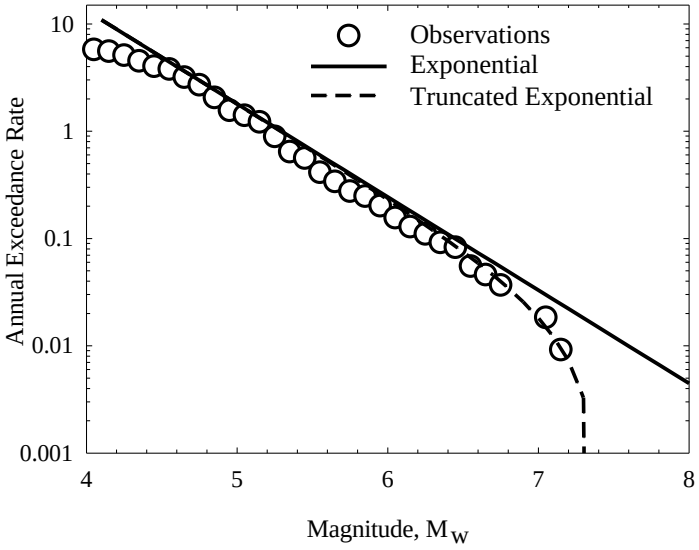


Figure 2.6 Application of Exponential (Guttenberg-Richter) and truncated exponential magnitude-recurrence relationship on the seismicity around the city of Van.

Characteristic model is developed by Schwartz and Coppersmith (1984) based on an assumption that the individual faults tend to produce earthquakes within a characteristic magnitude range. (Figure 2.7). The basic characteristic earthquake model suggests a

uniform distribution of characteristic earthquake magnitude, bounded by two limits. As the events on the background of a fault can be modeled by a truncated exponential model, a combination of truncated exponential and basic characteristic magnitude distribution functions is possible as shown on Figure 2.7.a (Youngs and Coppersmith, 1985). Instead of the basic characteristic model, the truncated normal distribution around a mean magnitude (Figure 2.7.b) is also suggested for modeling the characteristic earthquake magnitudes. The selection of magnitude distribution model may lead to uncertainty in hazard results and examined in Chapter 4 by using the city of Van case study.

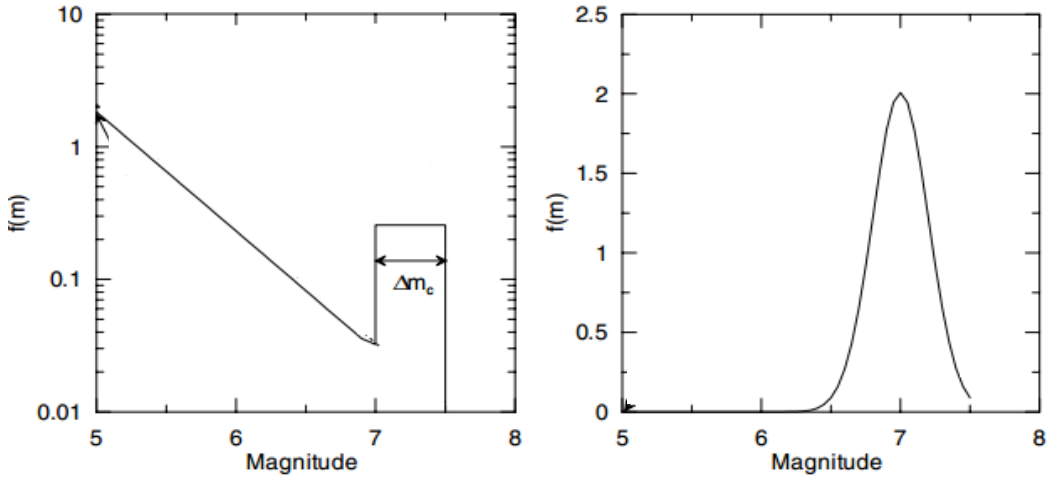


Figure 2.7 (a) The combined exponential and basic characteristic (uniform) magnitude density functions, (b) truncated normal characteristic magnitude density function (modified from Stewart et al, 2001).

### 2.3.3.2. Activity Rate

As described previously the frequency of earthquakes above a minimum magnitude is called as the activity rate $\nu_{Mmin}$. The seismological data (i.e., earthquake catalogs) and geologic information (i.e., slip-rate and maximum magnitude estimations) are useful data for the computation of $\nu_{Mmin}$ for truncated exponential magnitude-recurrence model of background seismicity and for characteristic magnitude-recurrence models of faults (Youngs and Coppersmith, 1985). It is necessary to build a declustered and unified-magnitude catalog of earthquakes before any statistical estimation of $\nu_{Mmin}$.

### 2.3.3.3. Probability Models of Earthquake Occurrences

Most probabilistic seismic hazard analyses are based on the assumption that the earthquake process is memoryless, that is, there is no memory of time, size and location of past events. If the mean number of particular rare events in a given time interval does not depend on

the history of those rare events, and if it is proportional to the length of the time interval, then the sequence of occurrence of rare events constitute a Poisson process. Thus, the occurrences of earthquakes with magnitudes greater than a target magnitude level, $M_t$, can be hypothetically considered as a Poisson process. For a Poisson process the probability of $x$ occurrences of an earthquake with a magnitude greater than $M_t$ in $t$ years is

$$P(x) = \frac{\nu(M>M_t)t^x}{x!} e^{-\nu(M>M_t)t} \tag{2.8}$$

where $\nu$ ($M>M_t$) represents the annual exceedance rate corresponding to $M_t$ in the recurrence model. Equation (2.10) is also known as the probability density function of a Poisson distribution. If no occurrence of events above $M_t$ is of interest, x will be equal to 0 and Eq. (2.8) will become

$$P(x = 0) = e^{-\nu(M>M_t)t} \tag{2.9}$$

In PSHA, the probability of at least one earthquake is of concern and it is computed by subtracting the probability of non-occurrence for $M>M_t$ from 1

$$P(M > M_t) = 1 - e^{-\nu(M>M_t)} \tag{2.10}$$

By taking the logarithm of both sides in Eq. (2.10) and writing it for $\nu$ ($M>M_t$), the modified form of Eq. (2.10) for the computation of annual rate of exceedance is

$$\nu(M > M_t) = -\frac{\ln(1-P(M>M_t))}{t} \tag{2.11}$$

A common way to represent dependency between earthquakes is to use renewal models. The renewal models put emphasis on the memory of past earthquakes. They are also known as time-dependent models and assume that the probability of a future earthquake increases with the elapsed time since the last earthquake. The consequences of this model are investigated to a limited extent and it is used occasionally in engineering practice and particularly in risk analysis (Cramer et al., 2000). There are two alternative forms of magnitude recurrence in renewal models. The first model is the slip-predictable model in which the time to the next earthquake is predicted from the slip in the previous earthquake provided that the fault slip rate is constant. The second one is time-predictable model that predicts the earthquake occurrence from the time since the previous earthquake regardless of earthquake magnitude (Thenhaus and Campbell, 2003). As one can infer from these discussions the renewal models require reliable information about the seismic moment accumulation (or stress and strain distribution) in the seismic sources. Such knowledge would yield consistent time-dependent earthquake recurrence modeling. Detailed

geological and geophysical information does not exist for the city of Van and surroundings and renewal model (or the uncertainty in renewal model) is not considered in the framework of this thesis.

The probability that a large earthquake occurs on a fault at time $\tau$ in the interval (T, T+$\Delta$T) is given by the probability density function $f_T(t)$

$$P(T \leq \tau \leq T + \Delta T) = \int_T^{T+\Delta T} f_T(t)dt \quad (2.12)$$

A lognormal probability density function is assumed for the recurrence time

$$f_T(t) = \frac{1}{t\sigma_{lnT}\sqrt{2}} \exp[-\frac{1}{2}\left(\frac{t/T^*}{\sigma_{lnT}}\right)^2] \quad (2.13)$$

The term $\sigma_{lnT}$ in Eq. (2.13) is the standard deviation of the logarithm of recurrence time and $T^*$ is the median recurrence time, which is related to the mean recurrence time ($T_m$) by the expression given in Eq. (2.14).

$$T^* = T_m \exp(\frac{1}{2}\sigma_{lnT}^2) \quad (2.14)$$

Other density functions, such as Weibull time predictable distribution, and Brownian passage time distribution are also suggested for modeling the recurrence time (Cornell and Winterstein, 1988).

## 2.4. Ground Motion Prediction Equations

Ground-motion prediction equations (GMPEs) or attenuation relationships are empirical equations derived to estimate ground-motion intensity parameters such as peak ground acceleration (PGA), peak ground velocity (PGV), and pseudo spectral acceleration (PSA) at different vibration periods. They describe the probability density function of ground motion conditioned on some important seismological parameters. The earthquake source properties are considered by magnitude and style-of-faulting whereas the wave propagation path effects are defined by source-to-site distance. The modification of waveform amplitudes are accounted by site response functions, which are sometimes simplified by dummy site classes. The general form of an attenuation relationship is expressed by

$$\ln(Y) = C + f(M) + f(R) + f(F) + f(S) + \varepsilon\sigma \quad (2.15)$$

The parameter Y in Eq. (2.15) represents the ground motion amplitude parameter, which is assumed to follow a lognormal distribution, the term C defines a constant that is determined by the regression analysis, the functions f(M), f(R), f(F) and f(S) describe the influence of magnitude, source-to-site distance, style-of-faulting and site response on the ground-motion intensity parameter, respectively. The inherent variability in ground motions is given by the standard deviation, $\sigma$ (sigma) and the number of standards deviation above or below the median estimation is defined by the term $\varepsilon$. When $\varepsilon = 0$, the ground-motion predictive model estimates the median ground motion.

The predictive models show differences in the median estimations of the ground motion due to the selection of functional form, regression techniques, and the differences in the definition of seismological parameters (Bommer et al., 2005). The quality of compiled strong-motion records (i.e., the strong-motion database) can also affect the estimations of model parameters (Strasser et al., 2009). The difference among the predictive models can lead to significant differences in median estimations. The standard deviation associated with each model also shows significant variations from one model to the other. This fact in turn affects the predicted ground motion towards the tails of the distribution as PSHA studies generally use $\pm 3\sigma$ (i.e., $\varepsilon = 3$) to account for the inherent ground-motion amplitude variability. The imperfections in the strong-motion database used in the derivation of GMPEs and the number of predictor variables in the functional forms of GMPEs can also affect the level of sigma (Akkar et al., 2012). Figure 2.8 shows the impact of sigma on the computed exceedance probabilities for PGA for a location selected from the city of Van. The hazard curves on this figure are calculated from the ground-motion predictive model of Akkar and Bommer (2010) by changing the sigma from 0.3 to 0.9 with increments of 0.1. As inferred from Figure 2.9 change in sigma implies significant variations in hazard levels that is discussed in Bommer and Abrahamson (2006) in detail. Hence, it is important to examine the effect of variability among different prediction equations on the results of PSHA. In this thesis, 13 candidate ground-motion prediction equations are selected while running the sensitivity analysis for the seismic hazard of the city of Van. Their important characteristics are given in Table 4.5. To emphasize the delicacy of GMPE variation in hazard results further Figure 2.9 (a) and (b) compare the median PGA estimations and the standard deviations of the equations listed in Table 2.1 for rock sites and for an earthquake magnitude of $M_w 7$. The style of faulting is chosen as normal fault.

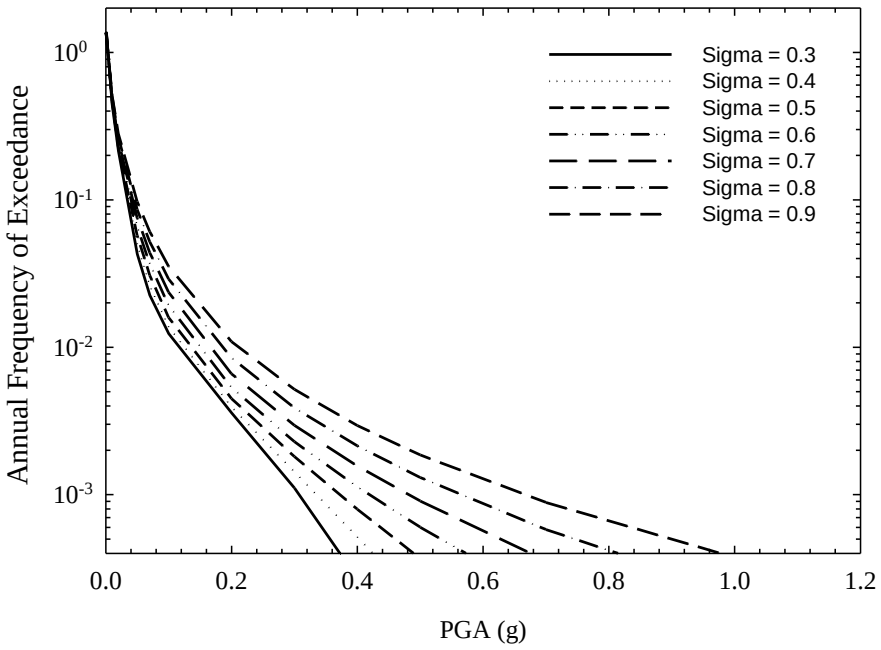


Figure 2.8 Effect of sigma (σ) on PSHA for a location in the city of Van.

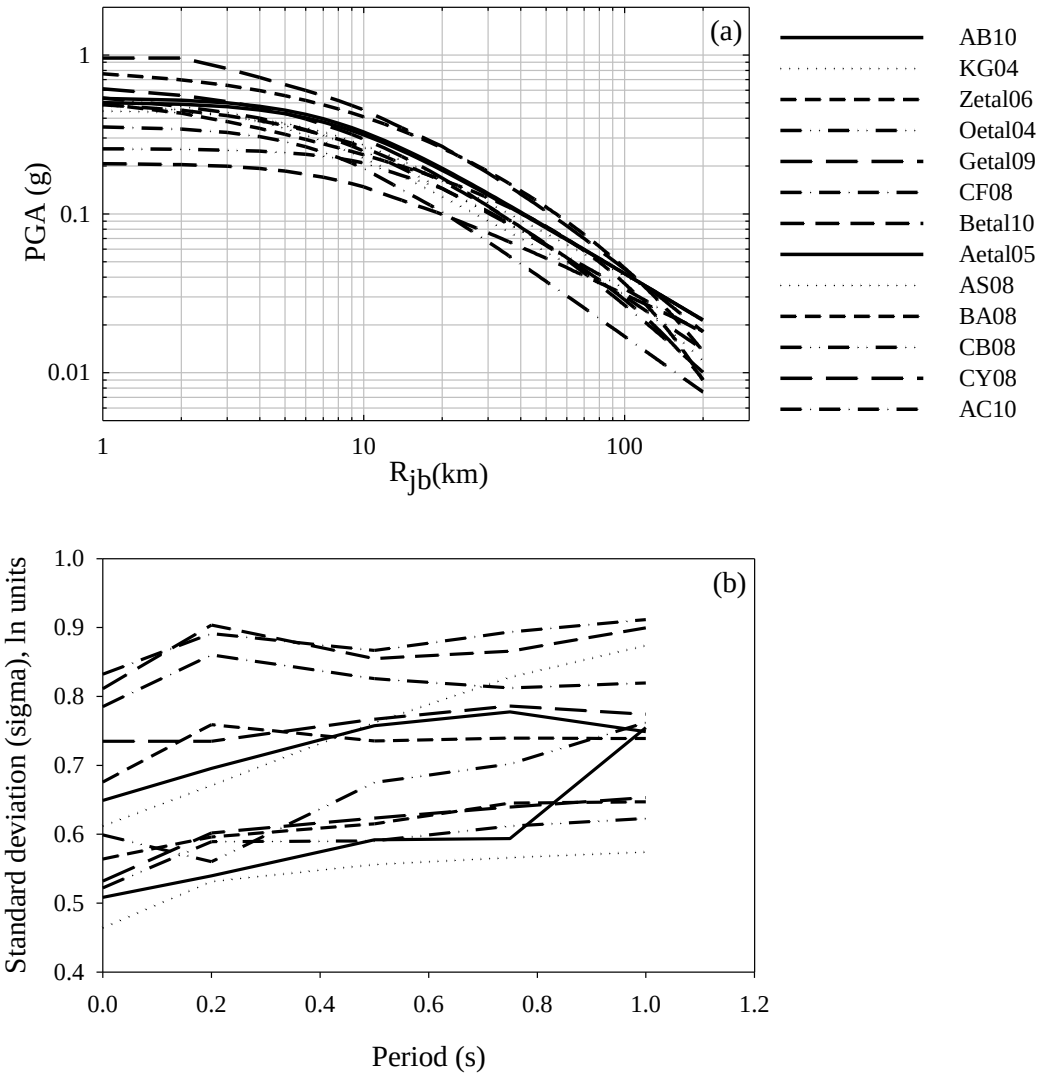


Figure 2.9 (a) Median PGA estimations and (b) period dependent standard deviation values of candidate ground-motion prediction equations (see Table 2.1 for the abbreviations given in the legend)

The idealizations imposed in the ground-motion predictive models result in differences between the observed and estimated ground-motion parameter. These differences are analyzed through residual analysis. A ground-motion predictive model that yields unbiased median estimations must have a residual scatter with zero mean. Assessment of unbiased estimations for GMPEs as well as their suitability in terms of tectonic activity is particularly important for the particular region or site where probabilistic hazard studies are conducted.

In order to justify the usability and applicability of the candidate ground-motion prediction equations (see Table 2.1) for the region of concern in this thesis, and to select the most appropriate set of ground motion prediction equations from candidate GMPEs, a methodology suggested by Kale and Akkar (2013) is applied. The method is called as Euclidian Distance Based Ranking (EDR).

The implementation of the method on the ranking of candidate GMPEs that are selected for this study and the interpretations of the results will be discussed in Chapter 4.

## 2.5. Mathematical Framework of PSHA

Once the seismic sources are characterized and the most appropriate GMPE(s) is (are) selected, probabilistic seismic hazard is computed. The probabilistic seismic hazard analysis (PSHA) accounts for all possible earthquake scenarios and ground motion probability levels that can occur on the seismic source(s) in the considered area. The basic methodology of PSHA considers how often a specified level of ground motion is exceeded at the site of interest. The resulting hazard consists of contributions from each independently defined source. The hazard equation that is introduced for the annual exceedance rate ($\gamma$) of the ground-motion intensity parameter Y, exceeding a threshold level y, from source j can be described by the following integral

$$\gamma_j(Y > y) = (\nu_{M,min})_j \int_{R_{min,j}}^{\infty} \int_{M_{min,j}}^{M_{max,j}} f_{M,j}(M) f_{R,j}(R) P\left(Y > y|_{M,R,SC,SoF}\right) dR dM \quad (2.19)$$

As described in the entire body of this chapter, the parameter $(\nu_{M,min})_j$ in Eq. (2.19) is the annual rate of earthquakes with magnitudes greater than or equal to $M_{min}$ for source j. The terms $f_{M,j}(M)$ and $f_{R,j}(R)$ define the probability density functions of magnitude recurrence and distance for source j, respectively. The concept of earthquake recurrence relationships for seismic sources is discussed in Section 2.3.3.1. The probability density function $f_{R,j}(R)$ considers the location uncertainty of events occurring on source j. The nucleation points of earthquake ruptures are generally assumed to be uniformly distributed on a seismic source. The term $P(Y>y|_{M,R,SC,SoF})$ is the conditional probability of the ground motion parameter Y exceeding a threshold level y conditioned on the given magnitude (M), distance (R), site class (SC) and faulting mechanism (SoF). The uncertainty involved in each probability density function and their likely contribution to total seismic hazard are emphasized in the previous sections of this chapter.

For multiple seismic sources, the total annual exceedance rate of a given ground motion exceeding a threshold y is determined by summing up the annual exceedance rates of all individual sources as shown in Eq. (2.20).

$$\gamma(Y > y) = \sum_j \gamma_j(Y > y) \quad (2.20)$$

## 2.6. Subjectivity in PSHA

Probabilistic seismic hazard analysis calculates the probability of exceeding a level of ground motion amplitude at a certain interval of time. The analysis requires identification of seismic sources and ground motion prediction models. There is no unique set of models that should be used in hazard analysis, because a significant level of uncertainty and variability is inherent in seismotectonic studies. Moreover the theoretical models are dependent on a number of assumptions. Selection and implementation of these models is generally made among a number of alternative choices, such that an expert's justification becomes crucial. Following the selection of source and ground-motion prediction models, the determination of model parameters also involves statistical uncertainty.

There are two main types of uncertainty in PSHA that are tried to be described by means of PSHA components in the previous sections. These are called as aleatory variability and epistemic uncertainty (SSHAC, 1997). Aleatory variability incorporates the inherent uncertainty due to natural randomness in a process. Epistemic uncertainty can be described as the scientific uncertainty in the model of the process which is associated with the choice of particular models or model parameters. It is due to the limited knowledge and the data.

Aleatory variability is accounted for directly in PSHA by means of a mathematical integration. Specification of standard deviation (σ) of a ground motion prediction relationship, earthquake magnitude given the rupture area and the location of the rupture given earthquake magnitude are a few sources of aleatory variability.

However, epistemic uncertainty is included in PSHA by explicitly including alternative models and parameters. Incomplete knowledge in predictive equations that are selected for the site under consideration, maximum earthquake magnitude, and the alternative probability distribution models accounting for earthquake recurrence, earthquake source delineation, the alternative procedures for earthquake catalog compilation, and the long term slip rate can constitute the major part of the epistemic uncertainty. The effect of epistemic uncertainty on PSHA can be investigated by considering construction of a logic-tree for alternative models and possible set of parameters (Figure 2.10). A subjective weight, justified whenever possible, is assigned to each branch of logic tree, depicting a particular set of models and their parameters. A ranking method, through sensitivity analysis, used for justification of weights is presented in Chapter 3. Consequently, the effect of epistemic uncertainty on PSHA is further examined in Chapter 4 by computing the probabilistic seismic hazard assessment of the city of Van.

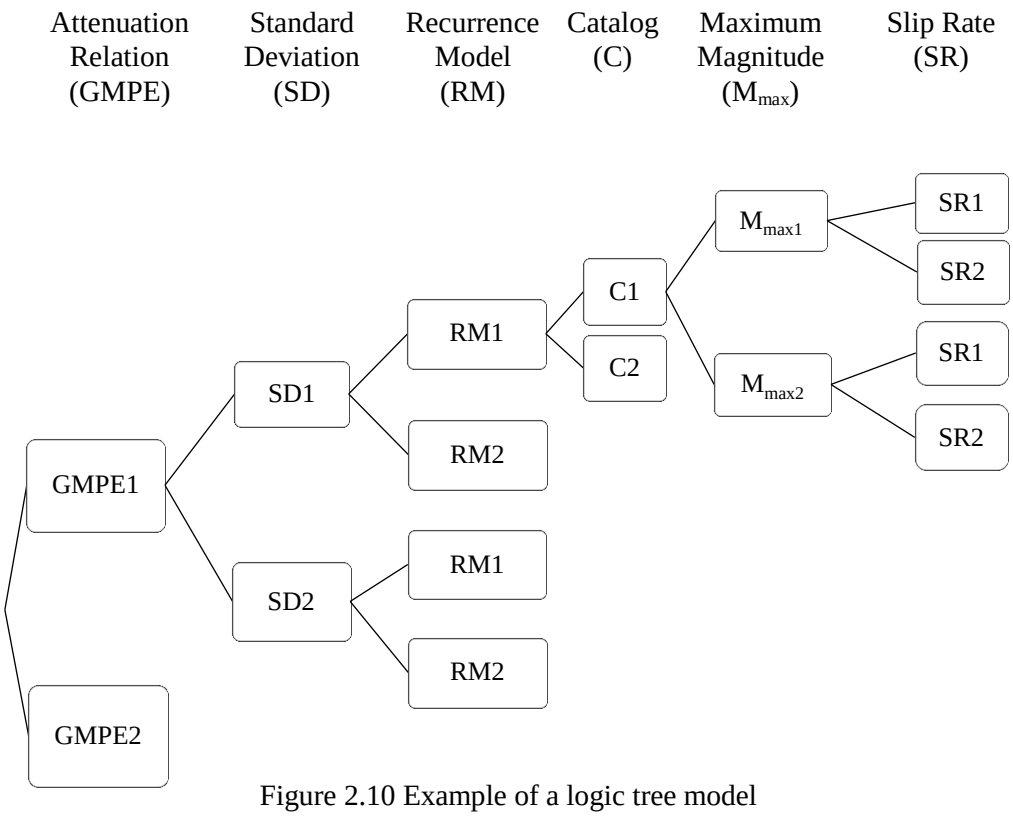


Figure 2.10 Example of a logic tree model

# CHAPTER 3

# SENSITIVITY ANALYSIS

## 3.1 General

The most significant parameters contributing to probabilistic seismic hazard assessment are discussed in the previous chapter to emphasize the importance of reliable seismic source characterization and ground-motion amplitude estimation. The uncertainties in the source parameters and ground motions require examination of their specific effects on PSHA results. To this end, the sensitivity analysis in PSHA helps the hazard expert to come up with the most viable set up to account for these modeling deficiencies. A prominent product of sensitivity analysis is a properly built logic-tree to consider different options in source and ground-motion models used in the analysis. The sensitivity analysis for probabilistic seismic hazard assessment can be done in various ways. One rigorous approach is to use probability distributions for unknown parameters. The probability distributions established in this way can be used by a sampling technique (e.g., Monte Carlo) to mimic a range of values that can be attained by these unknown parameters. Studies by Rhoades (1997), Moss and Kiureghian (2006), Moss (2009) and Kiureghian and Ditlevsen (2009) implement sampling techniques (such as Monte Carlo) to emphasize the modeling uncertainty in the particular components (e.g., GMPEs) of PSHA. The excessive computer time and difficulty in assessing the consistency of probability distribution of each uncertain parameter are the particular difficulties of such methods. Another approach for running sensitivity analysis is the use of limited number of values for representing the uncertainty in each seismic input parameter. PSHA is run simultaneously for these preselected values to assess the overall role of each uncertain parameter in PSHA outputs. These methods are more feasible in terms of computational burden. The sensitivity analysis that will be used in this study falls into this group. The seismic hazard of Van and surroundings is chosen as the specific case study to assess the efficiency of the chosen sensitivity method. The implemented sensitivity method not only focuses on the individual effects of each seismic input parameter but also portrays the interaction between them.

The following section of Chapter 3 examines the commonly used methods in the literature that describes the sensitivity of PSHA to the model parameters. The latter sections give information about the method for sensitivity analysis.

## 3.2 Proposed Sensitivity Methods in the Literature

Sensitivity analyses have been widely used in PSHA mainly because of the uncertainties in modeling parameters. Various approaches for sensitivity analyses are presented by McGuire and Shedlock (1981), Atkinson and Charlwood (1983), Rabinowitz and Steinberg (1991), and Grünthal and Wahlström (2008). Among these, the first two studies analyze the influence of each parameter by modifying one variable at a time and keeping the others as constants. Grünthal and Wahlström (2008) examine the sensitivity of each parameter by employing a logic-tree built on alternative parameter sets. The method proposed by Rabinowitz and Steinberg (1991) uses a multi-level approach to assess the significance of each parameter. A brief summary of each method is given in the following paragraphs.

The method described in McGuire and Shedlock (1981) examines the statistical uncertainty in the model parameters. Their method investigates the parameter sensitivities using point-source models built for the seismic hazard analyses of San Francisco, Bay Area. The point-source models lead to a coefficient of variation (COV) in the analysis results due to the uncertainty in the depth of energy release, in the activity rate, in Richter's *b* value and in the ground-motion prediction equation. The accuracy of the seismic models and their parameters is examined by comparing COVs obtained from multiple seismic hazard analyses. The basic assumption in the method of McGuire and Shedlock (1981) is that the uncertainties of different parameters are independent from each other. In other words, the method can be suitable if model parameters are estimated from the consideration of different datasets.

Atkinson and Charlwood (1983) conducted sensitivity analyses that are based on a method similar to that of McGuire and Shedlock (1981). Their study is focused on the PSHA of Vancouver, British Colombia, Canada. They observed that uncertainty in the source characterization parameters (i.e., upper magnitude limit and magnitude-recurrence parameters) employed for the seismic source models and for the ground motion predictions has a pronounced effect on PSHA results.

Grünthal and Wahlström (2008) investigated the sensitivity of each model parameter used in PSHA by considering a logic-tree approach. The logic-tree included different seismic source models, magnitude sets and ground-motion prediction equations. The sensitivity of PSHA results to parameter variability is assessed by using the hazard curves of PGA. The combined effect of model parameters that are shown as the branches of the logic-tree is expressed by the product $A \cdot M^s \cdot B^s \cdot H^s$. In this relationship A is the number of alternative

ground-motion prediction equations, M is the number of alternative maximum magnitudes, B is the number of alternative magnitude-recurrence parameter, H is the number of alternative hypocentral depths, and S is the number of seismic sources. In their sensitivity analysis, Grünthal and Wahlström (2008) assumed that M, B and H are statistically independent whereas they considered a dependency between M, B and S and assumed S = 1.0. While their assumptions are elucidating the effects of each model parameter on the computed hazard, it fails to examine the interactions between the parameters, and the coupled effects of parameters on the hazard results.

The method proposed by Rabinowitz and Steinberg (1991) considers the effect of model parameters and their interactions as well. Thus, the procedure gives a broader view about the significance of each parameter on PSHA. For this particular reason, their method is employed in this study in order to emphasize the importance of modeling parameters on PSHA. Details of the method are described in the following section.

## 3.3 The method of Rabinowitz and Steinberg (1991)

Rabinowitz and Steinberg (1991) proposed a multi-parameter approach for sensitivity analysis. The method examines whether the significance of a parameter depends on another parameter. A regular sensitivity analysis is not capable to determine such a link between two parameters. Specific to the probabilistic seismic hazard of Jerusalem, it is shown that there are different levels of interaction between seismic parameters contributing to hazard integral that can affect the final results. The method can be applied either in terms of annual exceedance rates for a given threshold level of a ground-motion parameter, or in terms of a ground-motion parameter of any given exceedance rate. The latter alternative is implemented in this study.

The idea behind the method, which is first developed by Fisher (1926), is based on the statistical theory of factorial design. The application of the method is easy and effective when the variability of several parameters is considered in the sensitivity analyses (Rabinowitz and Steinberg, 1991). The basics of this statistical theory are given in the following subsections.

### 3.3.1 Multi-Parameter Sensitivity

The theoretical basis of a multi-parameter approach in sensitivity analysis can be established efficiently using factorial designs. A general factorial design is done by selecting a fixed number of levels for each variable (or parameter) of concern. All possible combinations between the levels are then considered in the sensitivity analysis. If $l_i$ denotes the number of levels for the $i^{th}$ variable and k is the number of variables, the total number of combinations will be given by the product $l_1 \times l_2 \times l_3 \times \ldots \times l_k$ in factorial design. For

example, if there are three variables (k = 3) and the first variable has 2 levels ($l_1$ = 2) whereas the second and third variables have 3 and 4 levels ($l_2$ = 3 and $l_2$ = 4) respectively, then a 2×3×4 factorial design requires combinations of 24 parameter sets in the sensitivity analysis (Box et al., 1978). If two levels are considered for each variable, $2^k$ combinations should be generated. In this study, each variable (i.e., model parameter) is set to two possible alternatives: up and low levels. The up and low levels can be either quantitative or qualitative. For instance, the magnitude recurrence for faults can be either truncated normal or pure characteristic. If the parameter is a continuous variable, like maximum magnitude, the associated up and low levels can attain values slightly above or below the mean maximum magnitude computed from empirical equations (see details in Chapter 4). Setting one standard deviation above and below the mean value would be preferable if the uncertainty in parameter estimation is described by a symmetric probability distribution. Otherwise, it would be better to transform the parameter to obtain an almost symmetric distribution (Rabinowitz and Steinberg, 1991). Considering all possible combinations, the effects of selected parameters on the final hazard results and the interactions among them are obtained. Figure 3.1 shows the geometric representation of this sensitivity analysis. The main effects (effect of each individual parameter) can be viewed as a contrast between observations on the parallel faces of the cube (Figure 3.1 (a)). The two-factor interactions can be viewed as a contrast between the results on two diagonal planes (Figure 3.1 (b)).

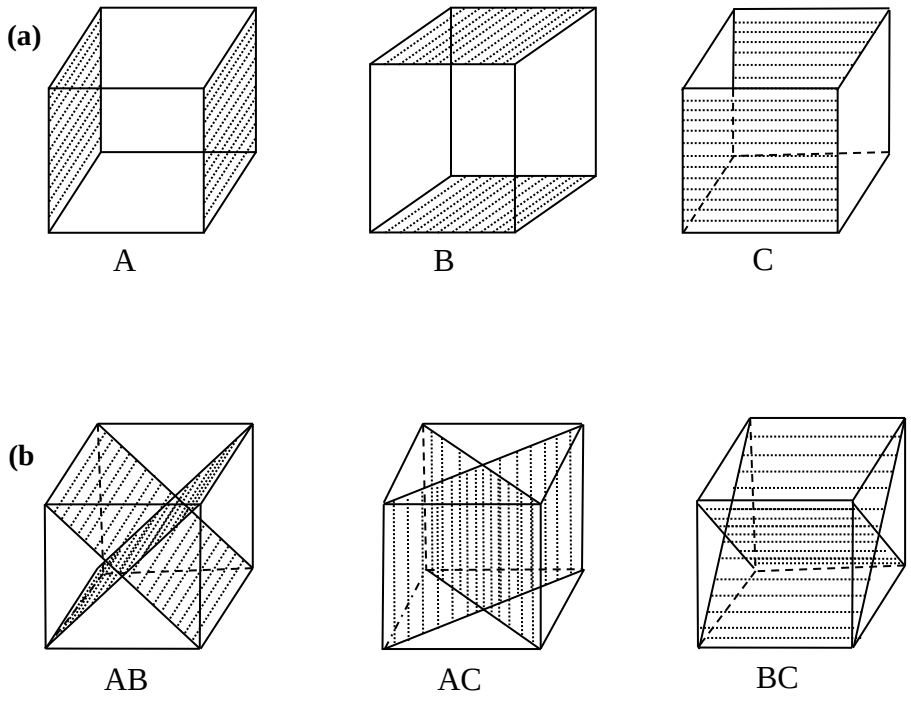


Figure 3.1 Geometric representation of the presented sensitivity methodology: (a) main effects (b) two-factor interactions (modified from Box et al., 1978)

### 3.3.2 Calculation Algorithm of Multi-Parameter Sensitivity Analysis

Hereafter the two levels of a variable that are defined as “up level” and “low level” will also be denoted as “+” and ”–“, respectively. The effect of each parameter considered in PSHA and the interaction between parameters are investigated by employing a two-level factorial design. The effect of a parameter is identified by a change in the PSHA results while varying that parameter from its low level to its up level. That is explained further in Table 3.1 by illustrating the possible combinations of dummy parameters A, B, and C, and the total number of PSHA runs necessary for identifying the main effects and two-factor interactions.

Table 3.1. $2^3$ combinations of 3 dummy parameters A, B and C

| Analysis # | A | B | C |
|---|---|---|---|
| 1 | - | - | - |
| 2 | + | - | - |
| 3 | - | + | - |
| 4 | + | + | - |
| 5 | - | - | + |
| 6 | + | - | + |
| 7 | - | + | + |
| 8 | + | + | + |

The average effect of the parameter A can be expressed as

$$A = \bar{Y}(A+) - \bar{Y}(A-) \tag{3.1}$$

The terms $\bar{Y}$(A+) and $\bar{Y}$(A-) represent the average acceleration values computed from all possible combinations when parameter A is at up and low levels, respectively. Thus, the effect of A on PSHA results is the difference between the average accelerations of all combinations when A is at up and low levels. The effects of A when B is either up (A(B+)) or low (A(B-)) are described by Eqs. (3.2) and (3.3), respectively.

$$A(B+) = \bar{Y}(A+, B+) - \bar{Y}(A-, B+) \tag{3.2}$$

$$A(B-) = \bar{Y}(A+, B-) - \bar{Y}(A-, B-) \tag{3.3}$$

Equations (3.2) and (3.3) indicate that the PSHA results should be considered in two parts according to the level of A (i.e., when A is at up and low levels). Each set should then be considered separately according to the up and low levels attained by B.

It should be noted that if the effects of A and B are independent, A(B+) will be equal to A(B-). Otherwise, there is an interaction between the parameters A and B. The interaction between A and B should consider the intersections of the cases when the parameters A and B are at the same levels (i.e., $\bar{Y}$(A=B)) and at the opposite levels (i.e., $\bar{Y}$(A≠B)). This is expressed mathematically in Eq. (3.4).

$$AB = \bar{Y}(A = B) - \bar{Y}(A \neq B) \tag{3.4}$$

The average effect of parameter A can also be calculated by Eq. (3.5) that considers the up and low levels of B. Moreover, the interaction between A and B can be expressed as in Eqs. (3.6) and (3.7) by considering the differences of the average effects of A when B is either up and low or the average effects of B when A is either up and low. Note that Eqs. (3.6) and (3.7) will not attain the same values unless the interaction is symmetric (i.e., AB = BA). The expressions that are given in Eqs. (3.1) to (3.4) lead to the derivations of Eqs. (3.5) to (3.7). These equations are given below.

$$A = [A(B+) + A(B-)]/2 \tag{3.5}$$
$$AB = [A(B+) - A(B-)]/2 \tag{3.6}$$
$$BA = [B(A+) - B(A-)]/2 \tag{3.7}$$

The above concepts are illustrated graphically in Figure 3.2 that shows the components that are used to compute the interaction between parameters A and B. The figure is plotted for a ground-motion intensity (e.g., PGA or spectral ordinates) with a predetermined return period (e.g., $T_R$ = 475 years) and separately describes the interaction between A and B for up and low levels of A. The combination of the plots essentially yields the interaction between A and B for the given ground-motion intensity at the designated return period. This is described in detail in the following paragraph.

The left-end points on Figure 3.2 indicate the average accelerations computed from the combination sets when B is at low level and A is up ($\bar{Y}(A+, B-)$; upper left point) and low ($\bar{Y}(A-, B-)$; lower left point). In a similar manner, the right-end points show the average accelerations for up level of B when A is at up ($\bar{Y}(A+, B+)$; upper right point) and at low levels ($\bar{Y}(A-, B+)$; lower right point). Note that the sum of left-end points defines the effect of A when B is low (A(B-); Eq. (3.3)). The sum of right-end points shows the effect of A when B is up (A(B-); Eq. (3.2)). The difference between these two terms (i.e., A(B+) and A(B-)) will yield the interaction between A and B (Eq. (3.6)). If the variation among the up levels of A when B is up and low is assumed to be linear, one would obtain the thicker black curve (designated as A+) on Figure 3.2. The thinner black curve (designated as A-) on Figure 3.2 is plotted by assuming a linear variation among the low levels of A when B attains up and low levels. If these two curves are parallel to each other, the up and low level variations of A are independent of the values attained by B.

This means that there is no interaction between A and B and eventually Eq. (3.6) will yield zero. This point is already highlighted in the previous paragraphs.

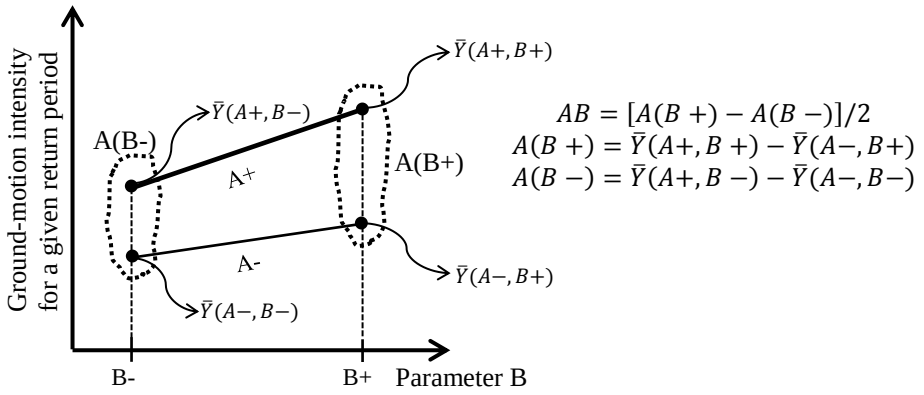


**Figure 3.2** An illustration that shows the elements that are used while computing the interaction between A and B by the factorial design approach. The equations on the right hand side are used in the computations and are already given in the text.

The effects A(B+) and A(B-) can also be calculated by

$$A(B+) = A + AB; \qquad A(B-) = A - AB \tag{3.8}$$

Equation (3.8) can be extended to the cases where there are more than two parameters. For instance, if the analyst seeks for the interaction of parameter A with parameters B and C, then

$$A(B+,C-) = A + AB - AC \tag{3.9}$$

Equation (3.9) defines the effect of parameter A on the hazard result when parameters B and C are at their up and low levels, respectively. The decision on adding or subtracting the interactions depends on the level of parameters. The specific case presented in Eq. (3.9) indicates that if the main effect of A is positive, and the interactions AB and AC attain positive and negative values, respectively, then setting the parameter B at its up level and C at its low level would increase the effect of A on the response. Alternatively, setting the parameter B at its low level and C at its up level would reduce the effect of the parameter A. Note that if the interactions are significant, consideration of B and C at low and up levels may yield to an opposite effect on the PSHA result when the level of A is switched from low to up. A specific example to that case is presented in Chapter 4 while describing the PSHA study of the city of Van.

### 3.3.3 Use of Multi-parameter Approach in Probabilistic Seismic Hazard Assessment

Since there are various assumptions regarding the model input parameters used in PSHA, the multi-parameter approach can be used to examine the sensitivity of hazard results to model parameters. The parameters are set to their up and low levels in PSHA runs while assessing their influence. The probabilistic seismic hazard is computed for all sets of combinations for the considered up and low levels. The hazard results that are expressed either as annual exceedance rates for a given ground-motion intensity level or ground-motion intensity for a predetermined annual exceedance rate are compared in order to understand the significance of interaction between the parameters. Consequently, the most critical parameters whose uncertainties have pronounced effects on PSHA can be assessed by sorting the annual exceedance rates or ground-motion intensities. Since the steps followed by this procedure yields quantitative results about the significance of each model parameter of concern, a logic-tree can be built for an efficient modeling of uncertainty in parameters. This way the cost of analysis is optimized by avoiding any preposterous discussion on the parameters that have very limited effects on PSHA.

The presented study focuses on the uncertainty of 6 parameters: the choice of ground-motion prediction equation, the standard deviation of ground-motion prediction equation (aleatory variability), the choice of magnitude-recurrence model, earthquake catalog completeness, maximum magnitude, and slip rate on active fault. These parameters are presumed to have the most pronounced effects on the PSHA results. The up and low levels of these parameters as well as their effects on the PSHA results of the city of Van are presented thoroughly in Chapter 4.

# CHAPTER 4

# MULTI-PARAMETER SENSITIVITY ANALYSIS FOR THE PROBABILISTIC SEISMIC HAZARD ASSESSMENT OF THE CITY OF VAN

## 4.1 General

This chapter describes the results of sensitivity analyses conducted for the probabilistic seismic hazard assessment of the city of Van. The calculations for the location with coordinates 38.50$^{o}$N and 43.40$^{o}$E are assumed to be representative of the probabilistic hazard to Van city. In the following, the seismotectonics and seismicity of Eastern Anatolia are presented by putting particular emphasis on the seismic sources surrounding the calculation location. Since particular emphasis is put on the effect of parameter uncertainty on seismic hazard, one close and one far active fault is considered for a simplified analysis. The activities of those sources are verified by earthquake records, and are supposed to represent the most significant characteristics of neotectonic frame around the calculation location. The background seismic sources, reflecting the low-magnitude activity on minor tectonic structures, are also simply modeled. Considering the complexity of tectonic frame in Eastern Anatolia, and the experience gained by 2011 Van earthquake, it is likely that other significant active faults of the region will be reported in literature. Then, the ranges of parameters considered in sensitivity analyses are presented. The chapter concludes with the observations made on the results of sensitivity analyses. The probabilistic seismic hazard is numerically computed by using EZ-FRISK software (Risk Engineering, 2011).

## 4.2 General Seismotectonic Features of Eastern Anatolia

Turkey is a seismically active country that has suffered from a significant number of destructive earthquakes. Turkey's seismotectonic structure is formed by the interaction

between Arabian, African, and Eurasian plates (Reilingier et al., 2006). Majority of Turkey constitute the geographic region known as Anatolia, also historically named as Asia Minor, which roughly extends from Asian borders of Turkey on the east to her shoreline on the west. The interactions between plates result in four major active fault systems on Anatolia: North Anatolian fault (NAF) zone, Aegean Graben system, Eastern Anatolian fault (EAF) zone and Bitlis-Zagros thrust belt. These major fault systems are illustrated in Figure 4.1. Figure 4.1 implies that northward motion of the Arabian plate relative to the Eurasian plate causes lateral escape of Anatolian subplate (or, block) to the west and Eastern Anatolia the east (McKenzie, 1972).

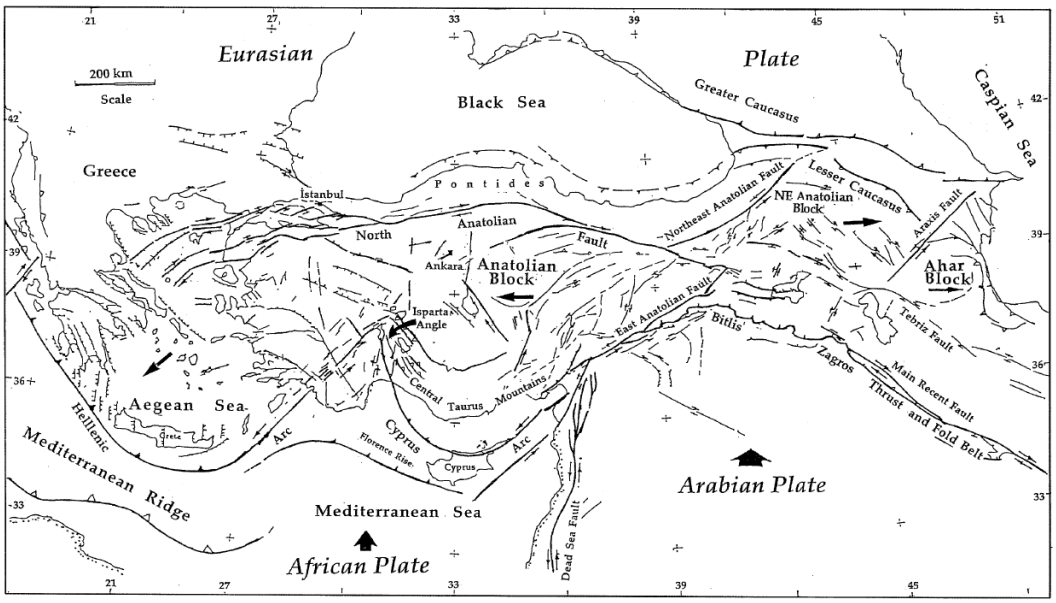


Figure 4.1 Major tectonic elements of Turkey (Barka and Reilinger (1997))

The North Anatolian and East Anatolian fault zones constitute the northern and southern boundaries of moving Anatolian plate. NAF is a 1500 km long seismically active right-lateral strike-slip fault that takes up the relative motion between Anatolian and Eurasian plate on the north. This fault zone extends from the triple junction (between Anatolian subplate, Euroasian plate, and Arabian plate) on Karlıova to the mainland Greece (Barka and Kadinsky-Cade, 1988). The converging motion of Arabian plate and Euroasia formed the Bitlis thrust zone, and the highlands on Eastern Anatolia. Similar to NAF and Bitlis thrust zones, the relative motion between Arabian plate and Anatolian subplate is accommodated by the 550 km long East Anatolian fault zone. This fault zone extends from Karlıova triple junction to the Mediterranean coast. East Anatolian fault zone is characterized by a series of major discontinues (i.e., stepovers and bends). The East Anatolian Fault Zone extends from Karlıova triple junction in the northeast to the Maraş triple junction in the southwest where it intersects the Dead Sea Fault. The age of the East

Anatolian Fault is still a debating issue. For instance, Şengör et al., (1985), Dewey et al. (1986), Arpat et al., (1976) place its formation in the Late Miocene-Early Pliocene. Şaroğlu et al. (1992), and Westaway and Arger (1996) argue that the East Anatolian fault is Late Pliocene. The total left-lateral displacement along this fault is in the range from 3.5 to 13 km according to Arpat and Şaroğlu (1972) whereas it is in the range from 15 to 27 km according to Emre et al., (2011). Those discrepancies depict a considerable level of uncertainty in slip-rate estimates even for major tectonic structures on the region of interest. The uncertainty in the slip rate introduces uncertainty in probabilistic seismic hazard, because of their relationship with the frequency of large earthquake magnitudes.

According to McKenzie (1972), the drift of the Arabian plate towards Eurasian plate results in a collision in the vicinity of Lake Van. The Eastern Anatolia was previously under a shallow sea. The collision of Arabian and Eurasian plates in Early Miocene began uplifting the region. In the late Miocene, the uplifting reached to a certain level and shortening of East Anatolia has been initiated. Consequently, the contraction yielded to formation of highlands, volcanic activity, and significant faulting. The lavas resulting from volcanic activity covered the region during this period. The Lake Van was formed when the lavas of the Nemrut volcano blocked the outward drainage of water in the Muş basin (Barka and Saroğlu, 1995). Although the thrust faulting could be prominent in the early stages of plate-shortening on East Anatolia, the characteristics of escape tectonics are more prominent in the region today. That is possibly due to advance of NAF towards Iran and South Caucasus, which ended the lithospheric shortening and crust thickening on East Anatolia. Hence, the present-day relative motion of East Anatolia is towards Caucasus on the east. (Barka and Reilinger, 1997; Örgülü et al., 2003; Copley and Jackson, 2006; Reilinger et al., 2006). Consequently, the complex neotectonic structure in Eastern Anatolia involves NE-SW trending sinistral fault zones, such as Horasan-Narman fault zone, NW-SE trending dextral fault zones, such as Çaldıran-Tutak fault zone, and EW trending thrusts, such as Muş-Van thrust (Barka and Reilingier, 1997). The Horasan-Narman and Çaldıran-Tutak fault zones are respectively 110 and 50 km long. Djamour et al., (2011) proposed that the Çaldıran fault lies in the same direction with Tutak fault, and they can be considered as a single fault (i.e., Çaldıran-Tutak Fault).

The recent 23 October ($M_w$ 7.2) 2011 and 9 November ($M_w$ 5.6) 2011 Van earthquakes that occurred in the eastern part of the Lake Van shook the surrounding area and caused more than 600 casualties along with 2000 injured people (METU, EERC 2011). These earthquakes caused significant damage in the cities of Van and Erciş that are located along the north coast of the lake. The epicenter of the 23 October 2011 Van earthquake ($M_w$ 7.2) is located about 25 km to Northeast of Van city. The epicenter of the latter earthquake ($M_w$ 5.6) is approximately 18 km to Southeast of Van city. The epicentral locations of the Van earthquakes determined by various seismological agencies are given in Tables 4.2 and 4.3. These tables imply that the seismological parameters of the Van earthquakes determined by different seismological agencies show significant variability. The variability in

reported parameters can be more significant for lower magnitude events of the region. Hence, the earthquake catalogs for the region may involve a level of uncertainty in information, which may eventually yield a certain level of uncertainty in PSHA.

The source mechanism solutions of the 23 October 2011 earthquake indicate a thrust faulting system. The main fault surface ruptured during this earthquake did not emerge at the surface. However, the thrust fault formed a 10 km wide deformation zone where 1-3 km long reverse fault segments striking N50$^o$-70$^o$ and dipping ~50$^o$ NW were observed (Özkaymak 2003; Özkaymak et al., 2004). Thus, the Van fault has been mapped as two segments as seen in Figure 4.4. On the other hand, the source mechanism of the 9 November 2011 earthquake shows a rupture on an unmapped strike-slip fault (METU/EERC 2012-2). The latter earthquake can be considered as an event on background seismicity, and depicts the relatively complex tectonic structure on the region.

Historical and instrumental seismicity also prove that Eastern Anatolia is a seismically very active region. The epicenter distributions of regional earthquakes in the instrumental period which are located between the longitudes of 37$^o$-40$^o$ and the latitudes of 41$^o$-45$^o$ are shown in Figure 2.3. The major instrumental-period earthquakes and major faults that generated some of these earthquakes were compiled and reproduced from the study of Barka and Reilinger (1997) and are displayed on Figure 4.2. Table 4.1 lists the major instrumental and historical period earthquakes occurred in the Eastern Anatolian region together with their magnitude, intensity and epicentral coordinates. The 1976 Çaldıran-Muradiye ($M_s$ 7.5), 1966 Varto ($M_s$ 6.8), 1983 Horasan-Narman ($M_s$ 6.8) earthquakes and the recently occurred 2011 Van ($M_w$ 7.2) earthquake are the examples of large events in this region. In the region, most large earthquakes in the last century have occurred on strike-slip faults (Toksöz et al., 1977).

One of the largest earthquakes that occurred in the area of interest is the 1976 Çaldıran (Muradiye) earthquake (Table 4.1). The epicenter of the Çaldıran (Muradiye) earthquake is in the province of Van. The surface-wave magnitude of the event is reported as $M_s$ 7.5 (KOERI, www.koeri.boun.edu.tr) whereas its body-wave magnitude is given as $m_b$ 6.3 (www.isc.ac.uk). The corresponding moment magnitude values are $M_w$ 7.3 (for $M_s$ 7.5) and $M_w$ 6.8 (for $m_b$ 6.3) according to the empirical magnitude conversion relationships proposed in Akkar et al. (2010). It is noted that Kandilli Observatory and Earthquake Research Institute (KOERI) reports a moment magnitude value of $M_w$ 6.3. This magnitude value is disregarded in this study while defining the uncertainty in maximum magnitude as it conflicts with the level of surface-wave magnitude reported by the same institute. It is not expected to have moment magnitude values smaller than the surface-wave magnitudes. The fault rupture was about 55 km and it is mapped on Figure 4.3. The motion was purely right-lateral strike-slip and the observed dip was nearly 90$^o$ (Toksöz et al., 1978). 1903 Malazgirt (Muş) earthquake is another major earthquake of East Anatolia with an epicenter close to Van.

The seismicity and the faulting mechanisms of large earthquakes indicate that East of Turkey can be separated into three dominant tectonic deformation zones. The approximate boundaries of these zones are shown with black solid lines on Figure 4.2. The seismotectonic properties of each zone show similar features in terms of faulting mechanisms and fault-plane solutions. The first deformation zone (Zone 1) extends from the east of Karlıova triple junction towards North. The northern boundary of the second deformation zone (Zone 2) extends from NAF and reaches Bitlis-Zagros thrust belt in Iran. The tectonic province on East Anatolia, showing characteristics of escape tectonics, is designated as Zone 3. The delineation of these zones carries a certain level of uncertainty as they are identified through the similarity of seismotectonic features within each zone. That uncertainty can also affect the PSHA results to a limited extent. The overall picture in Figure 4.2 together with the epicentral distributions shown in Figure 2.3 indicates that the Bitlis-Zagros thrust zone causes intensive seismic activity around the area of interest. The Çaldıran-Tutak fault, and the recently mapped Van fault, can be considered as two main faults structures around Van city.

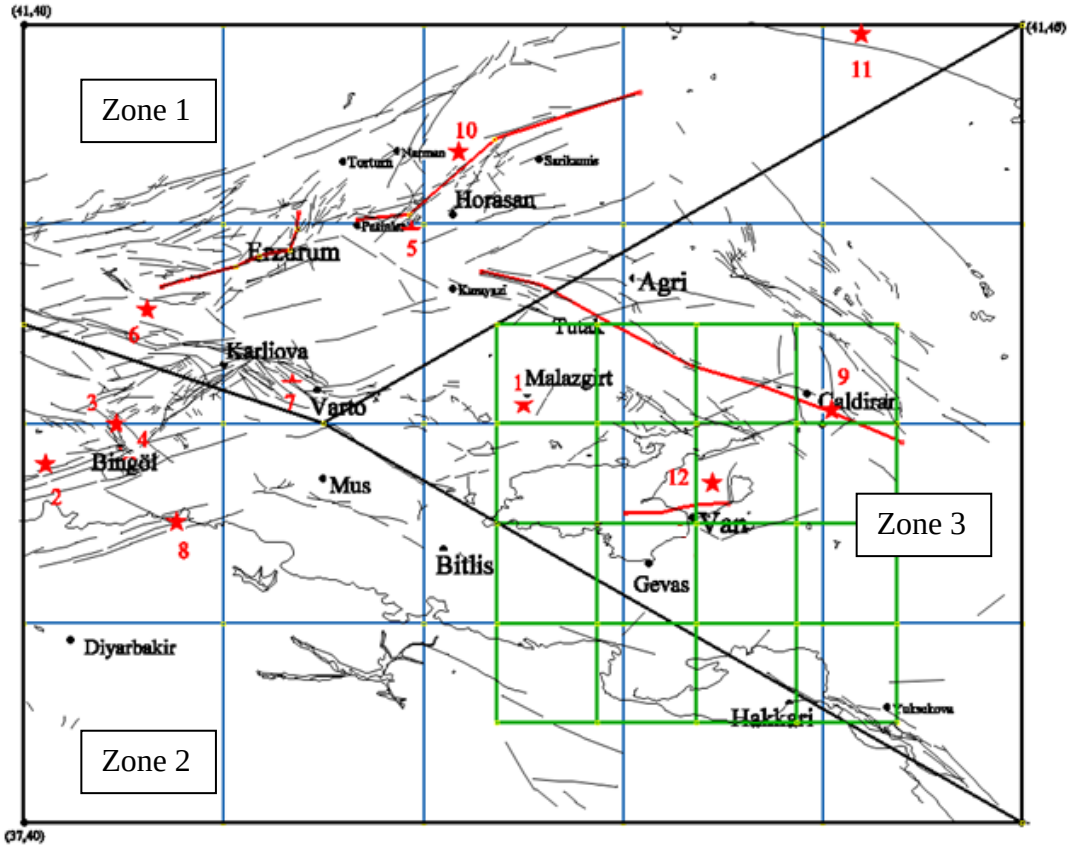


Figure 4.2 Epicentral locations major instrumental-period earthquakes (red stars) and major fault segments (red solid lines) considered in this study. Black thick lines are the approximate boundaries of three regions identified according to the similarity of seismotectonic features in each region. The red numbers next to each epicentral location correspond to the number indices listed in Table 4.1. The green squares represent the background sources in the area of interest of this study. The black thin lines are the other active faults according to Koçyiğit (2002).

Table 4.1. Major earthquakes occurred in the region of interest of this study

| | No | Date | Lon | Lat | Earthquake Name | Related fault | Intensity | $M_S$ | $M_L$ | $M_w$ | Style of Faulting |
|---|---|---|---|---|---|---|---|---|---|---|---|
| Instrumental Earthquakes | 1 | 29.04.1903 | 42.5 | 39.1 | Malazgirt (Muş) | Malazgirt fault | | 6.5 | 6.0 | | Strike Slip |
| | 2 | 08.03.2010 | 40.11 | 38.8 | Başyurt-Karakoçan | EAFZ | | | 6.0 | | Strike Slip |
| | 3 | 22.05.1971 | 40.53 | 38.87 | Bingöl | EAFZ | | 6.8 | | | Strike Slip |
| | 4 | 01.05.2003 | 40.46 | 39.00 | Bingöl | EAFZ | | 6.4 | | | Strike Slip |
| | 5 | 13.09.1924 | 41.94 | 39.97 | Horasan | Horasan-Pasinler | | 6.8 | | | Strike Slip |
| | 6 | 17.08.1949 | 40.62 | 39.57 | Karlıova | NAFZ junction | | 6.7 | | | Strike Slip |
| | 7 | 19.08.1966 | 41.34 | 39.2 | Varto | NAFZ junction | | 6.9 | | | Strike Slip |
| | 8 | 06.09.1975 | 40.76 | 38.51 | Lice | Lice Fault | | 6.6 | | | Thrust |
| | 9 | 24.11.1976 | 44.04 | 39.07 | Çaldıran (Muradiye) | Çaldıran Fault | | 7.5 | 6.9 | 6.3 | Strike Slip |
| | 10 | 30.10.1983 | 42.18 | 40.36 | Erzurum | Horasan-Pasinler | | 6.9 | | | Strike Slip |
| | 11 | 07.12.1988 | 44.19 | 40.96 | Kars or Armenia-Spitak | Pambak-Sevan | | 6.9 | | | Strike Slip |
| | 12 | 23.10.2011 | 43.45 | 38.71 | Van | Van fault | | 6.6 | | 7.2 | Reverse |
| Historical Earthquakes | 13 | 1581 | 42.1 | 38.35 | Van-Bitlis | | VIII | | | | |
| | 14 | 07.04.1646 | 43.7 | 38.3 | Van | | X | 6.7 | | | |
| | 15 | 12.08.1670 | 42 | 38 | Muş-Bitlis | | | 6.7 | | | |
| | 16 | 27.01.1705 | 41.7 | 38.7 | Bitlis | | IX | 6.7 | | | |
| | 17 | 08.03.1715 | 43.9 | 38.4 | Van | | IX | 6.6 | | | |

Magnitude information of the instrumental earthquakes is obtained from the International Seismological Centre (ISC, www.isc.ac.uk/) and Kandilli Observatory and Earthquake Research Institute (KOERI, www.koeri.boun.edu.tr)..

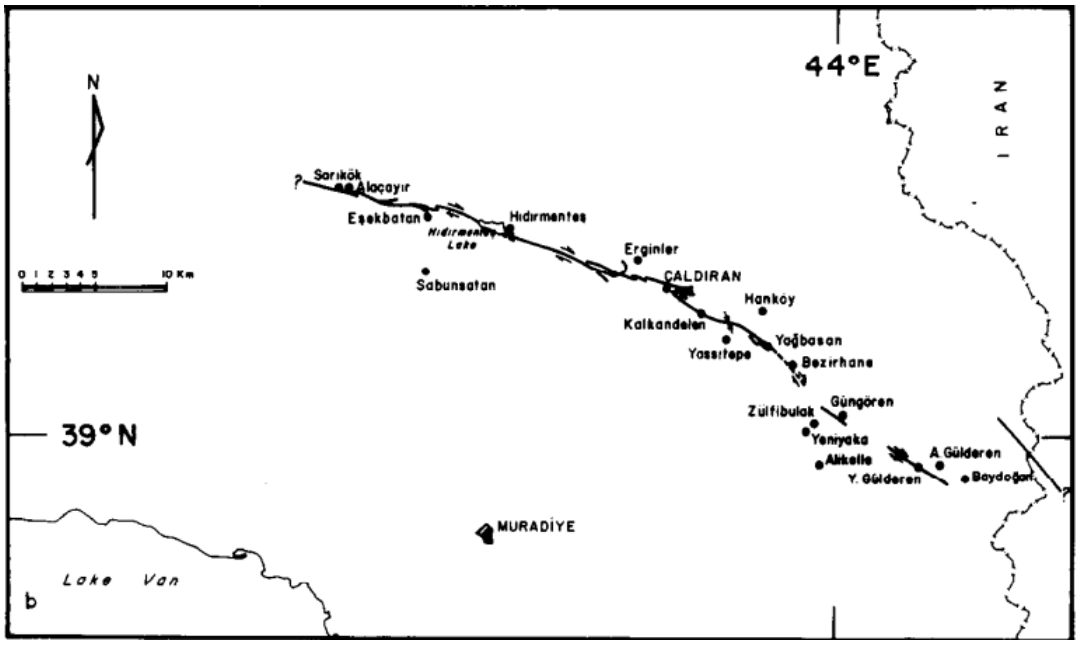


Figure 4.3 The 1976 Çaldıran (Muradiye) earthquake fault trace (Toksöz et al., 1978)

Table 4.2. Seismological parameters of the 23 October 2011 Van Earthquake obtained from different local and global seismological agencies (METU/EERC 2012-01)

| Agency* | Date | Epicenter Latitude (°N) | Epicenter Longitude (°E) | Focal Depth (km) | $M_w$ | $M_L$ |
|---|---|---|---|---|---|---|
| AFAD | 23/10/2011 | 38.68 | 43.47 | 19.02 | - | 6.7 |
| KOERI | 23/10/2011 | 38.758 | 43.36 | 5.0 | 7.2 | 6.6 |
| GCMT | 23/10/2011 | 38.67 | 43.42 | 15.4 | 7.1 | - |
| USGS | 23/10/2011 | 38.710 | 43.446 | 16 | 7.3 | - |
| GFZ | 23/10/2011 | 38.674 | 43.581 | 15 | 7.1 | - |
| EMSC | 23/10/2011 | 38.86 | 43.48 | 10 | 7.2 | - |
| INGV | 23/10/2011 | 38.86 | 43.48 | 10 | 7.3 | - |
| GeoAzur | 23/10/2011 | 38.627 | 43.535 | 16 - 23 | 7.2 | - |

* AFAD: Disaster Management and Emergency Presidency (www.afad.gov.tr); KOERI: Kandilli Observatory and Earthquake Research Institute (www.koeri.boun.edu.tr); GCMT: Global Centroid Moment Tensor Catalog (www.globalcmt.org); USGS: United States Geological Survey (www.usgs.gov); GFZ: German Research Center for Geosciences (www.gfz-potsdam.de); EMSC: European-Mediterranean Seismological Centre (www.emsc-csem.org); INGV: Istituto Nazionale di Geofisica e Vulocanologia (www.ingv.it); GeoAzur: www.geoazur.oca.eu

Table 4.3. Seismological parameters of the 9 November 2011 Van Earthquake determined by different local and global seismological agencies (METU/EERC 2012-02)

| Agency* | Date | Epicenter Latitude (°N) | Epicenter Longitude (°E) | Focal Depth (km) | $M_w$ | $M_L$ |
|---|---|---|---|---|---|---|
| AFAD | 09-11-2011 | 38.45 | 43.26 | 6.09 | - | 5.6 |
| EMSC | 09-11-2011 | 38.42 | 43.29 | 6 | 5.7 | - |
| GFZ | 09-11-2011 | 38.41 | 43.35 | 23 | 5.6 | - |
| GCMT | 09-11-2011 | 38.38 | 43.25 | 13.7 | 5.7 | - |
| KOERI | 09-11-2011 | 38.43 | 43.23 | 5 | - | 5.6 |
| USGS | 09-11-2011 | 38.43 | 43.23 | 8 | 5.6 | - |

* AFAD: Disaster Management and Emergency Presidency (www.afad.gov.tr); KOERI: Kandilli Observatory and Earthquake Research Institute (www.koeri.boun.edu.tr); GCMT: Global Centroid Moment Tensor Catalog (www.globalcmt.org); USGS: United States Geological Survey (www.usgs.gov); GFZ: German Research Center for Geosciences (www.gfz-potsdam.de); EMSC: European-Mediterranean Seismological Centre (www.emsc-csem.org)

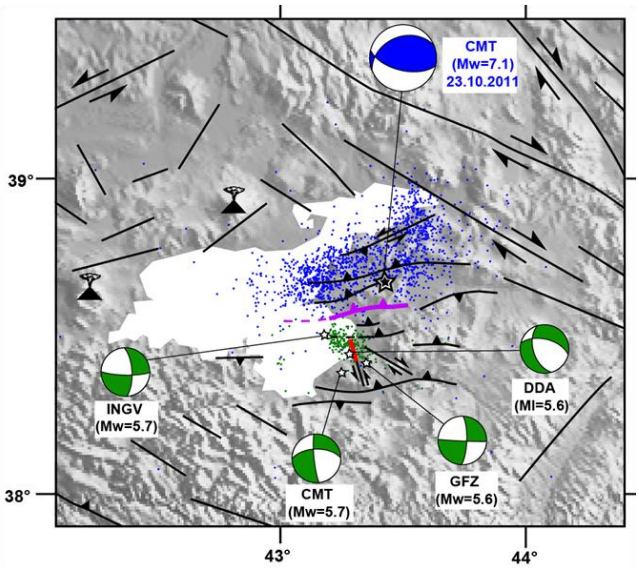


Figure 4.4 Mapped faults in the vicinity of the 2011 Van earthquakes. Blue dots show the aftershocks of the October 2011 earthquake. The blue beachball shows the fault-plane solution and the big star indicates the epicentral location of the same earthquake. The yellow dots are the aftershocks of November 2011 earthquake. Each green beachball is the fault-plane solutions of the November 2011 earthquake estimated by different agencies. The corresponding small stars are the estimated epicentral coordinates of the November earthquake from the same seismological agencies (METU/EERC 2012-02)

## 4.3. Seismic Hazard Input Parameters Used in the Multi-Parameter Sensitivity Analysis

As indicated in the previous chapters, the purpose of thesis study is to examine the influence of uncertainty in key hazard parameters on the probabilistic seismic hazard assessment considering the case of Van city. The most important parameters included in PSHA are already discussed in Chapter 2. In order to determine the significance of parameter uncertainty, the multi-parameter sensitivity analysis (Chapter 3) is used. The methodology is based on $2^k$ factorial design and considers two levels for each parameter (i.e., low and up levels). The combinations of low and high levels of these parameters allow a straightforward sensitivity analysis in PSHA. Hence, the main effect of each parameter and major interactions between parameters can be observed. The parameters that were included in the sensitivity analyses, their low and high levels used for each parameter are listed in Table 4.4. The description of each one of these parameters and the likely uncertainties associated with them are presented in Chapter 2. The detailed discussions on these parameters and the rationale behind the choice of low and high levels for each one of them are presented in the subsequent sections.

Table 4.4. The parameters used in the multi-parameter sensitivity analysis and corresponding low and high levels

| **Parameter** | **Low Level*** | **Up Level*** |
|---|---|---|
| GMPE | CF08 | AB10 |
| Sigma | 0.6 | 0.9 |
| Recurrence Model | Uniform<br>Characteristic | Truncated normal<br>Characteristic |
| Catalog | Incomplete | Complete |
| Maximum Magnitude | CTF=6.5,VF=6.9 | CTF=7,VF=7.3 |
| Slip Rate | CTF=6, VF=1.6 | CTF=13, VF=3.4 |

* CF08: Cauzzi and Faccioli (2008); AB10: Akkar and Bommer (2010); CTF: Çaldıran -Tutak fault; VF: Van Fault

### 4.3.1 Ground Motion Prediction Equations (GMPEs)

The influence of variations in GMPEs on PSHA is discussed in Chapter 2. At first, 13 candidate GMPEs are used for the multi-parameter sensitivity analysis, in order to emphasize the effect of GMPEs on probabilistic hazard results. The candidate GMPEs are collected by using the criteria established by Cotton et al (2006). Their important characteristics are listed in Table 4.5. Their moment magnitude range generally varies between 5 and 7.5. Most of the candidate GMPEs account for major faulting mechanisms. Their site terms are either continuous functions of $V_{S30}$ or they make use of generic site classifications. They are devised for estimating PGA and 5% damped pseudo-spectral acceleration (PSA).

The candidate GMPEs are tested in terms of their suitability and applicability for the considered region. In order to select the most appropriate GMPEs for the purposes of this study, a methodology that is proposed by Kale and Akkar (2013) was applied. The method is called as Euclidian Distance Ranking (EDR) and it is based on the calculation of Euclidian distances (DE). The influence of sigma on the ground motion estimations and bias between the observed data and median estimations are the two components that are assessed by this method. The computation of Euclidian distance definition for each data point of the ground-motion database specific to the region of interest is given in Eq. (4.1).

$$DE^2 = \sum_{i=1}^{N}(p_i - q_i)^2 \tag{4.1}$$

The parameters $p_i$ and $q_i$ represent the observed and estimated ground motion data pair. Given a GMPE, EDR considers the probability distribution of the absolute values of the differences (denoted by D) between natural logarithms of the observed and estimated data points to assess the influence of sigma on ground motion estimations. (Since each data in the database is a discrete point, the method defines the discrete values of *D* as $d_j$). The EDR method computes the probabilities of Euclidean distances, Pr ($|D| < |d_j|$), for a range of sigma values of the tested ground-motion prediction equation. Smaller probabilities for each data point indicate the better performance of the tested GMPE for that point. An index called as Modified Euclidian Distance (MDE) is computed in order to assess the performance of the tested GMPE for the entire ground-motion database. Equation (4.2) shows the MDE expression.

$$MDE_d = \sum_{j=1}^{n}\left|d_j\right|\Pr\left(|D| < \left|d_j\right|\right) \tag{4.2}$$

As indicated the EDR method also considers the bias between observed data and corresponding median estimations through a parameter called as κ. It is obtained by normalizing the original DE value by its corrected version, which represents the ideal performance of the tested GMPE (i.e., unbiased estimations of the considered GMPE for the entire ground-motion database). The optimum value of κ is 1.0 (when estimations show very close trends with the corresponding observations).

The final product of EDR is an index (called as EDR) that is obtained by considering the separate influences of MDE and κ. The formulation of EDR index is given in Eq. (4.3). The parameter N in Eq. (4.3) represents the total data number in the strong-motion database. A small EDR value indicates the better performance of the tested GMPE. The EDR procedure summarized here is described in detail in Kale and Akkar (2013).

$$EDR^2 = \kappa\frac{1}{N}\sum_{i=1}^{N} MDE_i^2 \tag{4.3}$$

Since EDR ranks the candidate GMPEs under a set of observed data a ground-motion dataset is compiled for the recorded horizontal accelerograms in the area of interest of this study. The accelerograms fall into the region enclosed by latitudes of $37^o$- $41^o$ and

longitudes of 40°- 45°. The total number of accelerograms in the compiled strong-motion database is 975 and they are from active shallow-crustal earthquakes occurred in the region. The strong-motion database is a subset of strong-motion databank compiled for the Earthquake Model of the Middle East project (EMME; www.emme-gem.org). Figure 4.5 shows the magnitude vs. distance distribution of the strong-motion database compiled for this thesis.

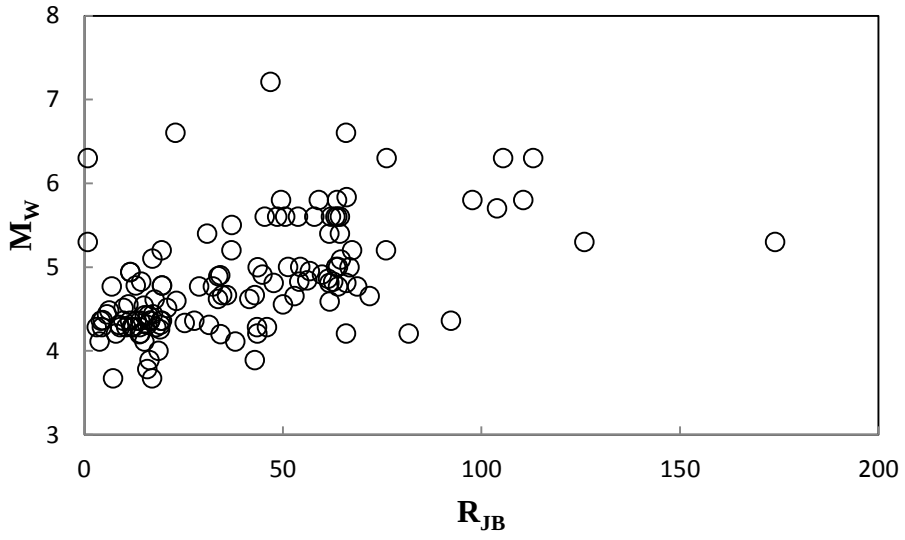


Figure 4.5 $M_w$ vs. $R_{JB}$ scatter plot of the strong-motion data used in this study

Table 4.5 GMPEs considered in this study

| Attenuation Relation | Acronym | Region | # of records, events | Min, Max $M_w$ | R type and $R_{max}$ [1] | Component type [2] | Style of Faulting [3] | Site Effect |
|---|---|---|---|---|---|---|---|---|
| Abrahamson and Silva (2008) | AS08 | Western US and Taiwan | 2754, 135 | 5.0, 8.5 | $R_{rup}$, 200 | PGA, PGV, PSA in GMRotI50 | S, N, R | $V_{S30}$ |
| Akkar and Bommer (2010) | AB10 | Europe and Middle East | 532, 131 | 5.0, 7.6 | $R_{JB}$, 100 | PGA, PGV, PSA in GM | S, N, R | Dummy |
| Akkar and Çağnan (2010) | AC10 | Turkey | 433, 137 | 5.0, 7.6 | $R_{JB}$, 200 | PGA, PGV, PSA in GM | S, N, R | $V_{S30}$ |
| Ambraseys et al. (2005) | Aetal05 | Europe and Middle East | 595, 135 | 5.0, 7.6 | $R_{JB}$, 99 | PGA, PSA in L | S, N, O | Dummy |
| Bindi et al. (2010) | Betal10 | Italy | 561, 107 | 4.0, 6.9 | $R_{JB}$, $R_{epi}$ 100 | PGA, PGV, PSA in L PGA, PGV, PSA in B | U | Dummy |
| Boore and Atkinson (2008) | BA08 | Western US and Taiwan | 1574, 58 | 5.0, 8.0 | $R_{jb}$, 200 | PGA, PGV, PSA in GMRotI50 | S, N, R | $V_{S30}$ |
| Campbell and Bozorgnia (2008) | CB08 | Western US and Taiwan | 1561, 64 | 4.0, 8.5 | $R_{rup}$, 200 | PGA, PGV, PSA in GMRotI50 | S, N, R | $V_{S30}$ |
| Cauzzi and Faccioli (2008) | CF08 | Japan | 1164, 60 | 5.0, 7.2 | $R_{hyp}$, 150 | PGA, PGV, PSA in GMRotI50 | S, N, R | Dummy |
| Chiou and Youngs (2008) | CY08 | Western US and Taiwan | 1950, 125 | 4.0, 8.5 | $R_{rup}$, 200 | PGA, PGV, PSA in GMRotI50 | S, N, R | $V_{S30}$ |
| Ghasemi et al. (2009) | Getal09 | Iran | 716, 200 | 5.0, 7.4 | $R_{rup}$, $R_{hyp}$ 10 | PSA in GMRotI50 | U | Dummy |
| Kalkan and Gülkan (2004) | KG04 | Turkey | 112, 57 | 4.0, 7.4 | $R_{JB}$, 250 | PGA, PSA in L | U | $V_{S30}$ |
| Özbey et al. (2004) | Oetal04 | Northwestern Turkey | 195, 17 | 5.0, 7.4 | $R_{JB}$, 300 | PGA, PSA in GM | U | Dummy |
| Zhao et al. (2006) | Zetal06 | Japan | 4726, 269 | 5.0, 8.3 | $R_{rup}$, 300 | PGA, PSA in GM | S, N, R | Dummy |

[1] R: distance; $R_{max}$: maximum distance; $R_{epi}$: epicentral distance; $R_{hyp}$: hypocentral distance, $R_{JB}$: Joyner-Boore distance (Joyner and Boore, 1981); $R_{RUP}$: rupture distance

[2] GM: geometric mean of horizontal components, L: larger horizontal component, GMRotI50: rotation-independent average horizontal component (Boore et al., 2006); B: both horizontal components; V: vertical component

[3] S: strike-slip faulting, N: normal faulting, R: reverse faulting, O: oblique faulting, U: unidentified

Figure 4.6 shows the EDR testing results of candidate GMPEs for a spectral period band ranging from T=0.0 s (PGA) to T=2.0 s. A total of 8 discrete period values (i.e., T=0.0s, 0.1s, 0.2s, 0.5s, 0.75s, 1.0s, 1.5s and 2.0s) were used in testing. The first two panels of Figure 4.6 shows the components of EDR index (i.e., $\sqrt{\frac{1}{N}\sum_1^N MDE_i^2}$ and $\sqrt{\kappa}$) that evaluate the performance of each candidate GMPE for record-to-record variability (aleatory variability described by the standard deviation of GMPE) and model bias (agreement between the median GMPE estimations and overall data trend). The last panel on Figure 4.6.c displays the product of these 2 components, which is the actual EDR index. Table 4.6 shows a similar type of information as of Figure 4.6. This table lists the average values of EDR components as well as the average EDR value computed for each predictive model over the entire period range of interest.

The immediate observation from Figure 4.6 and Table 4.6 is the different performance of each GMPE while addressing the aleatory variability (described by $\sqrt{\frac{1}{N}\sum_1^N MDE_i^2}$) and model bias (described by $\sqrt{\kappa}$). Smaller values of these indices suggest a better performance of tested GMPEs.

Ground-motion prediction equations that are abbreviated as AB10, AC10, Betal10 and CF08 (see Table 4.5 for the meanings of abbreviations used in candidate GMPEs) perform better in addressing the aleatory variability for the considered strong-motion database. On the other hand, the ground-motion predictive models AC10, CF08, Oeatl04 and Zetal06 perform better while representing the general trend of the observed data with respect to other candidate GMPEs. When the influence of these two factors is considered together AB10, AC10, CF08 and Oetal04 perform better with respect to other GMPEs. These observations are important depending on the objective of PSHA studies. The site-specific hazard studies may prefer the separate consideration of aleatory variability and model bias (Kale and Akkar, 2013). The EDR index that combines the effects of MDE and kappa is favorable for regional hazard studies as the trade-offs between aleatory variability and model bias might lose their significance for relatively short return periods (return periods up to 2475 years) considered in regional seismic hazard assessment. Since the subject study focuses on the site-specific hazard assessment of the city of Van, the separate consideration of MDE and kappa indices may be of use for selecting the most appropriate GMPEs that can be used to observe their effects on probabilistic hazard computations.

Under the light of above discussions, two GMPEs proposed by Akkar and Bommer (2010) and Cauzzi and Faccioli (2008) are selected for the purposes of the sensitivity analysis from the separate consideration of MDE and kappa attained by each candidate GMPE. AB10 and CF08 perform fairly well in terms of above two indices with respect to other candidate GMPEs. Besides median values of CF08 consistently draws the upper bound with respect to AB10 in spectral estimations that suits well for its designation as high-level GMPE. Consequently, AB10 is assigned as the low level GMPE in this study.

Table 4.6. Performances of tested GMPEs for components of EDR and the EDR

| **GMPE** | $\sqrt{\kappa}$ | $\sqrt{\frac{1}{N}\sum_{1}^{N} MDE_i^2}$ | EDR |
|---|---|---|---|
| AB10 | **1.33** | 1.13 | **1.50** |
| AC10 | **1.18** | **1.00** | **1.18** |
| Aetal05 | 1.34 | 1.19 | 1.59 |
| AS08 | 1.76 | 1.51 | 2.66 |
| BA08 | 1.73 | 1.44 | 2.49 |
| Betal10 | **1.30** | 1.18 | 1.54 |
| CF08 | **1.28** | **1.10** | **1.41** |
| CB08 | 1.77 | 1.47 | 2.60 |
| CY08 | 1.57 | 1.37 | 2.15 |
| Fetal03 | 2.00 | 1.80 | 3.61 |
| Getal09 | 1.47 | 1.24 | 1.82 |
| KG04 | 2.07 | 1.57 | 3.24 |
| Oetal04 | 1.37 | **1.05** | **1.44** |
| Zetal06 | 1.40 | **1.11** | 1.55 |

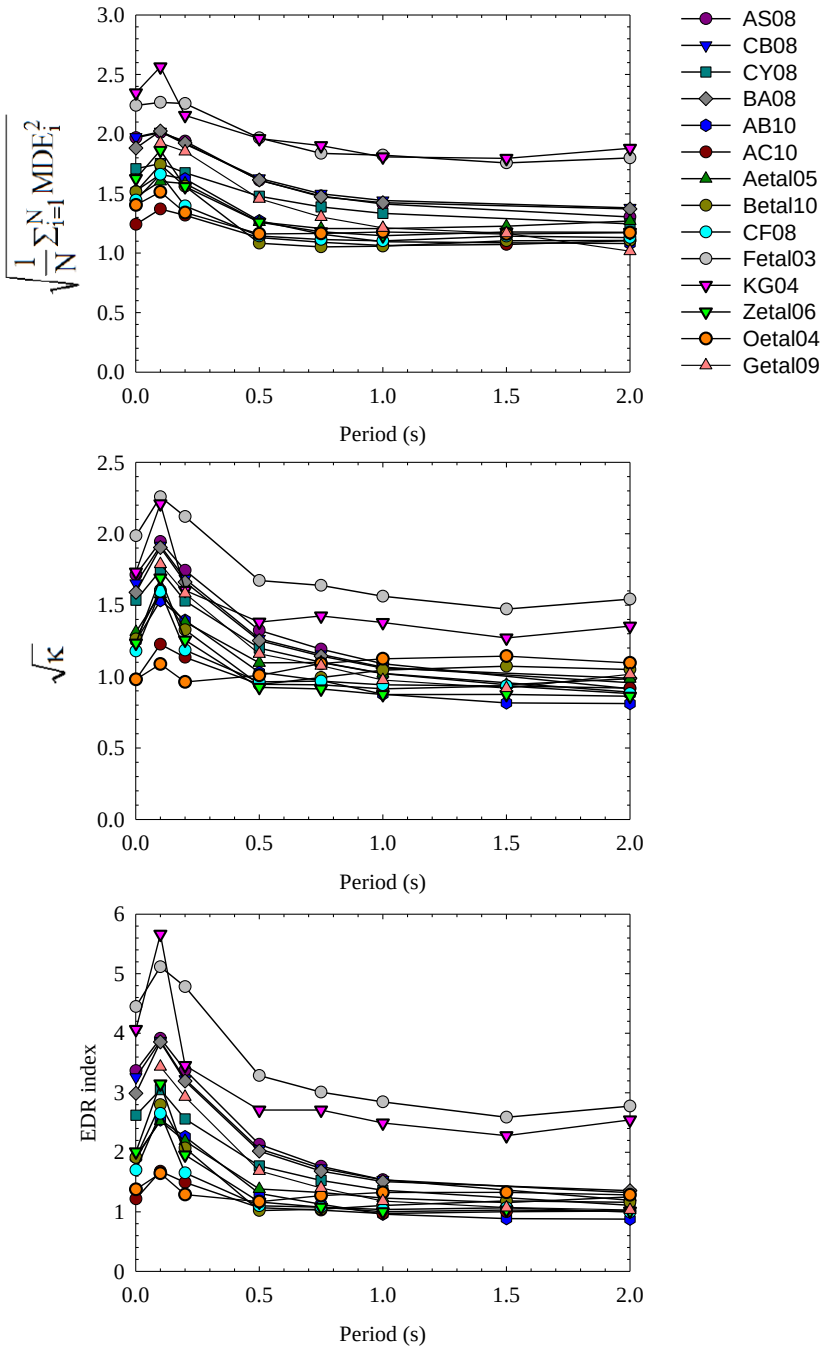


Figure 4.6 A representative figure that shows the EDR components (a) $\sqrt{\frac{1}{N}\sum_{1}^{N} MDE_i^2}$ and (b) $\sqrt{\kappa}$ and (c) the actual EDR

### 4.3.2. Standard Deviation (Sigma) of Ground Motion Predictive Models

As GMPEs are derived from observed acceleration data, the individual observations display considerable scatter about their median estimations (ground-motion variability or aleatory variability). This inherent behavior (i.e., aleatory variability) is mapped on to the probabilistic hazard analysis by including a range of standard deviation of the GMPE(s) considered in PSHA. The variations in standard deviations that are associated with GMPEs are discussed in Chapter 2 by Figure 2.9.b. The sigma variation presented by Figure 2.9.b indicates that the standard deviations of the candidate GMPEs change between 0.6 and 0.9 in logarithmic units. Hence, for the purposes of the sensitivity analysis the up and low levels of sigma are taken as 0.6 and 0.9 to study the level of influence of this parameter on PSHA results.

### 4.3.3. Earthquake Recurrence Models for Fault Sources

The uncertainty due to the selection of earthquake recurrence models are also discussed in Chapter 2. In brief, truncated exponential model is used for modeling the magnitude-recurrence relationship for background activity and characteristic earthquake model is used for modeling the earthquakes on the fault (line) sources (McGuire, 2004). The characteristic model suggests that the magnitude of the major earthquake on a fault is a characteristic property of the fault. On the other hand, the variability in interpretation of historical, geological and seismological parameters and limitations in available information yields a significant uncertainty in the estimation of characteristic magnitude. Therefore, the characteristic magnitude is considered as a random variable distributed between two possible limits for any particular line source. Two different distributions (Chapter 2 and Chapter 3) for characteristic magnitude are considered: a uniform distribution, and a truncated normal distribution between minimum and maximum plausible magnitudes. A preference between these two models may lead to uncertainty (or variations in hazard outputs) that has to be included in the sensitivity analysis. Pure characteristic model and truncated normal distributions are respectively selected as high and low levels of the earthquake recurrence model. The effect of the selection of this parameter is discussed in the subsequent sections.

### 4.3.4. Magnitude-Recurrence Parameters for Background Seismicity

This study considers the instrumental (contemporary) earthquake catalog of the events within the time period of 1904-2013 that is compiled from the International Seismological Centre (ISC; www.isc.ac.uk) and Boğaziçi Kandilli Observatory and Earthquake Research Institute (KOERI; www.koeri.boun.edu.tr). The catalog consists of earthquakes occurred in the Eastern Anatolia within the latitude range from $37^{o}$N to $41^{o}$N, and longitude range from $40^{o}$N to $45^{o}$E. The annual distribution of catalog events is shown in Figure 4.7. This figure indicates that the frequency of earthquakes has increased in last four decades. Figure 4.8 shows the histogram for $M_w$ of catalog events. Small and moderate size earthquakes (i.e., magnitudes smaller than 6) dominate the earthquake catalog.

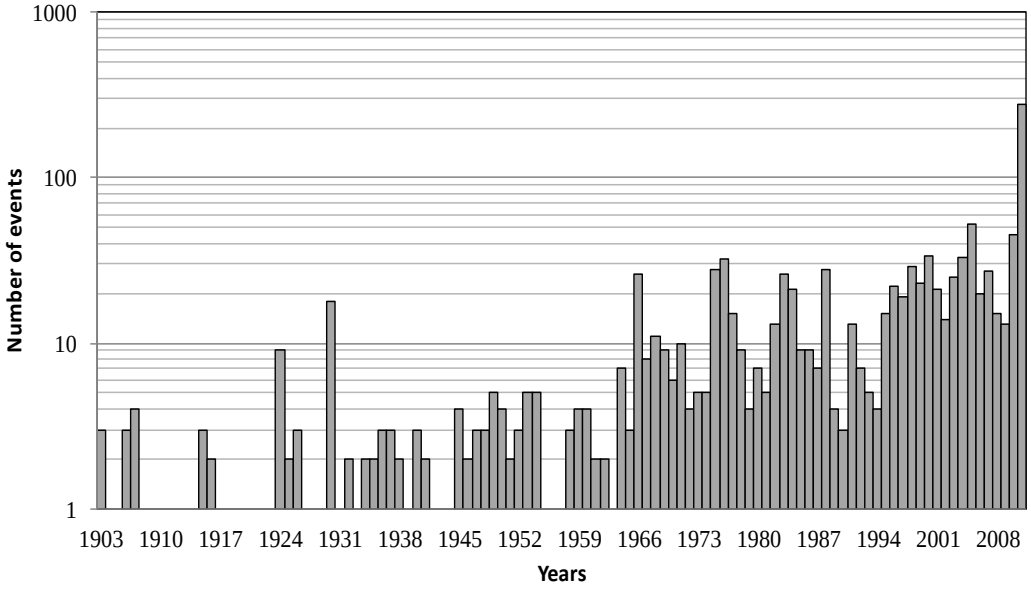


Figure 4.7 Annual distribution of earthquakes in the catalog utilized for the present study

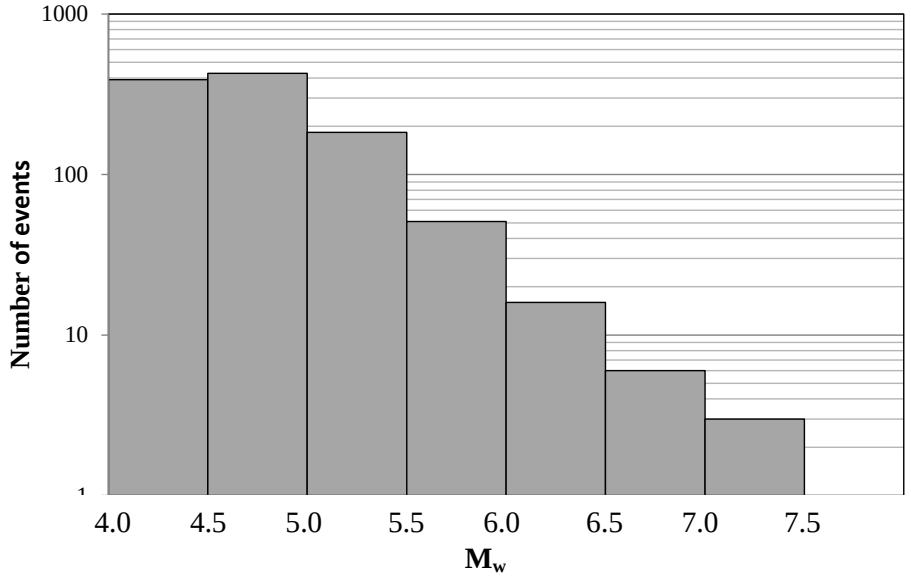


Figure 4.8 Moment magnitude histogram of the catalog events.

The effect of the catalog on probabilistic seismic hazard assessment was analyzed in two aspects. First, the probabilistic seismic hazard analyses are conducted by considering the original catalog data set. Second, the analyses are conducted after corrections for catalog completeness and eliminating aftershocks. In the first aspect, in order to estimate a- and b-values, original catalog data is used without any change. In the second aspect, aftershocks and possible foreshocks are eliminated from the catalog, such that the seismic moment of

aftershocks are added to the seismic moment of main shocks. The declustering method of Reasenberg (1985), explained in Chapter 2, is employed. Then, the catalog was analyzed for its completeness of magnitude ranges (see details in Table 4.7). The periods of completeness for different magnitude intervals are estimated according to the method discussed in Chapter 2. The computer program ZMAP is used (Weimer, 2001).

Table 4.7. Completeness of magnitude ranges for (a) Zone 1, (b) Zone 2, (c) Zone 3

(a) Zone 1

| $M_{min}$ | $M_{max}$ | Complete Year |
|---|---|---|
| 4.0 | 4.4 | 1980 |
| 4.5 | 4.9 | 1959 |
| 5.0 | 5.4 | 1948 |
| 5.5 | 7.2 | 1903 |

(b) Zone 2

| $M_{min}$ | $M_{max}$ | Complete Year |
|---|---|---|
| 4.0 | 4.4 | 1984 |
| 4.5 | 4.9 | 1956 |
| 5.0 | 5.4 | 1948 |
| 5.5 | 7.2 | 1903 |

(c) Zone 3

| $M_{min}$ | $M_{max}$ | Complete Year |
|---|---|---|
| 4.0 | 4.4 | 1991 |
| 4.5 | 4.9 | 1964 |
| 5.0 | 5.4 | 1945 |
| 5.5 | 7.2 | 1903 |

The well-known destructive earthquakes (generally with a magnitude greater than 6.5) in the catalog were associated with active faults in the region of interest (Table 4.1). These events are supposed to originate from line sources in PSHA. On the other hand, other moderate and small size earthquakes are usually not associated with an active fault and supposed to originate from sources in the background of those major tectonic structures. For background sources, the upper magnitude threshold level is selected as $M_w$ 6.5, which is the lowest of characteristic magnitude on fault sources in the considered region. The threshold $M_w$ 6.5 is selected according to the availability of maps on surface trace of fault rupture for past events in the region. Fault ruptures of several events with magnitudes less that that threshold are not shown on maps presented in literature, possibly due to unclear surface traces. Using the catalog data, earthquake recurrence model parameters such as a-value (activity rate) and b-value are estimated for background sources. However, since the variance of an estimate is dependent on sample size, it is necessary to gather a sample size that is sufficient for a reasonable convergence of estimate. It is assumed that the b-value is

uniform on a zone that shows a reasonable uniformity in tectonic characteristics. Hence, b-value is estimated separately for three seismotectonic zones (Zone 1, Zone 2 and Zone 3) that are shown in Figure 4.2 by dividing the events into three groups according to the location of epicenters. a-value is supposed to be nonuniformly distributed over a seismotectonic zone. Since the catalog is not complete for all magnitudes, the events with $M_w \geq 4.5$ after the year 1970 are considered for calculation of activity rates when catalog completeness is of concern.

Since none of the background sources (square-shaped cells shown in Figure 4.9) occupies any area of Zone 3, that zone was expelled from further analyses. Following the declustering of catalog data, the events with epicenters on Zone 1 and Zone 2 are analyzed for complete periods of magnitude ranges. Then, b-values are estimated for two zones separately by considering and ignoring catalog completeness. The calculated b-values for Zone 1 and Zone 2 are presented on Table 4.8. b-value of each cell is assigned according to location of cell's center. In order to reflect the spatial variability of a-value, the background activity was divided by cells (square areas) with dimensions $0.5^o$ by $0.5^o$ in spherical coordinates. The cell sides overlap with parallels and meridians. Figure 4.9 shows the grid cells with numbers from 1 to 16. Those square shaped areas constitute the background seismic sources. The activity rates (a-values) on each cell were calculated by considering the number of epicenters located in each cell. Then b-values of each square were attained in accordance with b-values calculated for Zone 1 and Zone 2, because none of the cells is located on Zone 3.

The a-value, the activity rate, is calculated by considering and ignoring the catalog completeness. Since the catalog is complete after 1970 for the magnitude (Mw) range greater than 4.5, that magnitude range and period of completeness is used for calculation of rates on each cell, in the case that catalog completeness is taken into consideration. The rate of lower magnitudes can be estimated by using the theoretical magnitude-recurrence relationship. In the case that completeness is not of concern, all events of catalog with magnitudes greater than 4.0 are used for calculation of a-value. Only the events with epicenters located in the pertinent cell are used for estimation of a-value for any particular background source.

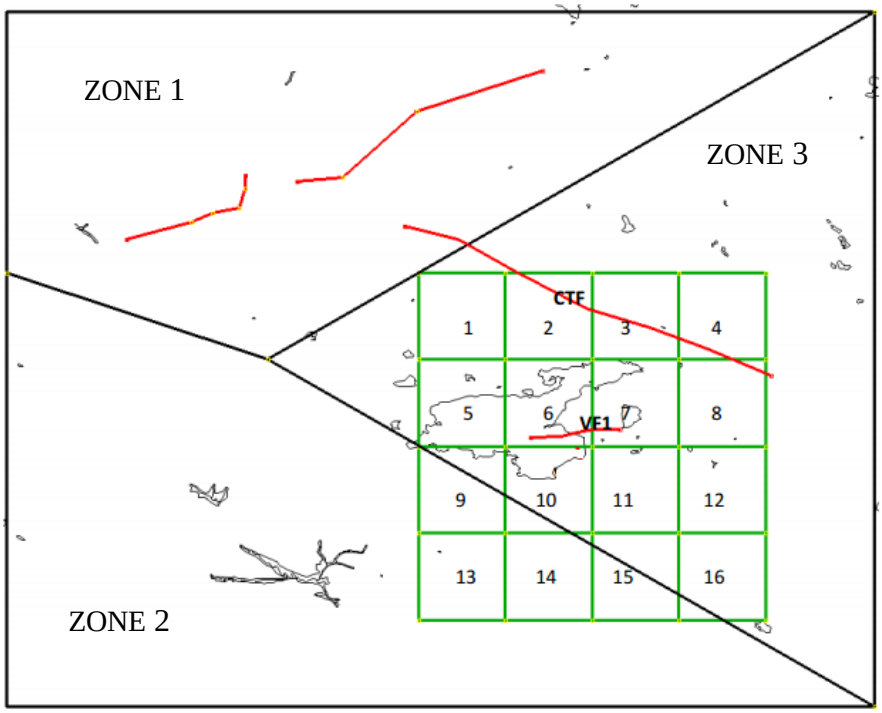


Figure 4.9 Background sources (0.5 $^{o}$ x 0.5$^{o}$ sized squares), deformation zones (Zone 1, Zone 2 and Zone 3) and well-studied fault sources (CTF: Çaldıran-Tutak Fault, VF: Van Fault)

Table 4.8 b-values of Zone 1 and Zone 2 obtained from analysis of catalog before and after completeness analysis

| Zones | Complete | Incomplete |
|---|---|---|
| | b-value | b-value |
| Zone 1 | 2.05 | 1.70 |
| Zone 2 | 1.77 | 1.61 |

Table 4.9 Seismological parameters obtained from analysis of catalog after completeness analysis and from original catalog

| Background Sources | Complete | | Incomplete | |
|---|---|---|---|---|
| | a-value | b-value | a-value | b-value |
| Square 1 | 0.0185 | 2.05 | 0.0183 | 1.70 |
| Square 2 | 0.0556 | 2.05 | 0.0183 | 1.70 |
| Square 3 | 0.1296 | 2.05 | 0.1193 | 1.70 |
| Square 4 | 0.1852 | 2.05 | 0.1468 | 1.70 |
| Square 5 | 0.0556 | 2.05 | 0.0734 | 1.70 |
| Square 6 | 0.0926 | 2.05 | 0.0734 | 1.70 |
| Square 7 | 0.0556 | 2.05 | 0.0734 | 1.70 |

Table 4.9 (Continued)

| Background Sources | complete | | Incomplete | |
|---|---|---|---|---|
| | a-value | b-value | a-value | b-value |
| Square 8 | 0.1111 | 2.05 | 0.1376 | 1.70 |
| Square 9 | 0.0926 | 1.77 | 0.1193 | 1.61 |
| Square 10 | 0.1111 | 2.05 | 0.0826 | 1.70 |
| Square 11 | 0.0556 | 2.05 | 0.0734 | 1.70 |
| Square 12 | 0.0185 | 2.05 | 0.0550 | 1.70 |
| Square 13 | 0.0556 | 1.77 | 0.0550 | 1.61 |
| Square 14 | 0.0926 | 1.77 | 0.0917 | 1.61 |
| Square 15 | 0.0926 | 1.77 | 0.0734 | 1.61 |
| Square 16 | 0.0370 | 2.05 | 0.0275 | 1.70 |

### 4.3.5. Maximum Magnitude for fault (line) sources

The prediction of maximum earthquake magnitude that a fault can generate introduces uncertainty in probabilistic seismic hazard assessment. The maximum credible magnitude can be assigned to a fault (line) source by compiling geological and seismological data. For a possible future earthquake, the estimated maximum rupture dimensions can be used for the prediction of maximum earthquake magnitude from empirical relationships of rupture geometry vs. magnitude. The past major earthquakes on the fault can guide the expert for likely rupture areas that can be generated by the fault. This approach is also followed in this study.

The empirical relationships between earthquake magnitude and geometrical properties of the fault rupture proposed by Wells and Coppersmith (1994) are considered in this study. Table 4.10 presents the relationships between rupture area and moment magnitude. Irrespective of the uncertainty in the estimations of maximum possible rupture area on a fault, the magnitude predictions involve a significant level of uncertainty as depicted by the standard deviations in Table 4.10. Sensitivity of PSHA to predicted maximum magnitude is investigated by considering two levels of maximum magnitude (i.e., up and low levels of maximum magnitude) for each fault. The accuracies of geological and geophysical investigations of the Van and Çaldıran-Tutak faults are not within the scope of this study. Hence, the precision in the estimation of rupture area for a future earthquake on these faults is not examined. Instead, the largest credible rupture areas on the two faults that are presumed to be consistent with the moment magnitudes of the Van and Çaldıran (Muradiye) earthquakes are computed. This approach is applied in the current PSHA practice. As discussed previously, the moment magnitude of the 23 October 2011 Van earthquake has already been estimated and reported by geologists and seismic networks considering the ruptured segments and kinematic properties of the new Van fault. The

moment magnitude of the Çaldıran (Muradiye) earthquake is unknown and its estimation is done by using the empirical magnitude conversion relationships proposed in Akkar et al. (2010). This topic is already indicated in the beginning of this chapter and moment magnitude for the Çaldıran (Muradiye) earthquake is estimated as $M_w$ 7.3 (for a surface-wave magnitude of 7.3) and $M_w$ 6.8 (for a body-wave magnitude of 6.3) via Akkar et al. (2010) empirical conversion relationships. Thus, for the Çaldıran-Tutak fault, the predictions on the maximum moment magnitude will involve further uncertainties as the estimated rupture area from the empirical relationships in Table 4.10 is based on an estimated $M_w$ from an empirical conversion relationship. This study prefers the use of $M_w$ 6.8 for estimating the rupture area of future earthquakes on the Çaldıran-Tutak fault because the area considered for the seismic hazard assessment does not cover the entire length of the Çaldıran-Tutak fault (see Figure 4.2). Thus, the likelihood of experiencing a larger magnitude earthquake (i.e., $M_w > 6.8$) on this fault is small if only the fault area that is within the boundaries of the study area is considered.

The upper and lower estimations of rupture areas for these two faults through the considerations of the 23 October 2011 and 24 November 1976 earthquakes are converted to up and low level maximum magnitude predictions as given in Table 4.11. These magnitude values account for the prediction interval of one standard deviation around mean estimate.

Table 4.10 Wells and Coppersmith (1994) magnitude vs. rupture area (RA) relationships. The abbreviations SS, R and N stand for strike-slip, reverse and normal faulting

| Equation | Slip type | Coefficients | | standard deviation |
|---|---|---|---|---|
| | | A | B | |
| M=a+b*log(RA) | SS | 3.98 | 1.02 | 0.23 |
| | R | 4.33 | 0.90 | 0.25 |
| | N | 3.93 | 1.02 | 0.25 |

Table 4.11 Up and low levels of maximum magnitudes of the Çaldıran -Tutak (CTF) and Van (VF) faults

| Faults | Maximum Magnitude | |
|---|---|---|
| | Low level | Up level |
| Çaldıran Tutak Fault | 6.51 | 6.97 |
| Van Fault | 6.85 | 7.35 |

### 4.3.6. Slip Rates on Faults

The slip-rate estimates are usually controversial issues even for well-studied faults. Usually, the measurements for offsets on geological formations around active faults and their estimated geological ages are used for calculation of slip rates. The developments on remote sensing also allowed monitoring of relative velocity between two spatial coordinates. A comparison of variability in slip rate estimates and consistency between two methods is presented for major tectonic structures around Anatolia by Reilinger et al. (2006). The limitations in remote sensing data and discrepancies in interpretation of geological data result in uncertainty in rate estimates. Besides, data for slip rate estimates on less significant tectonic structures may not be available as well. The slip rates on major tectonic structures can be used for constraining the slip rate estimates on faults wherever reliable data is not available (e.g., Westaway, 2003). The consequence of lack of slip rate estimate is not in the scope of this study. However, the uncertainty in slip rate estimates is a practical issue, since it will be inherent in any estimation of slip rate.

The slip rates of fault sources considered in this study are based on the study of Reilinger et al. (2006), presenting the interpretations of remote-sensing data. Consequently, a single hypothetical discontinuity located on northeast of Van lake accommodate 11.9 mm/year left-lateral slip, and about 3.0 mm/year closing with an error of 0.4 mm/year. Supposing that about %60 of slip rates can be coseismic, corresponding to fault slips during significant earthquakes (Paradisopoulou et al., 2010), and considering alternative tectonic models explained in literature, the slip-rate estimates presented on Table 4.12 are used in sensitivity analyses. Those slip rate estimates are only reasonable assumptions, and may not strictly represent the actual slip rates on two fault sources considered in this study. On the other hand, the ratio between two levels of slip rates is consistently about 2.1.

Table 4.12 Up and low levels of slip rate

| Faults | Slip Rate | |
|---|---|---|
| | Low level | Up level |
| Van Fault (VF) | 1.6 | 3.4 |
| Çaldıran Tutak Fault (CTF) | 6 | 13 |

## 4.4. Sensitivity Analysis

The sensitivity analysis on the probabilistic seismic hazard assessment for the city of Van is conducted using the upper and lower levels of the parameters that are discussed in the previous section. The combinations of these parameters are given in Table 4.13. The method used for combining different levels of parameters is presented in Chapter 3. A total of 64 combinations are analyzed in order to observe how the variations in these input parameters affect the PSHA results. The results are shown in terms of spectral acceleration

values. Peak ground acceleration (PGA) as well as pseudo spectral acceleration ordinates at T = 0.2s and T = 1.0s (i.e., PSA(T=0.2s) and PSA(T=1.0s)) are computed. These spectral quantities are generally used to derive design spectrum envelopes after site-specific hazard studies (ASCE, 2010). The return periods considered for these spectral parameters are 72, 475 and 2475 years. The return periods correspond to %50, 10%, and 2% exceedance probabilities for an exposure time of 50 years respectively, and are commonly used for designation of ground motion amplitudes to be considered in design and assessment of buildings (e.g., TEC, 2007; ASCE, 2010; CEN, 2004).

Table 4.13 Combinations of input parameters used in the sensitivity analysis

| No | GMPE | Sigma | Recurrence Model | Catalog | Maximum Magnitude* | Slip Rate* |
|---|---|---|---|---|---|---|
| 1 | AB10 | 0.6 | Pure Characteristic | Complete | CTF=7,VF=7.3 | CTF=13, VF=3.4 |
| 2 | AB10 | 0.6 | Pure Characteristic | Complete | CTF=6.5,VF=6.9 | CTF=13, VF=3.4 |
| 3 | AB10 | 0.6 | Pure Characteristic | Complete | CTF=7,VF=7.3 | CTF=6, VF=1.6 |
| 4 | AB10 | 0.6 | Pure Characteristic | Complete | CTF=6.5,VF=6.9 | CTF=6, VF=1.6 |
| 5 | AB10 | 0.6 | Pure Characteristic | Incomplete | CTF=7,VF=7.3 | CTF=13, VF=3.4 |
| 6 | AB10 | 0.6 | Pure Characteristic | Incomplete | CTF=6.5,VF=6.9 | CTF=13, VF=3.4 |
| 7 | AB10 | 0.6 | Pure Characteristic | Incomplete | CTF=7,VF=7.3 | CTF=6, VF=1.6 |
| 8 | AB10 | 0.6 | Pure Characteristic | Incomplete | CTF=6.5,VF=6.9 | CTF=6, VF=1.6 |
| 9 | AB10 | 0.6 | Truncated Normal | Complete | CTF=7,VF=7.3 | CTF=13, VF=3.4 |
| 10 | AB10 | 0.6 | Truncated Normal | Complete | CTF=6.5,VF=6.9 | CTF=13, VF=3.4 |
| 11 | AB10 | 0.6 | Truncated Normal | Complete | CTF=7,VF=7.3 | CTF=6, VF=1.6 |
| 12 | AB10 | 0.6 | Truncated Normal | Complete | CTF=6.5,VF=6.9 | CTF=6, VF=1.6 |
| 13 | AB10 | 0.6 | Truncated Normal | Incomplete | CTF=7,VF=7.3 | CTF=13, VF=3.4 |
| 14 | AB10 | 0.6 | Truncated Normal | Incomplete | CTF=6.5,VF=6.9 | CTF=13, VF=3.4 |
| 15 | AB10 | 0.6 | Truncated Normal | Incomplete | CTF=7,VF=7.3 | CTF=6, VF=1.6 |
| 16 | AB10 | 0.6 | Truncated Normal | Incomplete | CTF=6.5,VF=6.9 | CTF=6, VF=1.6 |
| 17 | AB10 | 0.9 | Pure Characteristic | Complete | CTF=7,VF=7.3 | CTF=13, VF=3.4 |
| 18 | AB10 | 0.9 | Pure Characteristic | Complete | CTF=6.5,VF=6.9 | CTF=13, VF=3.4 |
| 19 | AB10 | 0.9 | Pure Characteristic | Complete | CTF=7,VF=7.3 | CTF=6, VF=1.6 |
| 20 | AB10 | 0.9 | Pure Characteristic | Complete | CTF=6.5,VF=6.9 | CTF=6, VF=1.6 |
| 21 | AB10 | 0.9 | Pure Characteristic | Incomplete | CTF=7,VF=7.3 | CTF=13, VF=3.4 |
| 22 | AB10 | 0.9 | Pure Characteristic | Incomplete | CTF=6.5,VF=6.9 | CTF=13, VF=3.4 |
| 23 | AB10 | 0.9 | Pure Characteristic | Incomplete | CTF=7,VF=7.3 | CTF=6, VF=1.6 |
| 24 | AB10 | 0.9 | Pure Characteristic | Incomplete | CTF=6.5,VF=6.9 | CTF=6, VF=1.6 |
| 25 | AB10 | 0.9 | Truncated Normal | Complete | CTF=7,VF=7.3 | CTF=13, VF=3.4 |
| 26 | AB10 | 0.9 | Truncated Normal | Complete | CTF=6.5,VF=6.9 | CTF=13, VF=3.4 |
| 27 | AB10 | 0.9 | Truncated Normal | Complete | CTF=7,VF=7.3 | CTF=6, VF=1.6 |
| 28 | AB10 | 0.9 | Truncated Normal | Complete | CTF=6.5,VF=6.9 | CTF=6, VF=1.6 |
| 29 | AB10 | 0.9 | Truncated Normal | Incomplete | CTF=7,VF=7.3 | CTF=13, VF=3.4 |
| 30 | AB10 | 0.9 | Truncated Normal | Incomplete | CTF=6.5,VF=6.9 | CTF=13, VF=3.4 |

Table 4.13 (Continued)

| No | GMPE | Sigma | Recurrence Model | Catalog | Mmax* | Slip Rate |
|---|---|---|---|---|---|---|
| 31 | AB10 | 0.9 | Truncated Normal | Incomplete | CTF=7,VF=7.3 | CTF=6, VF=1.6 |
| 32 | AB10 | 0.9 | Truncated Normal | Incomplete | CTF=6.5,VF=6.9 | CTF=6, VF=1.6 |
| 33 | CF08 | 0.6 | Pure Characteristic | Complete | CTF=7,VF=7.3 | CTF=13, VF=3.4 |
| 34 | CF08 | 0.6 | Pure Characteristic | Complete | CTF=6.5,VF=6.9 | CTF=13, VF=3.4 |
| 35 | CF08 | 0.6 | Pure Characteristic | Complete | CTF=7,VF=7.3 | CTF=6, VF=1.6 |
| 36 | CF08 | 0.6 | Pure Characteristic | Complete | CTF=6.5,VF=6.9 | CTF=6, VF=1.6 |
| 37 | CF08 | 0.6 | Pure Characteristic | Incomplete | CTF=7,VF=7.3 | CTF=13, VF=3.4 |
| 38 | CF08 | 0.6 | Pure Characteristic | Incomplete | CTF=6.5,VF=6.9 | CTF=13, VF=3.4 |
| 39 | CF08 | 0.6 | Pure Characteristic | Incomplete | CTF=7,VF=7.3 | CTF=6, VF=1.6 |
| 40 | CF08 | 0.6 | Pure Characteristic | Incomplete | CTF=6.5,VF=6.9 | CTF=6, VF=1.6 |
| 41 | CF08 | 0.6 | Truncated Normal | Complete | CTF=7,VF=7.3 | CTF=13, VF=3.4 |
| 42 | CF08 | 0.6 | Truncated Normal | Complete | CTF=6.5,VF=6.9 | CTF=13, VF=3.4 |
| 43 | CF08 | 0.6 | Truncated Normal | Complete | CTF=7,VF=7.3 | CTF=6, VF=1.6 |
| 44 | CF08 | 0.6 | Truncated Normal | Complete | CTF=6.5,VF=6.9 | CTF=6, VF=1.6 |
| 45 | CF08 | 0.6 | Truncated Normal | Incomplete | CTF=7,VF=7.3 | CTF=13, VF=3.4 |
| 46 | CF08 | 0.6 | Truncated Normal | Incomplete | CTF=6.5,VF=6.9 | CTF=13, VF=3.4 |
| 47 | CF08 | 0.6 | Truncated Normal | Incomplete | CTF=7,VF=7.3 | CTF=6, VF=1.6 |
| 48 | CF08 | 0.6 | Truncated Normal | Incomplete | CTF=6.5,VF=6.9 | CTF=6, VF=1.6 |
| 49 | CF08 | 0.9 | Pure Characteristic | Complete | CTF=7,VF=7.3 | CTF=13, VF=3.4 |
| 50 | CF08 | 0.9 | Pure Characteristic | Complete | CTF=6.5,VF=6.9 | CTF=13, VF=3.4 |
| 51 | CF08 | 0.9 | Pure Characteristic | Complete | CTF=7,VF=7.3 | CTF=6, VF=1.6 |
| 52 | CF08 | 0.9 | Pure Characteristic | Complete | CTF=6.5,VF=6.9 | CTF=6, VF=1.6 |
| 53 | CF08 | 0.9 | Pure Characteristic | Incomplete | CTF=7,VF=7.3 | CTF=13, VF=3.4 |
| 54 | CF08 | 0.9 | Pure Characteristic | Incomplete | CTF=6.5,VF=6.9 | CTF=13, VF=3.4 |
| 55 | CF08 | 0.9 | Pure Characteristic | Incomplete | CTF=7,VF=7.3 | CTF=6, VF=1.6 |
| 56 | CF08 | 0.9 | Pure Characteristic | Incomplete | CTF=6.5,VF=6.9 | CTF=6, VF=1.6 |
| 57 | CF08 | 0.9 | Truncated Normal | Complete | CTF=7,VF=7.3 | CTF=13, VF=3.4 |
| 58 | CF08 | 0.9 | Truncated Normal | Complete | CTF=6.5,VF=6.9 | CTF=13, VF=3.4 |
| 59 | CF08 | 0.9 | Truncated Normal | Complete | CTF=7,VF=7.3 | CTF=6, VF=1.6 |
| 60 | CF08 | 0.9 | Truncated Normal | Complete | CTF=6.5,VF=6.9 | CTF=6, VF=1.6 |
| 61 | CF08 | 0.9 | Truncated Normal | Incomplete | CTF=7,VF=7.3 | CTF=13, VF=3.4 |
| 62 | CF08 | 0.9 | Truncated Normal | Incomplete | CTF=6.5,VF=6.9 | CTF=13, VF=3.4 |
| 63 | CF08 | 0.9 | Truncated Normal | Incomplete | CTF=7,VF=7.3 | CTF=6, VF=1.6 |
| 64 | CF08 | 0.9 | Truncated Normal | Incomplete | CTF=6.5,VF=6.9 | CTF=6, VF=1.6 |

*CTF: Maximum magnitude on Çaldıran-Tutak Fault, VF: Maximum magnitude on Van Fault

### 4.4.1. Results of Sensitivity Analysis

The sensitivity of PSHA to the combinations of input parameters (Table 4.13) are analyzed by following the steps described in Chapter 3. The uncertainties in input parameters are expected to have multiplicative effects on the annual exceedance probabilities. This assumption is one of the premises of Rabinowitz and Steinberg (1991). The main effect of each input parameter on PSHA results is computed as the difference in average log spectral accelerations computed by the pertinent combinations of high and low level of parameters according to Eq. (3.1). The interactions between input parameters are computed according to Eqs. (3.6) and (3.7). Separate analyses are done for each return period (i.e., $T_R$ = 2475 years, 475 years and 72 years) and for PGA, PSA (T=0.2s) and PSA (T=1.0s). The main effect of a parameter on PSHA is insignificant when the difference between computed average log spectral accelerations for the designated up and low levels tends to zero, or the ratio between anti-logs of average log spectral accelerations yields a value around unity. The anti-log of average log spectral accelerations is referred to as the factor of main effects in this study. These are illustrated in Figure 4.10 and are also listed in Table 4.14. The first three parameters that show significant deviations from 1.0 are shown in bold fonts in Table 4.14

Table 4.14 Main effects of the parameters on PSHA

(a) PGA

| Parameter | Main Effects | | |
|---|---|---|---|
| | 2475 years | 475 years | 72 years |
| **GMPE** | 1.51 | 1.71 | 1.87 |
| **Sigma** | 1.64 | 1.47 | 1.48 |
| Recurrence Model | 1.01 | 1.01 | 1.00 |
| Catalog | 1.04 | 1.08 | 1.14 |
| Maximum Magnitude | 0.84 | 0.79 | 0.86 |
| **Slip Rate** | 1.25 | 1.29 | 1.22 |

(b) T=0.2s

| Parameter | Main Effects | | |
|---|---|---|---|
| | 2475 years | 475 years | 72 years |
| **GMPE** | 1.86 | 2.06 | 2.21 |
| **Sigma** | 1.65 | 1.48 | 1.49 |
| Recurrence Model | 1.01 | 1.01 | 1.00 |
| Catalog | 1.03 | 1.07 | 1.13 |
| Maximum Magnitude | 0.84 | 0.79 | 0.86 |
| **Slip Rate** | 1.25 | 1.30 | 1.24 |

Table 4.14 (Continued)

(c) T=1.0s

| Parameter | Main Effects | | |
|---|---|---|---|
| | 2475 years | 475 years | 72 years |
| **GMPE** | 1.60 | 1.74 | 1.92 |
| **Sigma** | 1.57 | 1.46 | 1.45 |
| Recurrence Model | 1.00 | 1.01 | 1.00 |
| Catalog | 1.00 | 1.01 | 1.03 |
| Maximum Magnitude | 0.89 | 0.81 | 0.87 |
| **Slip Rate** | 1.36 | 1.44 | 1.41 |

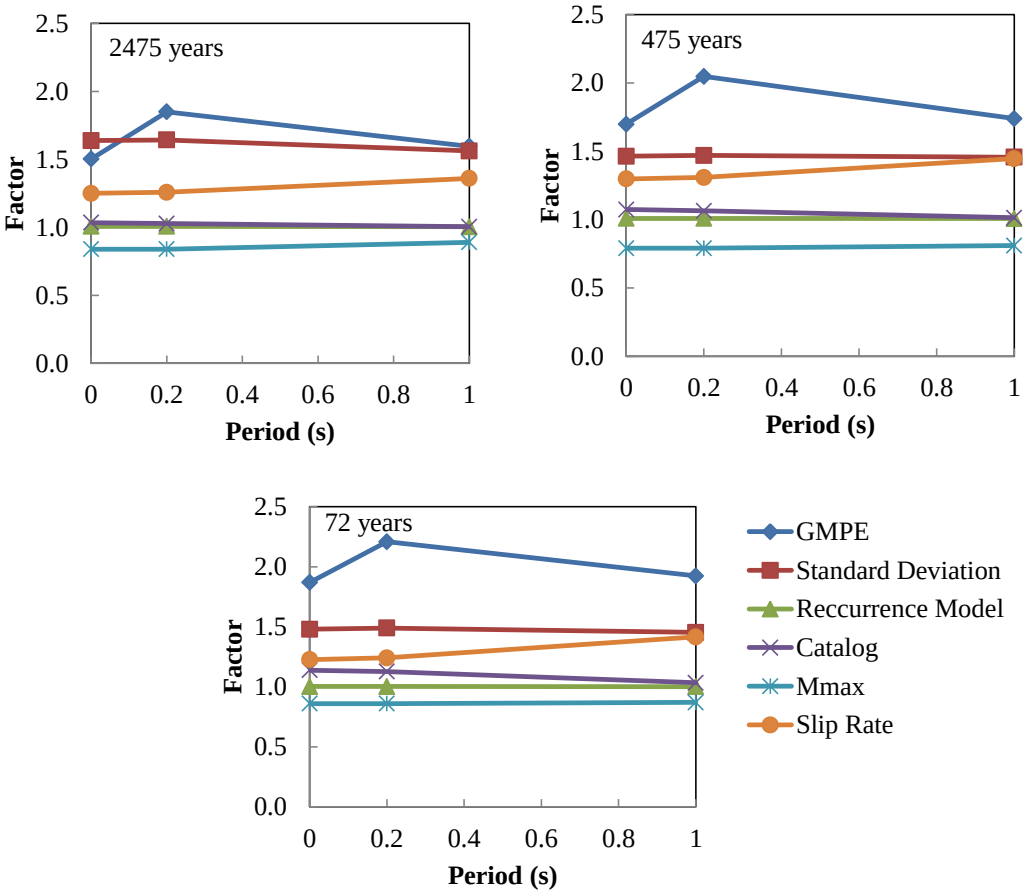


Figure 4.10 Main effects of each input parameter for different return periods as a function of spectral ordinates

Table 4.14 and Figure 4.10 can be interpreted better by focusing on the results of a particular ground-motion intensity parameter and a return period. For example, the results

given for PGA at the return period of $T_R$ = 475 years indicate that the most influential parameter for its hazard levels is the uncertainty (or the choice) in ground-motion prediction equation. The overall influence of the predictive model increases the PGA level by 71% for the city of Van when the Akkar and Bommer (2010) model is preferred instead of the Cauzzi and Faccioli (2008) GMPE.

The illustrations given in Figure 4.10 clearly show that the choice of GMPE affects the hazard results significantly for all return periods and the spectral ordinates chosen in this study. This input parameter is followed by the standard deviation of deviation of GMPEs that has a constant effect for the entire period range as the selected GMPEs in this study consider homoscedastic standard deviations that do not change with the variations of the estimator parameters of predictive models. The plots in Figure 4.10 indicate that the completeness of the earthquake catalog and the choice of recurrence models for faults do not play a significant role on the hazard results as the computed factors take values round unity. On the other hand the variations in the slip rate that directly affect the characteristic activity rates of faults are the third most contributing factor to hazard after GMPEs and their standard deviations. Slip rates changing from 1.6 mm/year to 3.4 mm/year for the Van Fault and from 6 mm/year to 13 mm/year for the Caldiran-Tutak Fault have an overall effect on hazard that approximately range between 25% and 50%. In other words, when low level slip rates of these faults are modified for their up levels the hazard for all spectral ordinates increase and the increase becomes significant towards longer periods. This is not surprising as larger slip rates would indicate the occurrence of larger magnitude earthquake on a fault that eventually affects longer period spectral ordinates. The interesting observation from Figure 4.10 and Table 4.14 is the negative effect of $M_{max}$ on hazard results. The increase in $M_{max}$ from low level to up level decreases the spectral ordinates by 10% to 15%. The reason for this adverse effect can be explained by the reduction in activity rates. In other words, in order to keep the moment rate constant due to the constraint on the slip-rate of a fault, the frequency of characteristic earthquakes should be decreased when the maximum magnitude increases. As the released seismic moment increases during characteristic earthquakes, the decrease in the frequency of characteristic earthquakes reduces the exceedance probability of PGA, PSA(T=0.2), or PSA(T=1.0) for a given threshold. Needless to say, this conclusion can be limited to the set of faults, spatial coordinates of the city of Van, and the ground-motion parameters considered in this study. However, the sensitivity analyses show that an increase in maximum magnitude does not necessarily increase the seismic hazard as expected.

The discussions in the above paragraph indicate the dominant influence of GMPE selection over other input parameters in PSHA for the city of Van. The other two input parameters that are influential on the seismic hazard are the standard deviation and slip rate. The following text discusses the interaction between the GMPEs and other three parameters in order to better understand the significance of the former parameter in the hazard results of Van.

Figure 4.11 displays the interactions between GMPE and standard deviation, between GMPE and maximum magnitude, and between GMPE and slip rate. The interaction factors are calculated by using Eq. (3.6). (The same plots would be obtained if Eq. (3.7) was used). The plots are given for the three spectral ordinates and return periods of interest in this study. The first conclusion from Figure 4.11 is that the interactions between GMPE and three input parameters decrease by decreasing return period. In all cases, the spectral ordinate at T = 0.2s is the most effected spectral quantity by the interaction between GMPE and the investigated input parameters. In general, PGA and spectral acceleration at T = 1.0s are influenced at the same level by the interactions between the parameters. The second important conclusion from Figure 4.11 is the significance of interaction between GMPE and standard deviation that is more pronounced with respect to the other two interactions. Hence, the effect of GMPE selection is important due to the combined effects of median and variance of estimated ground-motion parameter. Even when the standard deviations of GMPEs are set to a constant, changing the median estimation also changes the dispersion in the estimated ground motion. The standard deviation should be considered as the multiplier of median estimate because its definition is based on the logarithm of ground-motion parameter. This discussion also explains why the interaction effect is much more prominent for PSA(T=0.2s). This observation once again emphasizes the importance of selecting the most proper ground-motion predictive model for the probabilistic hazard studies in the city of Van. The effect of interaction is most significant for the longest return period ($T_R$ = 2475 years). Thus, the interaction effects may be overlooked except for the median and standard deviation of prediction equations at relatively long return periods (such as $T_R$ = 2475 years). This observation highlights the selection of GMPEs, such that not only the median but also the standard deviation of prediction equations should be taken into consideration.

The observations in the above paragraph can be understood better by interpreting the interactions that are given in Figures 4.12 – 4.14. These plots are prepared in the format as described in Figure 3.2. The interactions between GMPE and other three parameters are plotted for each return period and spectral ordinate by individually considering the up and low levels of GMPE. The interactions between GMPE vs. $M_{max}$ (Figure 4.13) and GMPE vs. slip rate (Figure 4.14) are plotted for the Van Fault: the closest line source to the city of Van that is expected to affect the hazard of Van the most. As indicated in Chapter 3, the interaction between GMPE and the other input parameter is significant whenever the up and low level curves of GMPE vary in a distinct manner with respect to the variations of the other input parameter. In other words, the parallel trends of up and low GMPE curves that vary as a function of up and low levels of the other input parameter would indicate insignificant interaction between these two parameters. Figure 4.12 shows the interactions between GMPE and standard deviation, which clearly indicates the strong influence between these two parameters that is particularly significant for $T_R$ = 2475 years and $T_R$ = 475 years. The interaction between these two parameters is relatively small for PGA at $T_R$ = 72 years. When the interactions between GMPE and maximum magnitude as well as GMPE and slip rate (Figures 4.13 and 4.14, respectively) are of concern, one can immediately observe the insignificance of interactions between these parameters for $T_R$ =

475 and $T_R$ = 72 years as the up and low level GMPE curves have trends almost parallel to each other. These observations once again certify the major observations made from Figure 4.11.

Figures 4.15 and 4.16 define the interactions between GMPE vs. $M_{max}$ and GMPE vs. slip rate for the Çaldıran-Tutak fault that is the distant line source considered in the hazard of the city of Van. The interaction plots display trends very similar to the corresponding ones given for the Van Fault. Their significance diminishes with decreasing return period and they are not prominent as in the case of interactions between GMPE vs. standard deviation. The observations on the GMPE vs. $M_{max}$ and GMPE vs. slip rate interactions are similar and are independent of the faults considered in this study. This fact emphasizes the importance of GMPEs and their associated standard deviations for the probabilistic hazard assessment of Van and surroundings. These two parameters should be selected in a careful manner for reliable probabilistic hazard assessment.

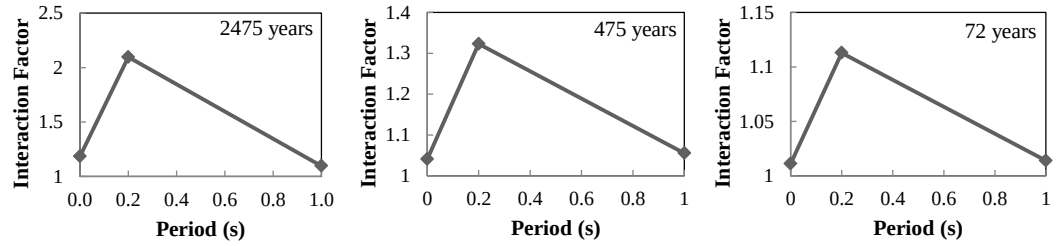


(a) Interaction between GMPE and Standard Deviation

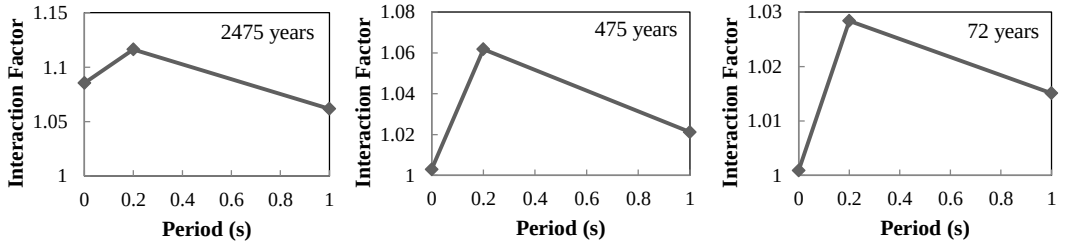


(b) Interaction between GMPE and Maximum Magnitude

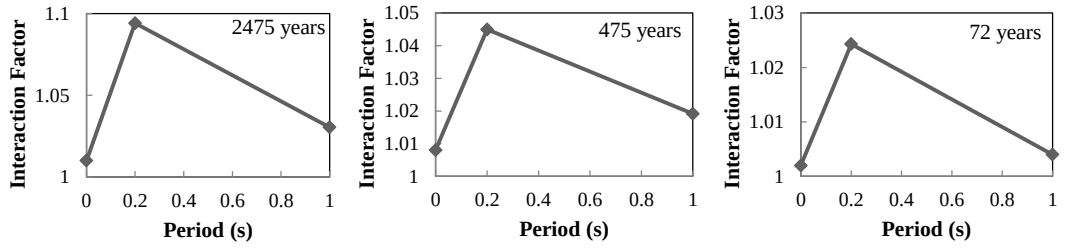


(c) Interaction between GMPE and Slip Rate

Figure 4.11 Interactions between GMPE and (a) standard deviation, (b) maximum magnitude and (c) slip rate.

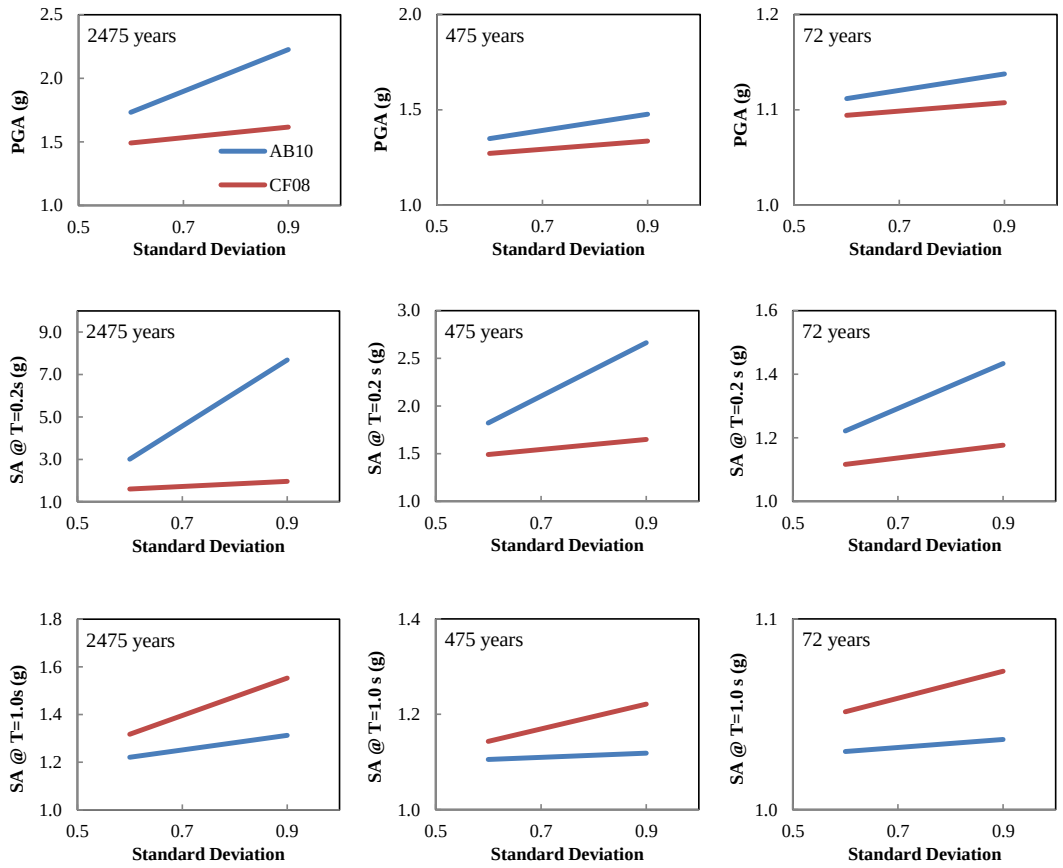


Figure 4.12 Major interactions between GMPE and standard deviation

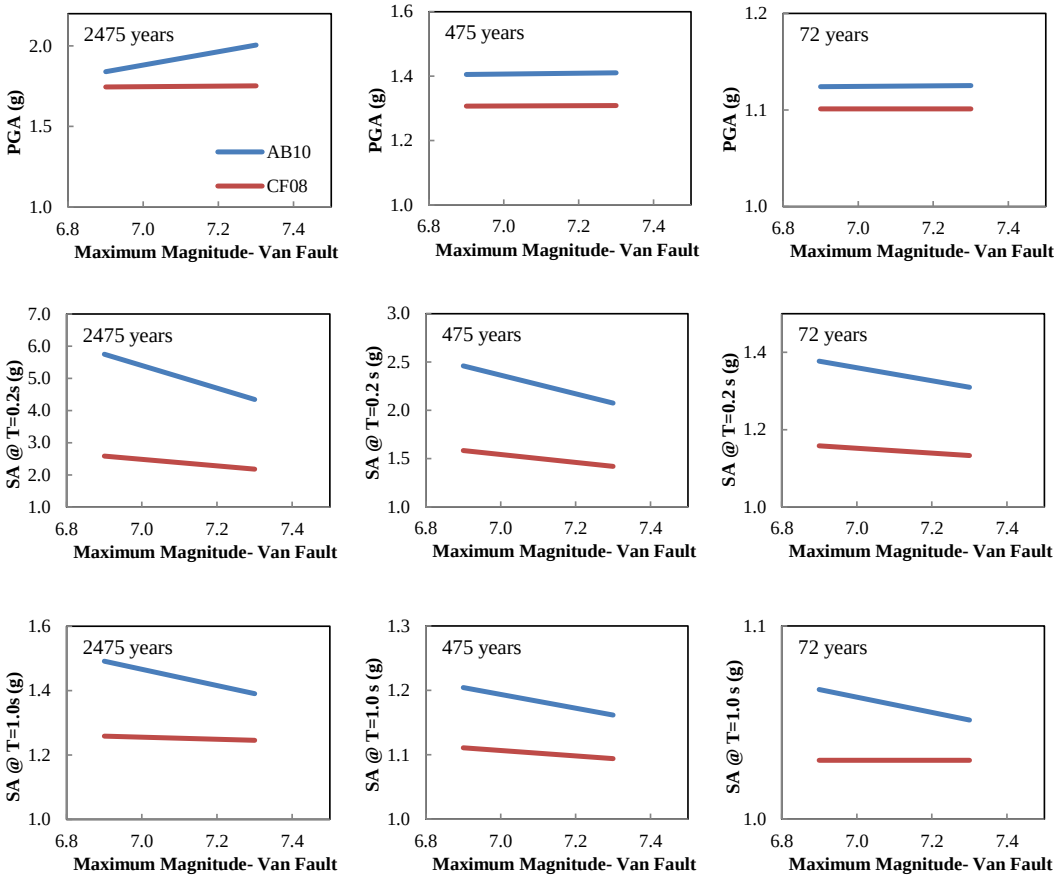


Figure 4.13. Major interaction between GMPE and $M_{max}$ for the Van Fault

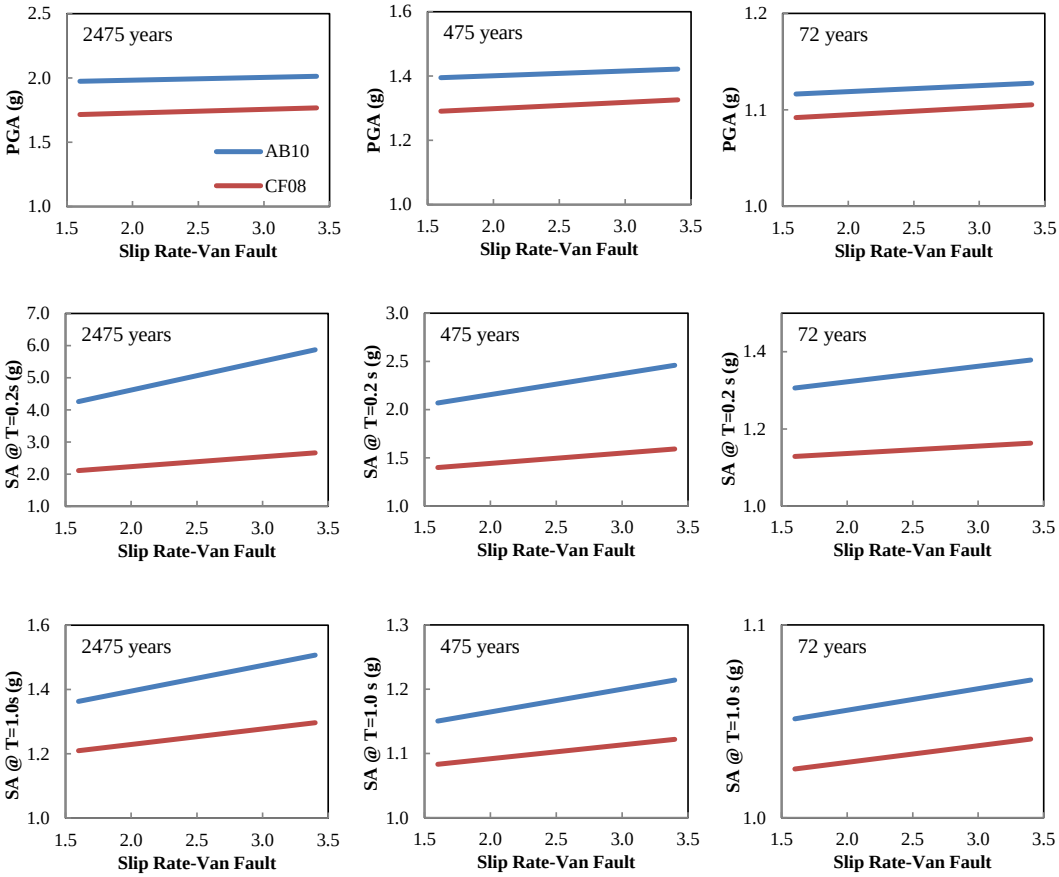


Figure 4.14 Major interaction between GMPE and slip rate for the Van fault

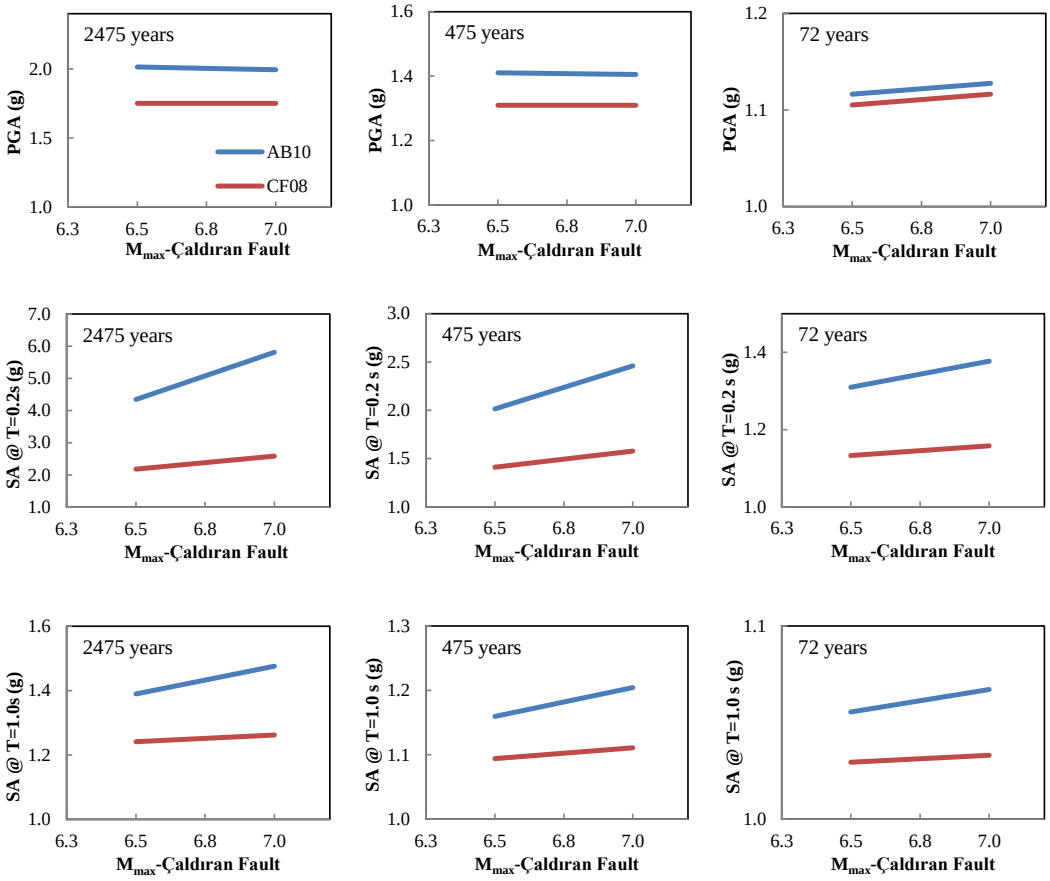


Figure 4.15. Major interaction between GMPE and $M_{max}$ for the Çaldıran-Tutak Fault

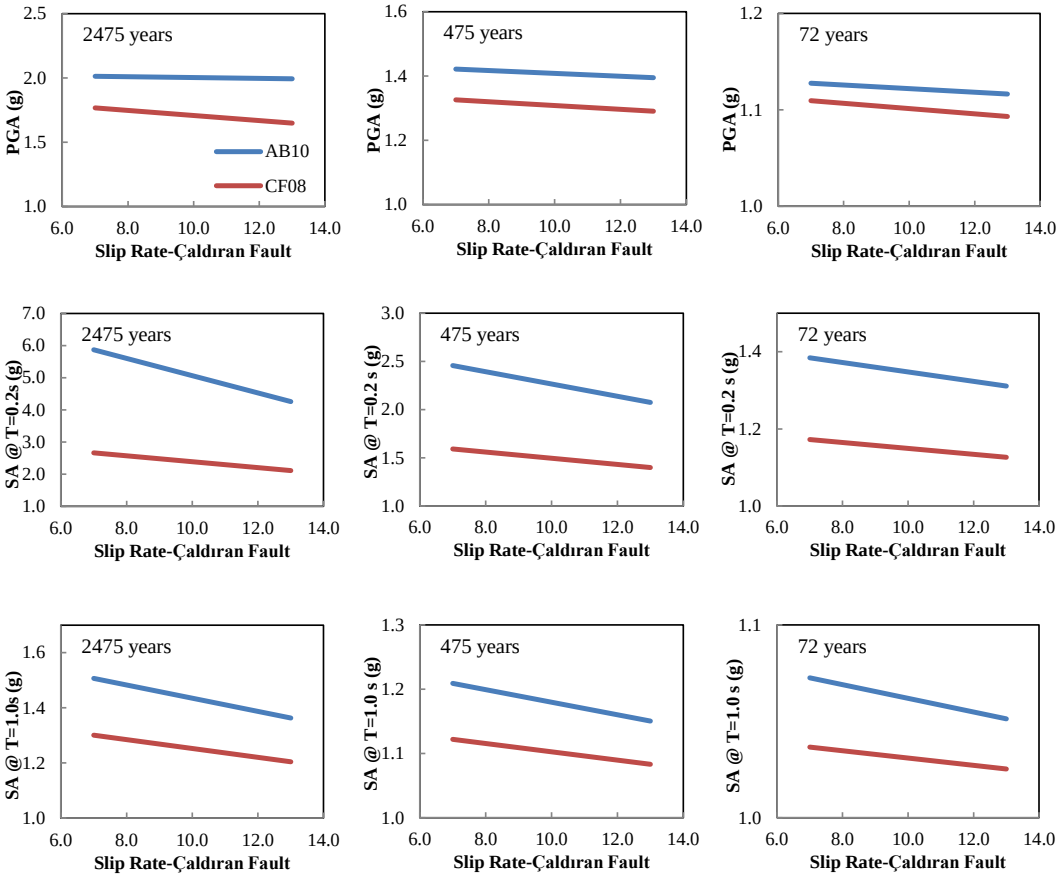


Figure 4.16 Major interactions between GMPE and slip rate for the Çaldıran-Tutak fault

# CHAPTER 5

# SUMMARY AND CONCLUSIONS

## 5.1. Summary

This study uses the multi-parameter sensitivity analysis approach (Rabinowitz and Steinberg, 1991) to assess the significance of input model parameters for site-specific PSHA. The approach is useful in the sense that the likely interactions between the seismic model parameters as well as their individual effects are considered through combinations (factorial design). In other words, the sensitivity method does not vary one parameter at a time while keeping the others constant to assess its effect on the overall hazard results (e.g., McGuire and Shedlock, 1981; Atkinson and Charlwood, 1983; Grüntahl and Wahlström, 2008). The combinations that account for the uncertainties associated with the model parameters are evaluated methodologically to see their overall effects as well as their combined effects on PSHA. Essentially, the hazard expert can assess the significance of uncertainty associated with each parameter; their contributions in the hazard results and can establish consistent logic-trees to describe the model uncertainty in hazard assessment. The multi-parameter sensitivity analysis is believed to be superior with respect to the sensitivity methods that employ probability distributions for each uncertain parameter. These alternative procedures use sampling techniques to assess the uncertainty for each model parameter. The difficulty in tailoring probability distributions for each seismic input parameter and computational burden with respect to the method assessed in this study are the practical difficulties of these methods.

The efficiency of the multi-parameter sensitivity analysis is tested for the city of Van that experienced two recent earthquakes in 23 October 2011 and 9 November 2011. These earthquakes caused significant damage and loss of life. Thus, it is believed that the hazard assessment for the city of Van is timely after these recent events. Moreover, the seismicity and seismic source characterization of the Eastern part of Turkey still suffers from significant unknowns. Thus, the consequence of uncertainties involved in each seismic

input parameter for the probabilistic seismic hazard assessment of Van and surroundings fit very well with the aims of this thesis. The center of the city with 43.5$^{o}$ E and 38.5$^{o}$ N is considered as the representative site for probabilistic hazard assessment in this study.

The study first discusses the major seismic model (input) parameters employed in PSHA. The uncertainty associated with each parameter is described and discussed by giving specific examples. The uncertainties in source characterization parameters (i.e., earthquake catalog, maximum magnitude, recurrence models for faults and area -or background-sources, slip rate) and ground-motion intensity (i.e., GMPEs and their standard deviations) are emphasized by making use of their underlying theory as well as by illustrating specific cases from the seismicity and seismotectonic features of Van and surrounding regions. The up and low levels that, in a way, bound the uncertainty of each hazard input parameter are assessed from above discussions as well as the particular seismic properties of the study area. In essence six parameters that are believed to be influential in seismic-source modeling and ground-motion variability are considered for the sensitivity analysis. The inter-variability of parameters is assumed to play a role in the seismic hazard of Van. The considered seismic model parameters are catalog completeness, slip rates on faults, maximum possible magnitude of earthquakes on specific faults and characteristic recurrence models. The parameters regarding the ground-motion variability are the median ground-motion estimations and the standard deviation that model the aleatory variability in ground-motion estimation. These two parameters are directly related to the GMPEs used in PSHA.

The multi-parameter sensitivity analysis is conducted for PGA (T = 0.0s) and spectral accelerations at T = 0.2s and T = 1.0s. The selected return periods are $T_R$ = 2475 years, $T_R$ = 475 years and $T_R$ = 72 years. The chosen spectral ordinates are generally used to establish site-specific design spectrum envelopes whereas the considered return periods are mostly used for code-based design and seismic performance assessment procedures. For each spectral period – return period pair the aforementioned seismic model input parameters result in 64 combinations. Thus, a total of 576 PSHA runs are made to observe the major effects of each one of these input parameters on hazard results as well as their effects due to interactions among each other.

## 5.2. Conclusions and Discussions

The multi-parameter sensitivity analysis indicates that the most influential factor in the probabilistic seismic hazard assessment for the city of Van is the decision on the selection of GMPEs. The decision between the up (Akkar and Bommer, 2010) and low (Cauzzi and Faccioli, 2008) levels of GMPEs may double the short-period spectral accelerations that are estimated from PSHA. The standard deviation is the second influential parameter on PSHA results that may increase the spectral accelerations by an amount of at least 50%

depending on the spectral period and return period of concern. These two parameters are followed by the slip rate and maximum magnitude of faults affecting the city of Van (Çaldıran-Tutak and Van faults). Interestingly, the change in maximum magnitude from low level to up level decreases the estimated spectral accelerations for all return periods. The underlying reason for this observation is the trade-off between the maximum magnitude and slip rate. Since slip rate is constrained to specific values, the increase in magnitude from a smaller to larger value causes a decrease in the activity rates (frequency of characteristic earthquakes) in order to preserve the seismic moment balance that is directly related to slip rate. A significant reduction in the activity results in reduced hazard although the capability of generating larger magnitude earthquakes are increased with incrementing the maximum magnitudes to larger values. The interactions between GMPE and the other most influential input parameters (i.e., standard deviation of GMPEs, slip rate and maximum magnitude) indicate that the level of standard deviation together with the selected GMPE should be considered seriously in logic-tree applications for the most proper estimations of spectral accelerations for the probabilistic hazard assessment in Van. The uncertainty in slip rate is the third significant parameter affecting the results of PSHAs.

It should be noted that the above discussions are only valid for the probabilistic hazard assessment of the city of Van and they are confined to the hazard model developed for this city. As it is summarized in the literature survey sensitivity analysis for uncertain input parameters may bring forward the importance of other parameters, such as those that characterize the seismic sources. As a matter of fact this study also indicates that slip rate and decision on maximum magnitude are the influential source parameters that lay roles on the seismic hazard outputs. Regardless of the input model parameter of significance affecting the hazard results of Van, the discussions that take place here clearly indicate that running PSHA without considering the uncertainty in each seismic model parameter may yield unreliable estimations of seismic demands. These seismic demands are essentially used by the engineers who design new buildings or assess the seismic performance of existing buildings. To this end, the multi-parameter sensitivity approach used in this study can be a proper tool to identify the most dominant seismic model parameter(s) influencing the hazard results for their careful consideration via logic-tree applications in PSHA.

## 5.3. Future Studies

The presented study constitutes a simple exercise to describe a useful sensitivity analysis method to identify the most significant seismic model parameters in a site-specific PSHA. The discussions are based on the chosen six model parameters and their up and low levels. The presented sensitivity analysis can be extended to other seismic model parameters with a much more refined seismic source characterization. Moreover, the up and low levels that account for the uncertainty in each seismic model parameter can be improved by adding

intermediate levels to monitor how the gradual change of uncertainty associated with each input parameter affects the ground-motion intensity estimations.

The other future study that can be conducted under the observations made by this thesis is proponing a transparent weighting strategy for addressing the modeling uncertainty in site-specific PSHA. Combination of sensitivity analysis methods that consider factorial design and variation of uncertain parameters one at a time with or without using sampling techniques can be implemented in many case studies. The observations from these extensive sets of analyses can be used to come up with a rationale logic-tree procedure for ranking and weighting the seismic input parameters according to their role on the results of PSHA. In fact, this cannot be studied in the thesis would have enabled the the computation of rational uniform hazard spectra for the city of Van at various return periods.

# REFERENCES


Abrahamson, N.A., (2006). Notes on Probabilistic Seismic Hazard Analysis – An Overview. Rose School, Pavia, Italy.

Abrahamson, N., and Silva, W., (2008). Summary of the Abrahamson & Silva NGA groundmotion relations. Earthquake Spectra, 24(1), 67-97.

Aki, K., (1965). Maximum likelihood estimate of b in the formula log N(M)=a -bM and its confidence limits, Bulletin of Earthquake Research Institute, Tokyo University 43, 237–239.

Akkar, S., and Bommer, J.J., (2010). Empirical equations for the prediction of PGA, PGV, and spectral accelerations in Europe, the Mediterranean Region, and the Middle East, Seismological Research Letters, Vol. 81 (2), 195-206.

Akkar, S., and Çağnan, Z., (2010). A local ground-motion predictive model for Turkey and itscomparison with other regional and global ground-motion models. Bulletin of the Seismological Society of America, 100(6), 2978-2995.

Akkar, S., Douglas, J., Di Alessandro, C., Campbell, K., Somerville, P., Cotton, F., Silva, W., Baker, J. (2012). Defining a consistent strategy to model ground-motion parameters for the GEM-PEER Global GMPEs Project, Proceedings of the Fifteenth World Conference on Earthquake Engineering.

Akkar, S., Çagnan Z., Yenier E., Erdoğan Ö., Sandıkkaya A., and Gülkan P., (2010). The recently compiled Turkish strong motion database: preliminary investigation for seismological parameters, Journal of Seismology,14, 457-479

Ambraseys, N.N., Douglas, J., Sarma, S.K., and Smit, P.M., (2005). Equations for the estimation of strong ground motions from shallow crustal earthquakes using data from Europe and the Middle East: Horizontal peak ground acceleration and spectral acceleration. Bulletin of Earthquake Engineering, 3(1), 1-53.

Annaka T., and Ohki H., (1992). A sensitivity analysis for seismic hazard estimation. Earthquake Engineering, Tenth World Conference, Balkema, Rotterdam.

Arpat, E., ve Şaroğlu, F., (1972). Doğu Anadolu fayı ile iilgili bazı gözlemler ve düşünceler: MTA DErg., 78:44-50 (in Turkish).

Arpat E., Saroğlu F., Iz H.B., (1976). Caldıran Earthquake, Yeryuvarı ve Insan 1977 2:29–41 (in Turkish).

Atkinson, G.M., and Charlwood R.G., (1983). Uncertainties in probabilistic seismic hazard assessment as a function of probability level: a case history for Vancouver, British Columbia, Bulletin of the Seismological Society of America Vol 73, 1225-1241.

Barka A., and Kadinsky-Cade K., (1988). Strike-slip fault geometry in Turkey and its influence on earthquake activity. Tectonics 7:663-684

Barka A., and Reilinger R., (1997). "Active tectonics of the Eastern Mediterranean region: deduced from GPS, neotectonic and seismicity data," Annali di Geofisica, XL(3): 587-610.

Barka, A., ve Şaroğlu, F., (1995). Van Gölü Su Yükselmesinin Tektonik İle İlişkisi. Van Gölü'nün Su Seviyesinin Yükselmesi Nedenleri, Etkileri ve Çözüm Yolları Sempozyumu, 20-22 Haziran 1995, Van. 74-90 (in Turkish).

Bindi, D., Luzi, L., Massa, M., and Pacor, F., (2010). Horizontal and vertical ground motion prediction equations derived from the Italian Accelerometric Archive (ITACA). Bulletin of Earthquake Engineering, 8(5), 1209-1230.

Bommer, J.J., Scherbaum, F., Bungum, H., Cotton, F, Sabetta, F., and Abrahamson, N.A. (2005). On the use of logic trees for ground-motion prediction equations in seisrnic-hazard analysis. Bulletin of the Seismological Society of America. 95:4, 377–389

Bommer, J.J., Abrahamson, N.A., (2006). "Why Do Modern Probabilistic Seismic-HazardAnalyses Often Lead to Increased Hazard Estimates?" Bulletin of the Seismological Society of America, 96(6), 1967-1977.

Bommer J. J., (2012). Challenges of Building Logic Trees for Probabilistic Seismic Hazard Analysis. Earthquake Spectra 28:4, 1723-1735

Boore, D.M., and Atkinson, G., (2008). Ground-Motion Prediction Equations for the AverageHorizontal Component of PGA, PGV, and 5%-Damped PSA at Spectral Periods between 0.01s and 10.0 s. Earthquake Spectra, 24(1), 99-138.

Box, G.E.P., Hunter, W.G., and Hunter J.S., (1978). Statistics for Experimenters, Wiley, New York.

Campbell, K.W., Bozorgnia, Y., (2008). "NGA Ground Motion Model for the Geometric Mean Horizontal Component of PGA, PGV, PGD and 5% Damped Linear Elastic Response Spectra for Periods Ranging from 0.01 to 10 s." Earthquake Spectra, 24(1), 139-171.

Cauzzi, C., and Faccioli, E., (2008). Broadband (0.05 to 20 s) prediction of displacement response spectra based on worldwide digital records. Journal of Seismology, 12(4), 453-475.

Chiou, B.S.J., and Youngs, R.R. (2008). An NGA model for the average horizontal component of peak ground motion and response spectra. Earthquake Spectra, 24(1), 173-215.

Copley and Jackson (2006). "Active tectonics of the Turkish-Iranian Plateau," Tectonics, 25: TC6006.

Cornell, C.A., and Winterstein S.R., (1988). "Temporal and Magnitude Dependence in Earthquake Recurrence Models," Bull. Seismol. Soc. Am. , 78, 1522–1537.

Cotton, F., Scherbaum, F., Bommer, J.J., Bungum, H. (2006). "Criteria for selecting and adjusting ground-motion models for specific target regions: Application to central Europe and rock sites," Journal of Seismology, Vol. 10, No. 2, pp. 137–156

Cramer, C.H., Petersen, M.D., Cao, T., Toppozada, T.R., Reichle, M., (2000). "A Time-Dependent Seismic- Hazard Model for California," Bulletin of Seismological Society of America, 90, 1–21.

Dewey J.F., Hempton M.R., Kidd W.S.F., Şaroğlu F., Şengör A.M.C., (1986). Shortening of continental lithosphere: the neotectonics of Eastern Anatolia-a young collision. In Collision Tectonics, eds. Coward MP and Ries AC, Geological Society Spectra Publication 19: 3-36.

Djamour Y., Vernant P., Ankali H.R., Tavakoli F., (2011). NW Iran-eastern Turkey present-day kinematics: Results from the Iranian permanent GPS network, Earth and Planetary Science Letters 307, 27-34

Emre Ö., Duman T.Y., Özalp S., Elmacı H. (2011). 23 Ekim 2011 Van depremi saha gözlemleri ve kaynak faya ilişkin ön değerlendirmeler. MTA Jeoloji Etütler Dairesi, Ankara, 22 pp (in Turkish).

Fisher, R. A. (1926). The arrangement of field experiments, Journal of the Ministry Agriculture. 33, 503-513.

Frankel, A., (1995). “Mapping Seismic Hazard in the Central and Eastern United States,” Bulletin of Seismological Society of America, 66, 8–21.

Fukushima, Y., Berge-Thierry, C., Volant, P., Griot-Pommera, D.-A. and Cotton, F. (2003). Attenuation relation for western Eurasia determined with recent near-fault records from California, Japan and Turkey. Journal of Earthquake Engineering, 7(4), 573-598.

Ghasemi, H., Zare, M., Fukushima, Y., and Koketsu, K., (2009). An empirical spectral groundmotion model for Iran. Journal of Seismology, 13, 499-515.

Grünthal G., and Wahlström R., (2008). Sensitivity Of Parameters For Probabilistic Seismic Hazard Analysis Using A Logic Tree Approach, Journal of Earthquake Engineering, 5:3, 309-328

Grünthal, G., Stromeyer, D., Wahlström, R. (2009). Harmonization check of Mw within the central, northern, and northwestern European earthquake catalogue (CENEC). - Journal of Seismology, 13, 4, 613-632

Gutenberg, B., (1945). Amplitudes of P, PP, & S and Magnitudes of Shallow Earthquakes. Bulletin of the Seismological Society of America., Vol. 35, pp. 57-69.

Gutenberg, B., and Richter C.F., (1956). Earthquake Magnitude, Intensity, Energy and Acceleration. Bulletin of the Seismological Society of America., Vol. 46, pp. 105-145.

Hanks, T.C., and Kanamori H., (1979). A moment magnitude scale, Journal of Geophysical Research 84~ 2348-2350.

Hassaballa A. E., Mohamed A. R. E., Sobaih M., (2011). Sensitivity Analysis of Parameters for Probabilistic Seismic Hazard for Sudan. Journal of Science and Technology, ISSN 1605 – 427X

Joyner, W. B. and Boore D.M., (1981). Peak horizontal acceleration and velocity from strong-motion records including records from the 1979 Imperial Valley, California, earthquake, Bull. Seism. Soc. Am. 71, 2011-2038.

Kale, Ö., and Akkar, S., (2013). A New Procedure for Selecting and Ranking Ground Motion Prediction Equations (GMPEs): Euclidean Distance-Based Ranking (EDR) Method, Bulletin of the Seismological Society of America, 103, 2A, 1069-1084.

Kalkan, E., and Gülkan, P., (2004). Site-dependent spectra derived from ground motion records in Turkey. Earthquake Spectra, 20, 1111-1138.

Kiureghian, D. A., Ditlevsen, O., (2009). Aleatory or epistemic? Does it matter?, Structural Safety 31 (2) 105-112, ISSN 0167-4730.

Koçyiğit A., (2002). Neotectonics and seismicity of East Anatolian.Workshop-2002 on the Geology of East Anatolian, Yüzüncü Yıl University, Van, Turkey, pp 2-4.

Kramer, S.L. (1996). Geotechnical Earthquake Engineering. New Jersey: Prentice Hill.

Leonard M. (2010). Earthquake Fault Scaling: Relating Rupture Length, Width, Average Displacement, and Moment Release. Bulletin of the Seismological Society of America 100, 1971-1988.

McCalpin, J., (1996). Paleoseismology. San Diego: Academic Press, 588 pps.

McGuire R.K., (2004). Seismic Hazard and Risk Analysis, Earthquake Engineering Research Institute Monograph, MNO-10, CA, 221p.

McGuire, R.K., and Shedlock K.M., (1981). Statistical uncertainties in seismic hazard evaluations in the United States, Bulletin of the Seismological Society of America Vol 71, 1287-1308.

McKenzie D.P., (1972). Active tectonics of the Mediterranean region. Geophysical Journal of the Royal Astronomical Society. 30: 109-185.

Moss, R. E. S., Der Kiureghian, A., (2006). Incorporating Parameter Uncertainty into Attenuation Relationships, in: Eighth U.S. National Conference of Earthquake Engineering (100th Anniversary Earthquake Conference), San Francisco, CD-ROM.

Moss, R. E. S., (2009). Reduced Uncertainty of Ground Motion Prediction Equations through Bayesian Variance Analysis, Pacific Earthquake Engineering Research Center, PEER report PEER 2009/105.

Örgülü G., Aktar M., Türkelli N., Sandvol E., ve Barazangi M., (2003). "Contribution to the seismotectonics of the eastern Anatolian Plateau from moderate and small size events", Geophysical Research Letters, 30(24), No. 8040.

Özbey, C., Sari, A., Manuel, L., Erdik, M. and Fahjan, Y., (2004). An empirical attenuation relationship for northwestern Turkey ground motion using a random effects approach. Soil Dynamics and Earthquake Engineering, 24(2), 115-125.

Özkaymak Ç., (2003). Van şehri ve yakın çevresinin aktif tektonik özellikleri. Dissertation, Yüzüncü Yıl Üniversitesi, 77 pp.

Özkaymak Ç., Yürür T., Köse O., (2004). An example of intercontinental active collisional tectonics in the Eastern Mediterranean region (Van, eastern Turkey). 5th International Symposium on Eastern Mediterranean Geology, Thessaloniki, Greece, Proceedings Book, pp 591-593.

Paradisopoulou, P.M., Papadimitriou, E.E., Karakostas, V.G., Taymaz, T., Kilias, A. and. Yolsal, S., (2010). "Seismic hazard evaluation in Western Turkey as revealed by stress transfer and time dependent probability calculations. Pure and Applied Geophysics, 167, 1013-1048.

Rabez, A., Slejko D., (2000). Sensitivity analysis on the input parameters in probabilistic seismic hazard assessment. Soil Dynamics and Earthquake Engineering, Vol. 20, Issues 5–8, Pages 341–351

Rabinowitz N., and Steinberg D.M., (1991). Seismic hazard sensitivity analysis: A multi-parameter approach. Bulletin of the Seismological Society of America Vol. 81:796-817

Reasenberg, P., (1985). "Second-order moment of central California seismicity,1969–1982," Journal of Geophysical Research, 90: 5479–5495.

Reilinger R., McClusky S., Vernant P., Lawrence S., Ergintav S., Cakmak R., Ozener H., Kadirov F., Guliev I., Stepanyan R., Nadariya M., Hahubia G., Mahmoud S., Sakr K., ArRajehi A., Paradissis D., Al-Aydrus A., Prilepin M., Guseva T., Evren E., Dmitrotsa A., Filikov S.V., Gomez F., Al-Ghazzi R., Karam G., (2006). GPS constraints on continental deformation in the Africa-Arabia-Eurasia continental collision zone and implications for the dynamics of plate interactions. Journal of Geophysical Research 111, B05411, 10.1029.

Rhoades, D. A., (1997). Estimation of attenuation relations for strong-motion data allowing for individual earthquake magnitude uncertainties, Bulletin of the Seismological Society of America 87 (6), 1674-1678.

Richter C. F., (1935). An instrumental earthquake magnitude scale. Bulletin of Seismological Society of America 25: 1-32

Saltelli, A., Ratto M., Andres T., Campolongo F., Cariboni J., Gatelli D., Saisana M., Tarantola S., (2008). Global Sensitivity Analysis: The Primer. Chichester, England: John Wiley & Sons.

Schwartz, D.P., and Coppersmith K.J., (1984), "Fault Behavior and Characteristic Earthquakes: Examples from the Wasatch and San Andreas Fault Zones," Journal of Geophysical Research, 89, 5681–5698.

SSHAC (Senior Seismic Hazard Assessment Committee), (1997), "Recommendations for PSHA: Guidance on Uncertainty and Use of Experts," Report NUREG/CR-6372, U.S. Nuclear Regulatory Commission, Washington, D.C.

Sokolov V. Y., Venzel F., Mohindra R., (2009). Probabilistic seismic hazard assessment for Romania and sensitivity analysis: A case of joint consideration of intermediate-depth (Vrancea) and shallow (crustal) seismicity. Soil Dynamics and Earthquake Engineering Vol. 29, Issue 2, Pages 364–381

Stepp, J.C., (1973). Analysis of Completeness of the Earthquake Sample in the Puget Sound Area. Contributions to Seismic Zoning: U.S. National Oceanic and Atmosphere Administration Technical Report ERL 267-ESL30, pp. 16-28.

Stewart, J. P., Chiou S. J., Bray D., Graves R.W., Somerville P. G., N. Abrahamson N., (2001). Ground Motion Evaluation Procedures for Performance-Based Design. PEER Report 2001/09.

Strasser, F. O., Abrahamson N. A., and Bommer J. J. (2009). Sigma: Issues, insights, and challenges. Seismological Research Letters 80, 41–56.

Şaroğlu F., Emre Ö., Kuşçu İ., (1992) Active fault map of Turkey. Publ Miner Res Explor Ins Turk, Ankara, Turkey. 38

Şengör A.M.C., Görür N., and Şaroğlu F., (1985). Strike-slip faulting and related basin formation in zones of tectonic escape: Turkey as a case study, in Strike-Slip Faultingf and Basin Formation, edited by K.T. Biddke and Christie-Blick, Society Economic Paleontologists Mineralogists Special Publication, 227-264

Thenhaus, P.C., and Campbell, K.W.(2003). Seismic Hazard Analysis, in: Earthquake Engineering Handbook, edited by: Chen, W.-F. and Schawthorn, C., CRC Press, VIII1-50

Toksöz M.N., Arpat E., Şaroğlu F., (1977). East Anatolian earthquake of 24 November 1976. Nature 270:423-425.

Toksöz M.N., Nabelek J., Arpat E., (1978). Source properties of the 1976 earthquake in eastern Turkey: a comparison of field data and teleseismic results. Tectonophysics 49:199-205.

Toro, G. and McGuire R., (1987). Calculational procedures for seismic hazard analysis and its uncertainty in the eastern United States. Proceedings,. Third International Conference on Soil Dynamics and Earthquake Engineering, Princeton, NJ, pp. 195-206.

Ulusay, R., Tuncay, E., Sonmez, H., Gokceoglu, C., (2004). An attenuation relationship based on Turkish strong motion data and iso-acceleration map of Turkey. Engineering Geology 74 (3–4), 265–291.

Utkucu, M., (2013a). 23 October 2011 Van, Eastern Anatolia, earthquake (MW =7.1) and seismotectonics of Lake Van Area, Journal of Seismolology, 17, 783–805.

Wang J., and Gao M., (1996). Parameter sensitivity analysis in seismic hazard. Institute of Geophysics, State Seismological Bureau, Beijing 100081, China

Weichert D.H., (1980). "Estimation of the earthquake recurrence parameters for unequal observation periods for different magnitudes," Bulletin of the Seismological Society of America, 70(4): 1337-1346.

Weimer, D.R., (2001). An improved model of ionospheric electric potentials including perturbations and application to the Geospace Environment Modeling November 24, 1996, event, Journal of Geophysical Research, 106, 407.

Wells, D. L., and Coppersmith K.J., (1994). New empirical relationships among magnitude, rupture length, rupture width, rupture area, and surface displacement, Bulletin of the Seismological Society of America.. 84, 974-1002.

Westaway (2003). "Kinematics of the Middle East and Eastern Mediterranean Updated", Turkish Journal of Earth Science, 12: 5-46.

Westaway, R., and Arger, J., (1996). the Gölbaşı basin, southern Turkey : a complex discontinuity in a major strike-slip fault zone. Journal of the Geological Society London, 153, 729- 744.

Wyss, M., Hasegawa A., and Nakajima J., (2001a). Source and path of magma for volcanoes in the subduction zone of northeastern Japan, Geophysical Research Letters.

Yılmaz Öztürk N. (2008). Probabilistic Seismic Hazard Analysis: A Sensitivity Study with Respect to Different Models, PhD Thesis, Department of Civil Engineering, Middle East Technical University, Ankara, Turkey.

Youngs, R.R. and Coppersmith K.J. (1985). Implications of fault slip rates and earthquake recurrence models to probabilistic seismic hazard estimates, Bulletin of the Seismological Society of America. 75, 939-964.

Zare, M. and Bard, P. Y., (2002). Strong motion dataset of Turkey: data processing and site classification, Soil Dynamics and Earthquake Engineering, Vol. 22, pp.703-718.

Zechar J. D., and Frankel K. L., (2009). Incorporating and reporting uncertainties in fault slip rates. Journal Of Geophysical Research, Vol. 114, B12407.

Zhao, J.X., Zhang, J., Asano, A., Ohno, Y., Oouchi, T., Takahashi, T., Ogawa, H., Irikura, K. Thio, H.K., Somerville, P.G. and Fukushima, Y. (2006). Attenuation relations of strong ground motion in Japan using site classification based on predominant period. Bulletin of the Seismological Society of America, 96(3), 898-913.